Martin Minarič, BSc.

Investigation of flange bolt joints between carbon fiber-reinforced plastic and aluminum

MASTER'S THESIS

to achieve the university degree of

Diplom-Ingenieur

Master's degree programme: Mechanical Engineering

submitted to

Graz University of Technology

Supervisor

Assoc.Prof. Dipl.-Ing. Dr.techn., Norbert Enzinger

Institute for Material Science and Welding of Graz University of Technology

Dipl.-Ing. Robert Szlosarek

Graz, February 2015

AFFIDAVIT

I declare that I have authored this thesis independently, that I have not used other than the declared sources/resources, and that I have explicitly indicated all material which has been quoted either literally or by content from the sources used. The text document uploaded to TUGRAZonline is identical to the present master's thesis.

Date	Signature

Preface

Firstly I would like to thank the Virtual Vehicle Research Center and the Institute of Material Science and Welding of Graz University of Technology, which made this master thesis possible. I should not forget to mention also the Composite Material & Lightweight Structures Group and my group leader, who were supporting me and made my stay at the Virtual Vehicle Research Center as pleasant as possible.

Explicitly I would like to thank my supervisor from Virtual Vehicle Research Center Dipl.-Ing. Robert Szlosarek for his unbelievable patience and for the fact, that he was always ready to help me. On the other hand I would like to thank to my supervisor form the Institute for Material Science and Welding Professor Norbert Enzinger for his knowledge, constructive criticism and a friendly atmosphere, which always drove me forward.

I would like to acknowledge the financial support of the "COMET K2 - Competence Centres for Excellent Technologies Programmeöf the Austrian Federal Ministry for Transport, Innovation and Technology (BMVIT), the Austrian Federal Ministry of Economy, Family and Youth (BMWFJ), the Austrian Research Promotion Agency (FFG), the Province of Styria and the Styrian Business Promotion Agency (SFG).

Furthermore I would like to express my gratitude to the supporting industrial and scientific project partners, namely Audi AG, ESI GmbH, Institut für Werkstoffkunde and Schweißtechnik at TU Graz, Fachgebiet Konstruktiver Leichtbau and Bauweisen at TU Darmstadt, and the Graz University of Technology.

I want to thank as well my girlfriend Ivanka and my family, because without their mental and financial support the study at the University of Technology in Graz would not be possible.

Graz, February 2015 Martin Minarič

Abstract

Carbon fiber-reinforced plastic (CFRP) represents for many manufacturers in automotive industry a material with high potential for future. It is so thanks to its low specific mass, beneficial mechanical properties and a high mass specific absorption of energy. Therefore, a deeper understanding of the CFRP is necessary. The most frequently used joining technology for the CFRP in automotive industry nowadays is a bolted joint between the CFRP and other materials. Bolted joints include rivet and screw joints. Consequently a detailed knowledge of the failure modes of the bolted joints between the CFRP and metals is crucial. The four basic failure modes are bearing failure, tensile failure, shear failure and cleavage. These failure modes are a result of failure phenomena in the CFRP like fiber failure, inter-fiber failure and delamination. From these four failure modes the bearing failure is the only safe failure. Safe failure is a failure without a separation. Therefore, the bearing failure represents the commonly required failure mode in automotive industry. The finite element method represents the perfect tool for designing mechanical and geometrical properties of bolted joints.

Based on literature research, an investigation of the influence of various properties on the results was performed. In this investigation three material models were used. The evaluation of the quality of each of the material models was based on a comparison. In this comparison major differences were discovered.

In the next step these three material models were compared with an experimental investigation. For this investigation a flow drill screw joint between CFRP and aluminum was tested. It was observed how the failure mode of the CFRP specimen varies depending on the end distance and the stacking sequence of the CFRP specimen. Parallel to these experimental tests, numerical simulations with various material models were performed. The comparison of the experimental tests with the simulations also showed that the quality of the material models varies significantly.

Content

List of abbreviations

Abbreviation	Description
2D	Two-dimensional
3D	Three-dimensional
CFRP	Carbon fiber-reinforced polymers
ECH	Epichlorhydrin
EE	Element Elimination
EP	Epoxy Resins
FEA	Finite Element Analysis
FEM	Finite Element Method
HT	High Tensile
IFF	Inter-fiber failure
KSII	Head shear tensile
PA	Polamide
PAEK	Polyaryletherketone
PAN	Polyacrylonitrile
PEEK	Polyetheretherketone
PEI	Polyetherimed
PET	Polyethylenterephthalat
PF	Phenol Resins
PI	Polyimide Duroplastics
PP	Polyprophylene
PTFE	Polytetraflouoroethyle
PVDC	Polyvinylidene Chloride
UP	Unsaturated Polyester Resins
VE	Vinylester Resins

List of symbols

Latin lower case

Symbol	Description
c	Compression
d	Diameter, Damage
e	End distance, Tensor trace, Fiber failure value
$elim$	Elimination
f	Fiber
f_E	Stress exposure
fp	Fracture plane
i	Initial
l	Displacement, Length, Intermediate
m	Matrix
n	Amount of holes
p	Pressure
t	Thickness, Tension
$true$	Real
u	Ultimate
v	Volume
w	Bolt distance, Width

Latin upper case

Symbol	Description
A	Surface area
B	Bearing
C	Celsius
E	Young's modulus, Elastic modulus
F	Force
FF	Fiber failure
G	Shear modulus
O	Initial
R	Strength
UD	Unidirectional
V	Volume, Ply volume, Pretension

greek lower case

Symbol	Description
α	Fiber volume ratio
δ	Deflection
ϵ	Strain
θ	Angle
μ_0	Coefficient of static friction
ν	Poisson's ratio
σ	Stress
τ	Shear stress

Greek upper case

Symbol	Description
Δ	Difference

Coordinate system

Symbol	Description
$1, 2, 3$	Coordinate system of the unidirection laminate
$1, n, t$	Coordinate system of the action plane in the unidirection laminate
i, j, k	Local coordinate system of an element
x, y, z	Global coordinate system

Symbol

Symbol	Description
$(+)$	Tension
$(-)$	Compression
°	Degree
$\parallel$	Parallel with respect to the fiber direction
$\perp$	Perpendicular with respect to the fiber direction

1 Introduction

The recent trend in automotive industry takes the direction to lighter cars with stronger materials. This is a result of the higher emission restrictions, lower consumption expectations and customer demand for higher performance. All these reasons require a lighter automobile construction. This development started with aluminum alloys, magnesium alloys and titanium alloys and went up to carbon fiber-reinforced plastic (CFRP). [1] [2]

CFRP are complex materials. The mechanical properties depend not only on the engineering constants and geometry, but because of the strong anisotropic properties, they depend as well on the direction of the load, the number of laminas combined together and the fiber direction of the laminas [3].

CFRP materials are used in automotive industry mostly in the construction of the car body and chassis, but can be found also in engine components. With the rapid growth of CFRP usage in car production a deeper understanding of the joining technology and interaction between CFPR and other materials has been crucial to utilize the maximum advantage from the CFRP. Bolted joints play among others an important role in the automotive joining technology. From experiments it is known that the CFRP can fail depending on the geometry and stacking sequence of the laminas either in a non-save failure (tensile failure, shear failure and cleavage) or a save failure (bearing failure). Whereas the save failure is always required due to the possibility to detect the failure before the separation of the jointed materials. It is capable as well to absorb higher amount of kinetic energy. [4]

To save time and cost of the experiments engineers seek for a numerical solution of CFRP in combination with a bolt joint. The finite element method (FEM) is trying to solve this problem while it considers the anisotropic properties of CFRP, inter-fiber failure, fiber failure, delamination, geometry of the components and the stacking sequence.

Due to the large amount of variables a question arises, whether a standard material description from the software producer or a user-defined material description are capable to predict the proper failure and the maximum force transmitted depending on all variables mentioned above.

This thesis describes principles behind the failure modes, stacking sequence, inter-fiber and fiber failure. Simulations of bolted joints in different variations and a attempt to fully use the possibilities of two standard material descriptions (shell and solid) provided by the producer and one user-defined material model description were done. It is important

to find out, whether it is possible to fully predict the failure and if not, to which level it is possible. Than it is interesting to define what should be modified or enhanced to achieve the goal. Simulations done in this thesis will be compared with experiments done in this field of interest. [5]

Fig. 1.1: Car frame produced from carbon fiber-reinforced plastics [6]

2 Theoretical Background

This chapter firstly introduced the topic fiber composites, which is supposed to inform the reader about the fundamentals. It describes many possible fiber and matrix types as well the important properties of each of this phases.

The CFPR is discussed. The manufacturing process of CFRP and all advantages which are provided with CFRP are explained.

The third part of this chapter writes about bolt joints. Types of bolt joints and their failures are introduced. Then optimization possibilities and characteristics are introduced.

The last section of this chapter describes the finite element analysis (FEA) and all necessary steps, which lead from a problem to a solution.

2.1 Fiber Composites

The number of applications using CFRP in automotive engineering rapidly increases every day. The demand for lighter and stronger materials with beneficial properties is the main propulsion for the production and utilization of fiber composites.

Figure 2.1 compares some of the material used in automotive industry and shows their mechanical properties.

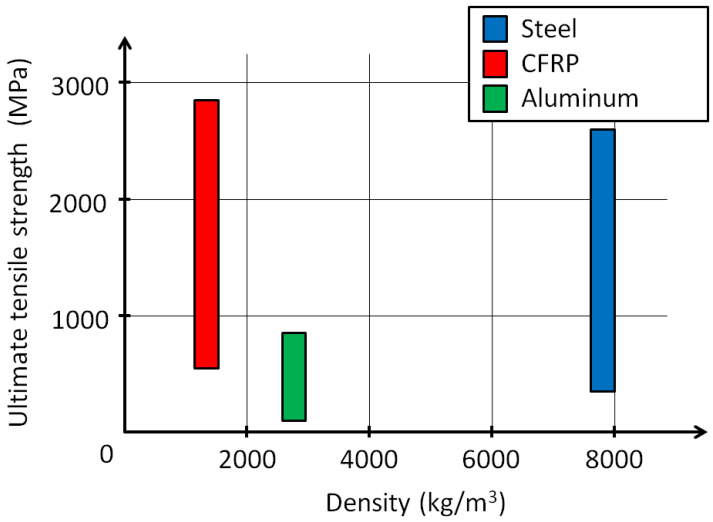

Fig. 2.1: Materials used in automotive industry [7], [8], [9]

Composite materials find their use in a variety of applications like: automotive industry, sport, aeronautic industry and shipbuilding. The figure 2.2 shows a use of composite material in wind turbine construction.

Fig. 2.2: Wind turbine [9]

Fiber composites consist of two basic parts, the fiber and the surrounding matrix. The purpose of the fibers is to transfer the tensile forces and the stresses which act on the composite, but on the other hand, they are not capable to transfer pressure or bending forces. Therefore the combination of fiber and matrix is crucial.

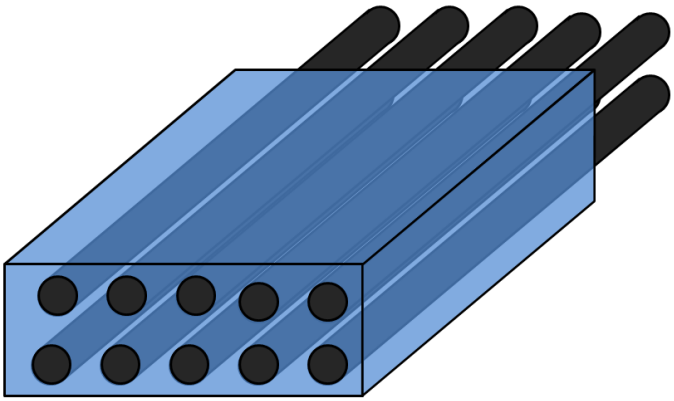

Fig. 2.3: Cut through fiber composite

The original idea of fiber composites came from nature. In nature it is possible find the perfect synergy between the fibers and the matrix. Wood is one of the most common fiber composite in the nature. The fibers in wood consist of high tensile strength cellulose and the matrix consists of light and binding lignin. In this way the nature developed a material that has a low density, but a high tensile strength [4].

Human body is also a part of the nature and therefore, it is possible to find composite materials as well within. The hip joint bone is a great proof of the ability of a bone to adapt to external conditions. In the figure 2.4 the bone trabeculae are shown. Trabeculae are microscopic tissue elements that create very small rods or beams. Trabeculae are composed of dense collagenous tissues. Trabeculae are the main reason, why bones are light, stiff and stable compared to other supporting body parts. The direction of trabeculae depends on the long term load on the bone. When a bone of a person standing the whole day on her feet and a sports athlete is compared it can be found out, that there is a big difference in the trabeculae direction. While the bones of a sport athlete have more isotropic properties and the bones of the person standing a lot has strongly anisotropic properties. [10]

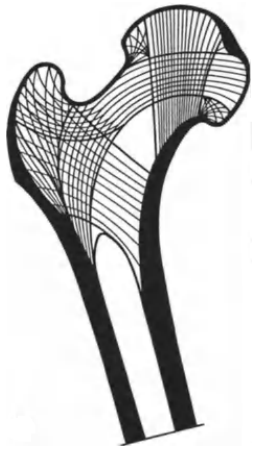

Fig. 2.4: Bone trabeculae [10]

2.1.1 Fiber

Already 3500 years ago the Egyptians discovered the use of fibers. In their times it was just a simple mixture of pieces of glass. Glass was in that time produced from milled quartz-pebble, chalk and ashes from wood. This mixture was rolled and burned and so the Egyptians produced the first artificial fiber. [11]

Fibers play an important role in composites. They change the properties of composites and give them higher strength and stiffness compared to matrix. Fibers alone are stiff and have high tensile strength, but should not be loaded by pressure or bending due to their low toughness. There is a variety of fiber types like natural fibers (hair, cotton, wool), organic fibers (carbon, aramid), anorganic fibers (glas, boron, quartz) and metallic fibers (steel, aluminum, copper).

The production of parts, which would be made of fibers without matrix, is impossible.

The fibers can be identified as long or short fibers. The composite with the long fibers have the highest mechanical properties. Depending on the application it is even possible to choose the direction of fibers with which the mechanical properties change. Almost all fibers have an elastic behavior up to the failure load. The most important fibers in mechanical engineering and their properties are shown in the table 2.1 and illustrated in the figure 2.5. Even the specific fiber types have deviations of their mechanical properties based on structure, production procedure, etc. These deviations are represented in the table by the range. [4]

Tab. 2.1: Mechanical properties of fibers [7]

Type	**Density** ($g\,cm^{-3}$)	**Young's Modulus** (GPa)	**Tensile strength** (MPa)
Alumina	3.70-3.96	370-410	1725-21000
Aramid	1.45	131-186	3400-3800
Boron	2.50	395	3450
Carbon	1.76-1.81	230-290	3100-5170
Glas	2.49-2.54	73-86	3450-4500
Graphite	1.67-2.02	390-720	1725-2070
Silica	2.19	73	5800
Tungsten	19.3	410	4140

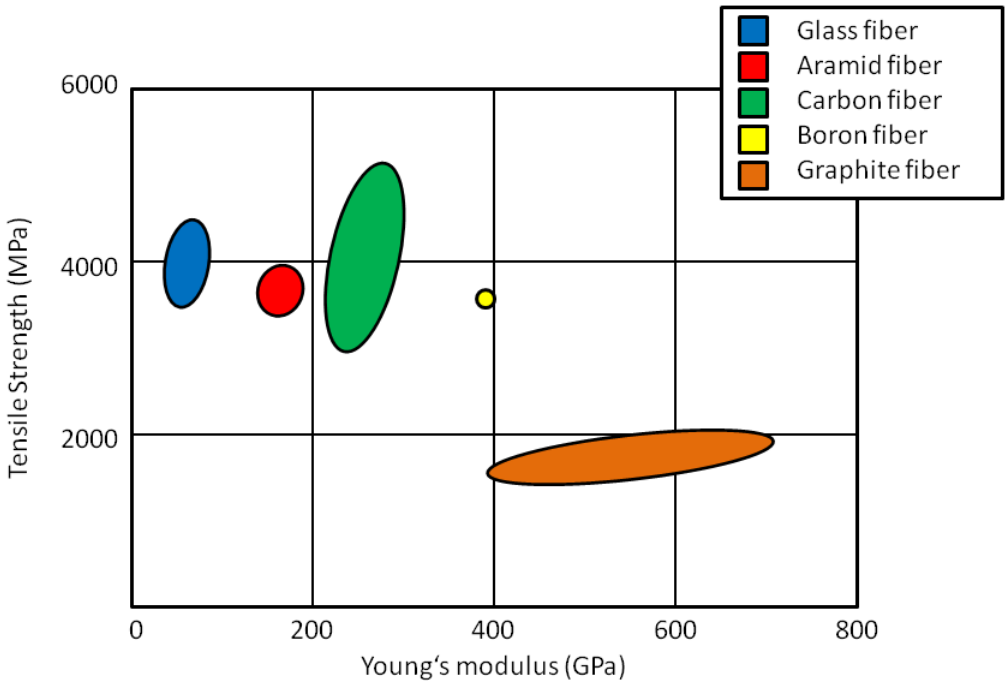

Fig. 2.5: Mechanical Properties of Fibers [7]

2.1.2 Matrix

The primary role of the matrix is to serve as a binding element. To take advantage of the mechanical properties of the composite it is necessary that the matrix fulfills certain conditions. The failure strain of the matrix must be higher than that of the fiber. The Young's modulus must be high enough to support the composite in pressure loads to avoid micro buckling. There exist a specific trade off curve for the failure strain and the Young's modulus for the matrix and therefore a compromise based on application is inevitable. The temperature resistance of matrix is lower than the temperature resistance of the fiber and limits the composite. [12]

Matrices might be produces from unsaturated polyester resins (UP), vinylester resins (VE), epoxy resins (EP), polyimyde duroplastics (PI), phenol resins (PF), polyprophylene (PP), polyamide (PA), polyethylenterephthalat (PET), polysulfide, polyetherimed (PEI), polyaryletherketone (PAEK), polyetheretherketone (PEEK), metalls, ceramics and carbon. Mechanical properties of some matrix materials are shown in table 2.2 and illustrated in the figure 2.6.

The most important one for us is the combination of carbon fiber with epoxy resin. [12]

Tab. 2.2: Mechanical properties of matrices [7]

Type	**Density** ($g\,cm^{-3}$)	**Young's Modulus** (GPa)	**Tensile strength** (MPa)
Epoxy resin	1.17-1.28	3.4-4.3	69-80
Polyester	1.1-1.5	3.2-3.5	40-90
Polyimides	1.4-1.9	3.1-4.9	70-120
Vinylester	1.15	3-4	65-90

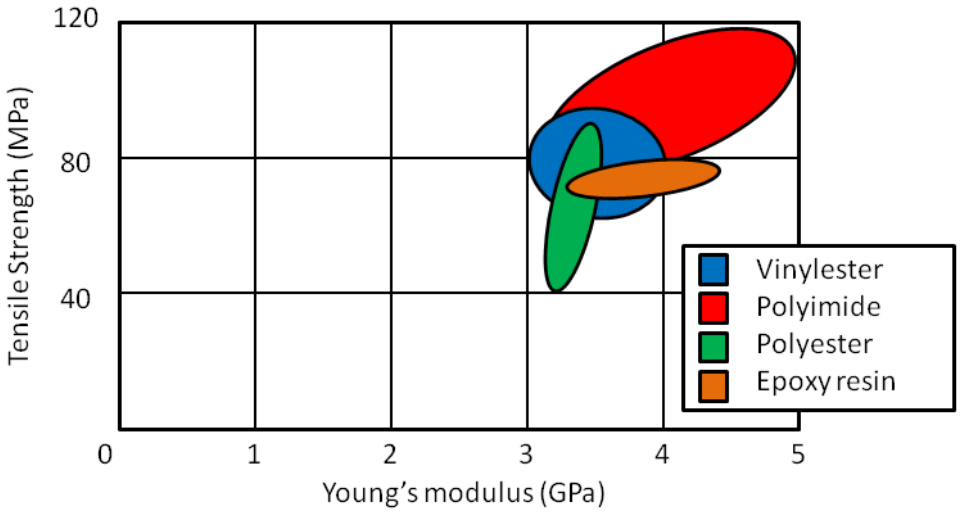

Fig. 2.6: Mechanical Properties of matrices [7]

2.2 Carbon fiber-reinforced plastic

CFRP is a composite material that contains of a matrix produced from epoxy resin and a fiber that is manufactured from carbon in one of many ways discussed below.

2.2.1 Carbon fiber

First mentions of carbon fiber come from 1879, when Thomas Alva Edison searched for a suitable filament material for his electric lamp. After many unsuccessful attempts and more than a year of work he came to the idea to burn a loop of cotton in vacuum. In

the year 1880 he patented his invention. It took up to 70 years to make carbon fiber commercially interesting. [13]

Nowadays carbon fibers are produced by three basic methods. Fabrication of carbon fibers is possible either from pitch fibers, polymer fibers or carbonaceous gases. While the fabrication of carbon fibers from pitch or polymers involves pyrolysis, the fabrication from carbonaceous gases involves catalytic growth of carbon. Most of the carbon fibers are produced from polymer precursors like rayon cellulose, polyvinylidene chloride (PVDC), polyvinyl alcohol and polyacrylonitrile (PAN) while PAN is the most common one and fabrication process is shown in figure 2.7. [3]

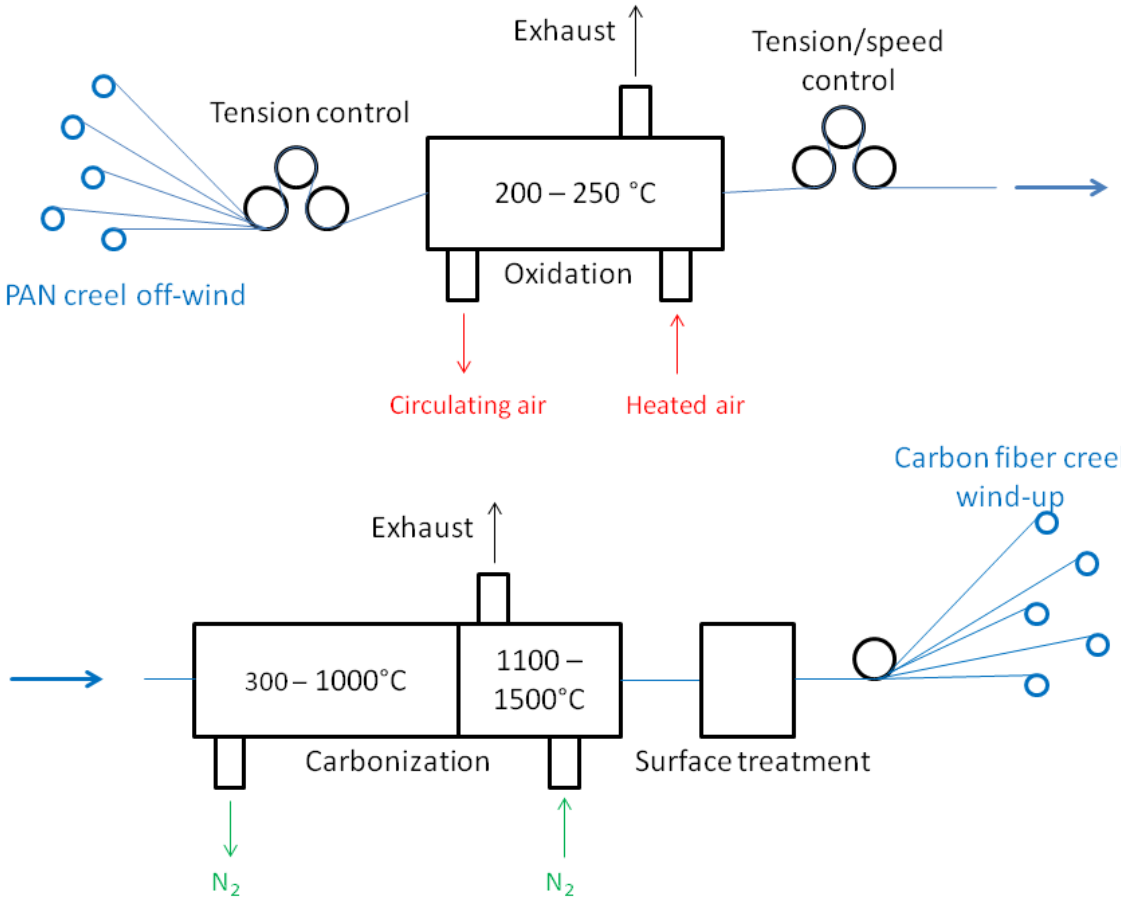

Fig. 2.7: Carbon fiber fabriction from PAN precursor [14]

2.2.2 Epoxy resin

The production of epoxy resin was patented by the company IG Farben in the year 1934. In the 40s and 50s the epoxy resin experienced a rapid increase in commercial use as a

glue of metals. Afterwards in the combination with textile glass it was possible to fabricate a material with high mechanical/dynamic properties.

Epoxy resin is a polymer that is produced through polycondensation of bisphenol A or bisphenol F or polymers which are produced by polycondensation of aliphatic or cycloaliphatic Carbon-Hydrogen bounds with Epichlorhydrin (ECH) with cleavage of hydrogen chloride.

The viscosity of epoxy resins at a room temperature is middle or high and their mechanical, dielectric and thermal properties are very good. Epoxy resins find their utilization in composite and binding technology as a matrix or glue. The basic mechanical properties are shown in table 2.2.

Epoxy resins have a wide variety of usage as for example in lightweight structure in automotive, rail, aircraft and space engineering, production of ducts and vessels used in chemistry tools, weapon technology as well as in construction engineering. They have very good corrosion properties and are therefore used in electrotechnics, electronic and tool production. [11]

2.2.3 Production of carbon fiber-reinforced thermosets

Thermosets are thermosetting resins that cure irreversibly above defined temperature. The majority of thermoset composites are produced either by lay-up, filament winding, liquid molding or pultrusion methods. Depending on the complexity, quality, material and series of the part some processes offer advantages compared with others. In the sections below two most commercially interesting methods are described. [9]

Lay-up processes

Lay-up processes are suitable for low-volume, medium or large sized parts, but the quality of the product strongly depends on the workers skills. It has to be distinguished between wet lay-up, prepreg lay-up and low temperature curing/vacuum bag prepreg lay-ups. [9]

Wet lay-up suits well for production of large parts with very low tooling costs. Therefore it is mostly used for production of prototype parts. Dry reinforcement material is placed in a form and a low viscosity resin is afterwards poured, brushed or sprayed on the reinforcement material. [9]

Prepreg lay-up involves ply cutting, ply collation or lay-up and curing. The most widely used procedure for production of high-performance, complex and high quality parts is automated ply cutting, manual ply collation and autoclave curing. [9]

Ply collation is accomplished either by hand, automated tape lying or fiber placement. Manual collation is the most labor expensive one, but in a case of prototype production it might be economical. Automated tape lying is the favorite method for flat or mildly contoured large parts. Fiber placement method is a hybrid between fiber winding and tape lying and allows to construct a complicated ply shapes. [9]

Then the laminate is sealed in a vacuum bag for curing as shown in figure 2.8. To avoid resin escape cork, silicon rubber or metal dams are used. In the first step a porous release material is placed on surface. This layer allows resin and air to escape without that the bleeder material would bond to the laminate surface. The art of bleeder depends on the laminate thickness and the desired amount of resin to be removed. Over the bleeder a inner bag made of polyester, polyvinyl fluoride or polytetraflouoroethyle (PTFE) is placed to allow the air to escape but to keep the resin in. A breather is then place over the layer. Its purpose is to allow air and volatiles to evacuate during the cure. The last layer is the vacuum bag which provides the membrane pressure necessary for the lamination process. Depending on the material of the bag it can withstand temperatures up to 350 °C. [9]

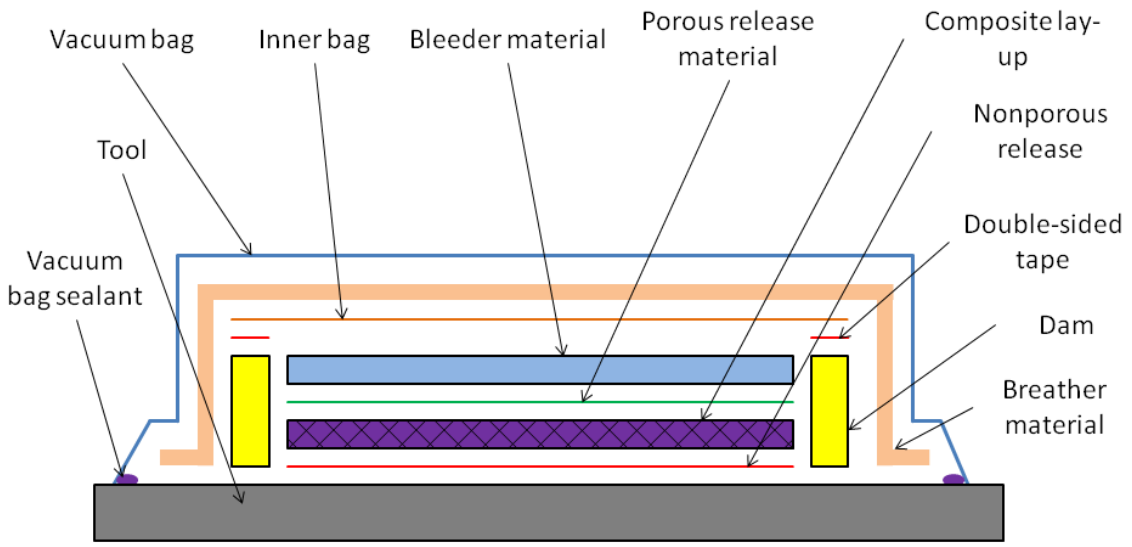

Fig. 2.8: Vacuum bagging [9]

Curing is the most important step of the whole procedure. It determines the final quality of the part. Most common curing method is autoclave curing. Autoclave evacuates the air from the vacuum bag and provides gas pressure from outside with inert gas. Almost any shape can be autoclave cured, while the only limitations are the initial expenses. A typical cure cycle is show in the figure 2.9 with two ramps. In the first ramp the semi-solid resin melts and is able to flow and escape. The second ramp polymerizes the resin and it gels into a solid. [9]

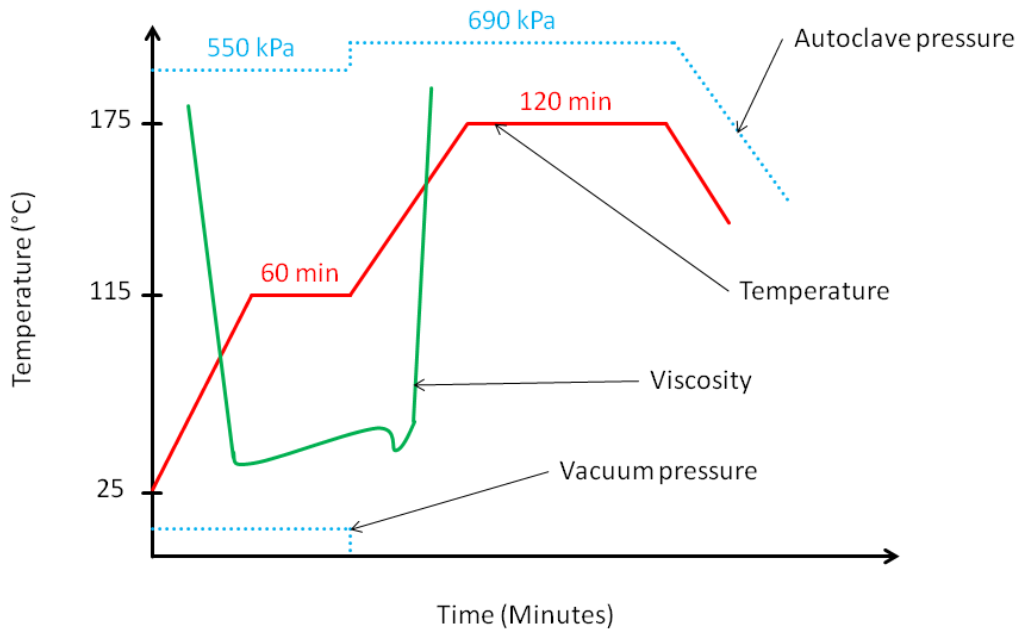

Fig. 2.9: Autoclave cure cycle [9]

Low-Temperature Curing/Vacuum Bag Systems usually use carbon fabric pre-pregs with a low-temperature curing epoxy resin. The advantages delivered by this method include tighter control of resin, avoidance of mixing error as can happen with liquid resins, higher possible fiber volume and no need for the resin to bleed during the cure process. These abilities allow to produce large parts with low tool expenses. Due to the fact that the material is supposed to cure at a lower temperature it includes reactive agents which shorten the working life of the material. [9]

Filament Winding

Filament winding is a high rate manufacturing process with a continuous fiber band. The most important limitation of this process is the geometry of the part. It is impossible to manufacture concave surfaces because in that case the fiber bridges the surface. The process includes dry fibers drawn though liquid resin bath, creating a band and winding around a mandrel. In case where hollow parts are produced the mandrel must be removable. It can be either washed-out, break-out, tapered, inflatable or it can shrink during the cool-down. [9]

2.3 Bolted Joints

To be able to combine parts produced from CFRP mostly bolted joints are chosen. Bolted joints are mechanical joints that can be disassembled and include screw and rivet joints.

Figure 2.10 shows a simple bolted joint. The bolted joints are chosen in applications where the thicknesses of the parts, which are supposed to be combined, are high. The screw and bolted joints share many similarities and therefore all design assumptions mentioned in this chapter can be applied as well to screw joints. The optimization of the bolt is not considered, because it is expected that the composite material fails before the bolt. [4]

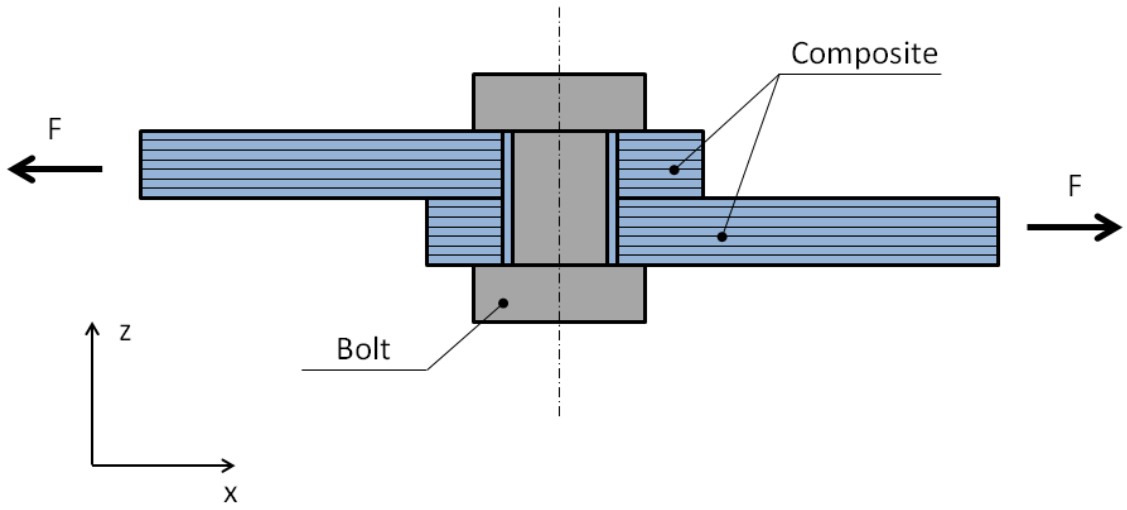

Fig. 2.10: Loaded bolted joint. F - Loading force

2.3.1 Advantages and disadvantages of bolted joints

Bolted joints are one of the basic types of joints. Depending on the application it is possible to utilize the advantages of it. However it is necessary to know and count with the disadvantages as well. The bolted joint brings with it many advantages like[4], [15]:

- possibility to combine different materials

- temporary joint

- bolts are easy and cheap to produce

- the bolted joints are easier to control visually compared with glued joints

- bolted joints are capable to absorb large portions of energy due to deformation

- no friction corrosion between CFPR plies

- there is no need to harden the joint as it is in glued joints

- combination of bolted and glued joint can elongate the lifetime of the joint significantly

- no sensitivity to surface preparation, service temperature or humidity

On the other hand there are as well some disadvantages to be considered[4]:

- due to the hole the strength of the parts that are joined is reduced

- due to the necessary overlap of the parts there is an added weight

- chemical corrosion

- punctual force transition

- the form and the shape of the bolted joint is not aerodynamically optimal

2.3.2 Failure modes

Depending on many parameters like bolt diameter, density of bolts, thickness of the joining parts, stacking sequence and others, a wide variety of failures can occur. The four basic types of failure are bearing, tension, shear and cleavage.

When a CFRP laminate and a metal bolts are combined the strength of the bolt is higher as that of the composite in most applications.

It is highly recommended to design a joint always for bearing failure of CFRP. Bearing failure is the only fail safe failure. That means that when the failure appears the hole starts to deform, but there is no separation of the material and the joint can transmit load. Therefore it is possible to control and identify a failure. In the other cases, when the failure occurs the material breaks and the joint cannot transmit any shear load. Bearing failure can as well absorb the highest amount of kinetic energy. [4], [16]

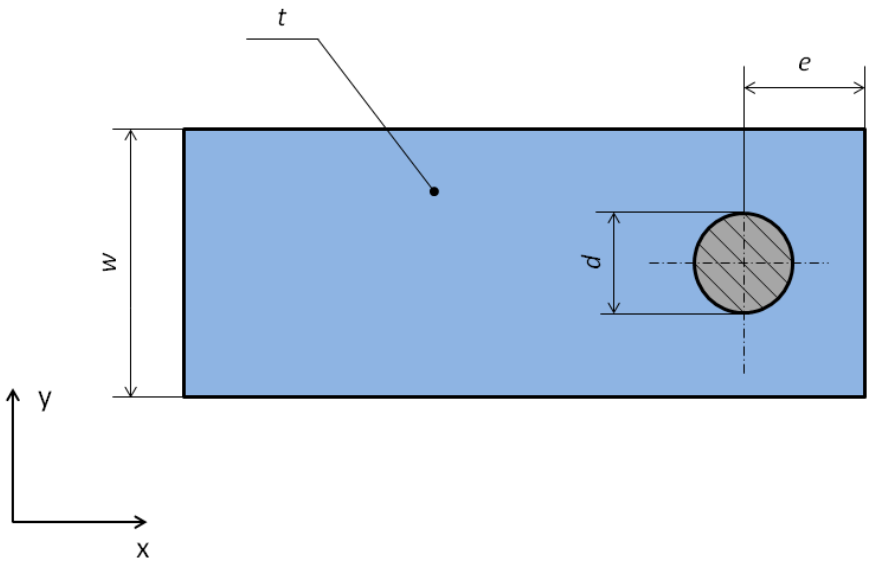

Fig. 2.11: Important dimensions of bolted joint. d - Bolt diameter, e - End or edge distance, t - Thickness, w - Width or bolt distance

Bearing failure

Bearing failure is a pressure loading failure. If a bearing failure occurs in a joint it can include few different phenomena like inter-fiber failure, delamination, compression kinking and enlargement of the hole. When the bearing strength is reached the CFRP behaves similar to elastic-plastic metals. The CFRP reduces the local stiffness through inter-fiber failure and delamination. Delamination occurs near the hole and reduces the stress concentration factor. [16]

The bearing failure force can be calculated with the equation (2.1).

$$F_u = \hat{R_B} \cdot d \cdot t \tag{2.1}$$

where

F_u – Force at bearing failure
$\hat{R_B}$ – Bearing strength of the weakest laminate

The parameters that can be optimized to improve the bearing strength are:

- bolt diameter d can be increased

- thickness t can be increased

- stacking sequence can be modified (Bearing is a pressure loading failure and the pressure strength of the CFRP increases with the amount of $0°$ plies. Due to the cylindrical form of the hole and the inclination of the force component a very high amount of 0° plies is not useful).

Some of the recommended bearing failure optimizations:

- edge distance to bolt diameter $e/d \geq 3$

- width to bolt diameter $w/d \geq 5$

- in case of high load or multiple bolts the width to bolt diameter $w/d \geq 4$.

There is a general rule for bearing failure, that says that the amount of plies with one fiber direction in laminate should never exceed 3/8 and never be lower than 1/8 [17].

Figure 2.12 shows bearing failure. The bolt is pulled through the CFRP and there is no laminate separation. The area below the curve in the force-displacement diagram represents the kinetic energy absorbed by the CFRP as shown in figure 2.13. [4]

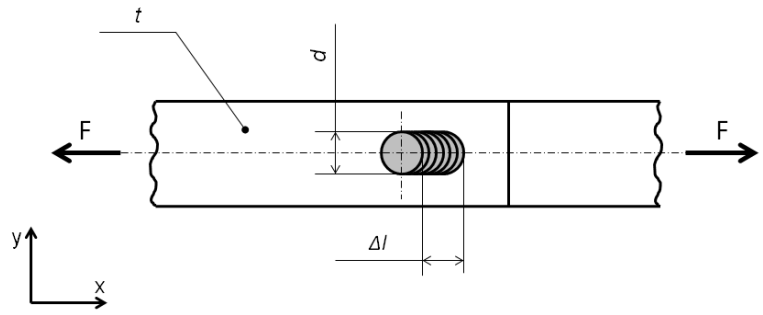

Fig. 2.12: Bearing failure. Δl - Displacement

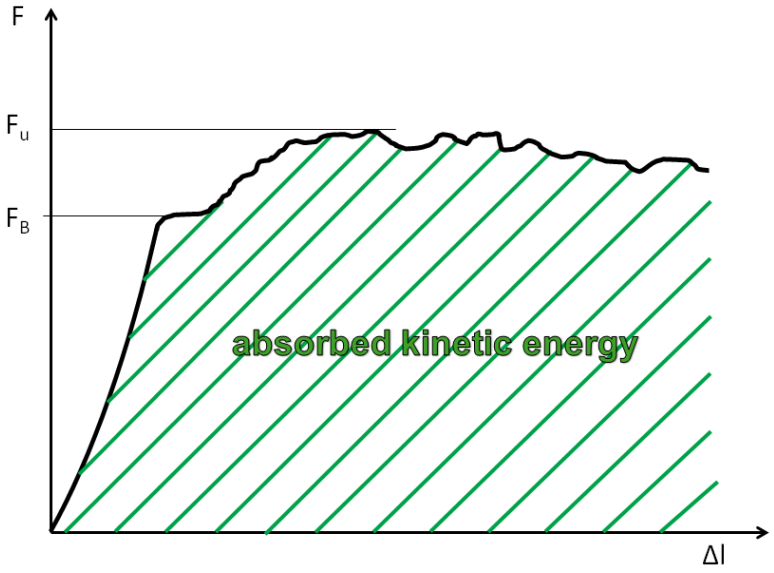

Fig. 2.13: Graph: Bearing failure. F_B - Force at the beginning of the bearing

Tensile failure

The main reason for a tensile failure is the reduction of cross-section area. Tensile failure is shown in figure 2.14.

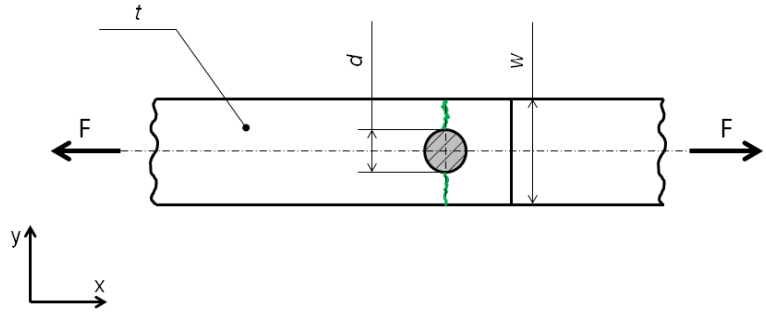

Fig. 2.14: Tensile failure

The equation (2.2) calculates the force at the tensile failure.

$$F_u = \hat{R}_x^+ \cdot (w - d) \cdot t \tag{2.2}$$

where

F_u – Force at tensile failure
$\hat{R}_x^+$ – Tensile strength of the weakest laminate in x-direction

Ways to optimize tensile failure:

- width w can be increased (empirical value used to avoid tensile failure is $w \geq 5 \cdot d$)

- thickness *t* can be increased - stacking sequence can be modified (additional 0° plies increase the tensile strength $\hat{R}_x$). [4]

Shear failure

Shear failure occurs in two cases. Either when the edge distance e of CFRP is to low or if the stacking sequence of the CFRP does not include high shear strength plies in x-direction. Figure 2.15 shows shear failure.

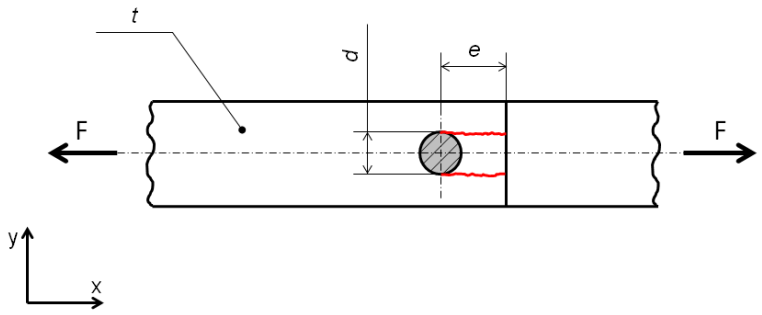

Fig. 2.15: Shear failure

The force at the shear failure can be calculated using the equation (2.3)

$$F_u = \hat{R_{xy}} \cdot 2e \cdot t \tag{2.3}$$

where

F_u – Force at shear failure
$\hat{R_{xy}}$ – Shear strength of the weakest ply in xy-direction

Possibilities to avoid shear failure include:

- edge distance e can be increase

- thickness t can be increased (empirical value used to avoid shear failure is $e \geq 3 \cdot d$)

- stacking sequence can be modified (additional $\pm 45°$ plies increase the shear strength $\hat{R_{xy}}$). [4]

Cleavage

Cleavage occurs when strength of the joining part perpendicular to the loading direction, which means in y-direction, is low. Figure 2.16 shows cleavage. This type of failure mostly appears in parts with only $0°$ plies. The force at the cleavage can be calculated using equation (2.4).

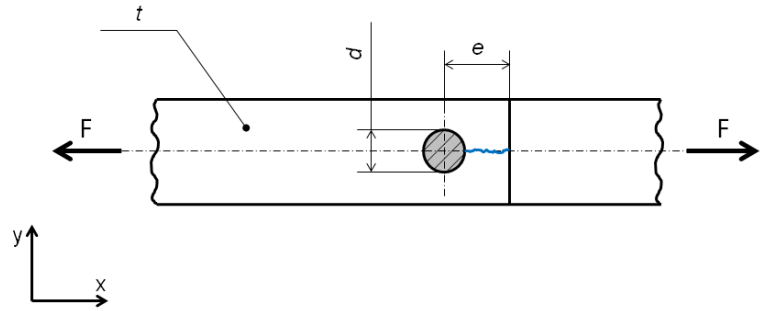

Fig. 2.16: Cleavage

$$F_u = \hat{R}_y^+ \cdot (e - \frac{d}{2}) \cdot t \tag{2.4}$$

where

F_u – Force at cleavage
$\hat{R}_y^+$ – Tensile strength of the weakest laminate in y-direction

Possibilities to optimize cleavage include[4]:

- edge distance e can be increase

- thickness of the joining parts can be increased

- stacking sequence can be modified (additional $\pm 45°$ or $90°$ plies increase the tensile strength $\hat{R}_y^+$).

2.3.3 Pretension of bolted joints

Bolted joints are designed to transmit the load through a frictional connection and positive locking. There is a linear relation between the applied torque and the load transmissible through friction. That brings advantages like:

- the pressure distribution around the hole decreases the stress on the edges, which are the crucial area for failure

- the kinking of the bolt is prevented

The pretension can bring improvements from 60 % up to 170 % of the bearing strength depending on the hole size. The pretension limit is approximately 22 MPa. Above this limit the higher pretension brings just minor improvements. [5], [18]

The equation (2.5) describes the force at bearing failure [4].

$$F_u = \hat{R_B} \cdot (d \cdot t) + \mu_0 \cdot F_V \tag{2.5}$$

where

μ_0 – Coefficient of static friction
F_V – Pretension force

2.4 Finite element analysis

Finite element analysis (FEA) is a important numerical tool that helps nowadays to solve, analyze and interpret problems in mechanics, heat transfer, acoustics, fluid mechanics and more. It splits the object of interest in a finite amount of elements with simple geometry and solves differential equations describing the local behavior. FEA consists of pre-processing, solving and post-processing. In this section only stress-strain analysis is considered. [19], [20]

2.4.1 Pre-processing

Pre-processing is the first step in numerical modeling using FE. It includes model construction, meshing, specification of material properties and specification of boundary, initial and loading conditions.

Model construction

Model construction enables to create even a complex structure with help of simple elements like points, nodes, lines, curve, surfaces and volumes. Figure 2.17 illustrates a simple component constructed by a pre-processing software.

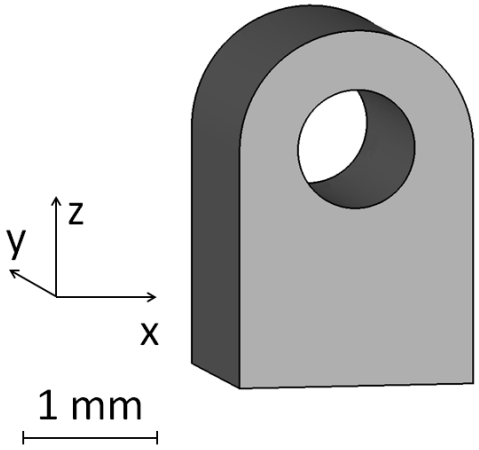

Fig. 2.17: Constructed component

Meshing

Meshing is the second phase of pre-processing which is often also called discretization. Meshing splits the structure into a finite amount of simple elements. The accuracy of the structure is defined by the size of elements. The higher the amount of elements that describes the structure the smaller they can be and can describe the complex surface better. On the other hand the higher amount of element increases the computational costs. Therefore a compromise is necessary.

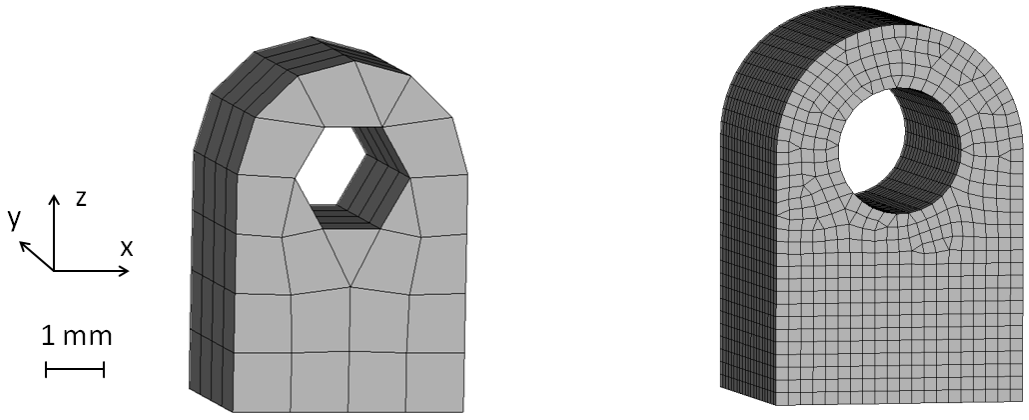

(a) Coarse mesh (b) Fine mesh

Fig. 2.18: Geometry meshing

Definition of material and medium properties

The next step in the procedure defines the properties of involved materials. It is possible to define properties to either a group of elements or to a single element. Properties that can be defined in mechanical problems excluding the effect of heat include: Young's modulus, shear modulus, density, Poisson's ratio, strengths and many more depending on the type of material.

Definition of boundary, initial and loading conditions

The definition of boundary, initial and loading conditions is the last step of pre-processing. The basic types of conditions include displacements, accelerations, velocities, forces, moments, stresses, pressures, temperatures, heat fluxes and so on.

Figure 2.19 illustrates the definition of boundary, initial and loading conditions. The arrows represent the loading force acting on specified nodes and the triangles represent a nodal constraint.

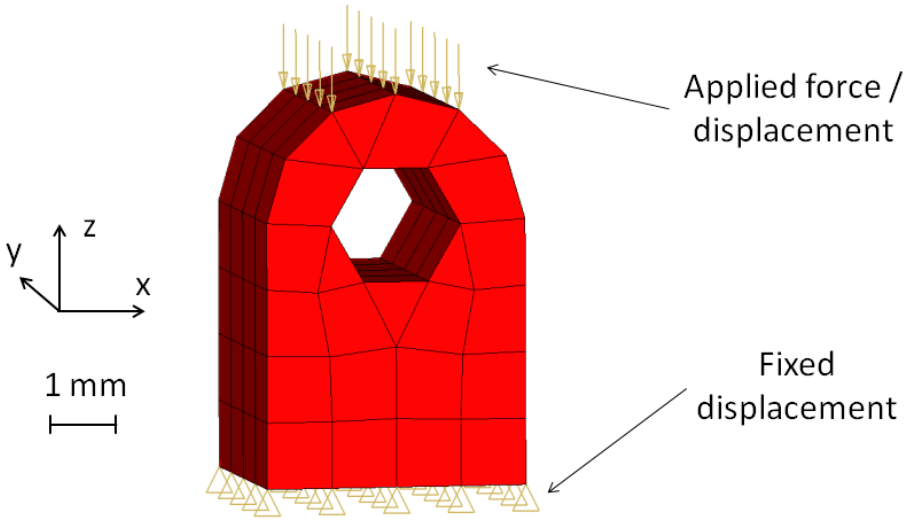

Fig. 2.19: Boundary conditions

2.4.2 Processing

Processing is the core process of a FEA. It is done with help of FEM. FEM is a numerical method which approximates the result of a problem in which it is very difficult or impossible to achieve results by closed analytical procedure. This is done in displacement assumption for each element. From this assumption an element equation is obtained. All elements together form global finite element equation for the whole system [19], [20].

2.4.3 Post-processing

Post-processing includes the processes which are done after the solver has finished. As a result of the solving process a big amount of data is obtained. To be able to analyze, interpret and present this data visualization is used. In the figures 2.20 - 2.22 results of a simple solid from figure 2.19 is displayed. The nodes of the solid are fixed on the bottom in translation but can rotate. The nodes on the top of the solid have predefined translation in z-direction. The stresses in the z-direction σ_{zz} are shown at different time steps.

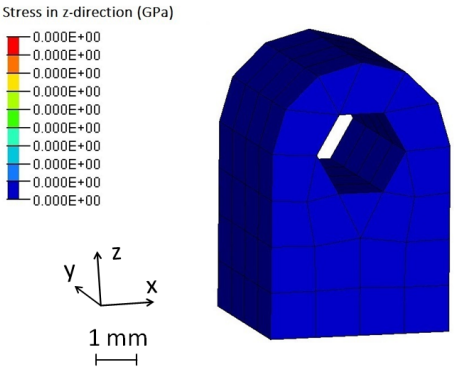

Fig. 2.20: Stress in z-direction at 0 % time

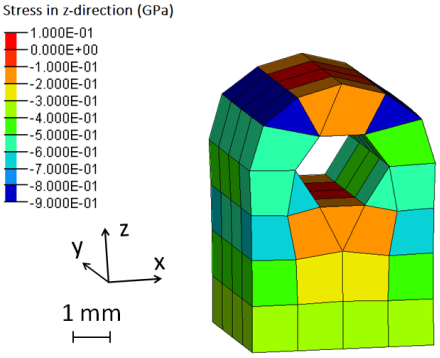

Fig. 2.21: Stress in z-direction at 50 % time

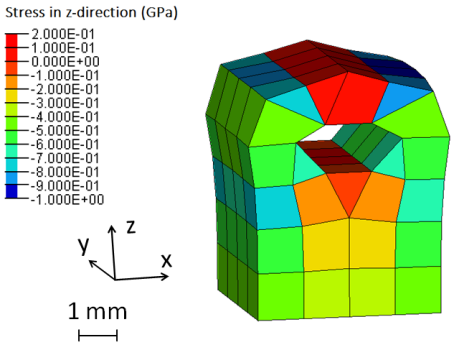

Fig. 2.22: Stress in z-direction at 100 %

3 Simulation of carbon fiber-reinforced plastic

In this chapter simulation of mechanical behavior of carbon fiber-reinforced plastic is described. This chapter takes a closer look to phenomena in CFRP and the various simulation capabilities of different material types.

3.1 Simulation tools

In this thesis all simulations were solved by $PAM - CRASH\ 64 - Bit\ Solvers\ 2013.0$ from ESI Group. Pre-processing and post-processing was done by $Hyperworks\ 11.0$ and 12.0 from Altair.

3.2 Material types

In this work three material types were used: Standard material type 30 and 131 and user-material type 81.

Material type 30 is unidirectional composite bi-phase material for solid elements [21].

User-material type 81 is a user defined material type. The number in 81 in this case is just a free slot in the software used for user-defined material types [22].

Material type 131 is multilayered shell element material type. All their abilities are going to be explained in following chapters [21].

3.3 Anisotropic material

Anisotropic material as opposed to isotropic material has got different material properties in different directions. As known isotropic material like steel have Young's modulus, Poisson's ratio, Shear modulus, ultimate strength, etc. identical in all directions. In case of anisotropic, for example CFRP, these properties depend on the materials of the fibers and the matrix, on the volume of fibers and the direction of fibers. Table 3.1 shows an example of construction steel S355 and unidirectional CFRP(AS4/3501-6).

Tab. 3.1: Mechanical properties of isotropic and anisotropic materials [7], [23], [24]

Mechanical Properties	**Steel S355**	**CFRP (AS4/3501-6)**
Density (kg m^{-3})	7840	1600
Longitudinal modulus E_1 (GPa)	210	147
Transverse modulus E_2 (GPa)		10.3
Major Poisson's ratio ν_{12}	0.3	0.27
Minor Poisson's ratio ν_{21}		0.02
Longitudinal tensile strength F_{1t} (MPa)	295	2280
Transverse tensile strenght F_{2t} (MPa)		57

These anisotropic properties are defined in the simulation in a way that the values for various mechanical properties like Young's modulus, Poisson's ratio and others in multiple directions are prescribed.

3.4 CFRP failure criteria in PAM-CRASH

Depending on the load specific failure may be considered. The basic failures which are considered in $PAM-CRASH$ in CFRP are fiber failure, inter-fiber failure and delamination.

3.4.1 Fiber failure

Theory

Fiber failure occurs mainly due to the stress parallel to the fiber direction σ_1 and fractures the fibers. This approach describes fiber failure in tension as in equation (3.1) and in compression as in equation (3.2). [25], [4]

$$f_{E,FF} = \frac{\sigma_1}{R_1^+} \qquad \text{if} \qquad \sigma_1 \geq 0 \tag{3.1}$$

$$f_{E,FF} = \left| \frac{\sigma_1}{-R_1^-} \right| \qquad \text{if} \qquad \sigma_1 < 0 \tag{3.2}$$

where

$f_{E,FF}$ – Fiber failure stress exposure
σ_1 – Stress in the fiber direction
R_1^+ – Tensile strength in fiber direction
R_1^- – Compression strength in fiber direction

If the fiber failure stress exposure $f_{E,FF}$ reaches the value one fiber failure occurs. The compression strength of fiber has a minus because the strengths only have positive values and the stress σ_1 provided by compression has got a negative value.

However for more precise calculation the contribution of the stresses perpendicular to the fiber direction σ_2 and σ_3 to the stress in fiber direction σ_1 must be taken in consideration. The more sophisticated criterions exceed the scope of this master thesis.

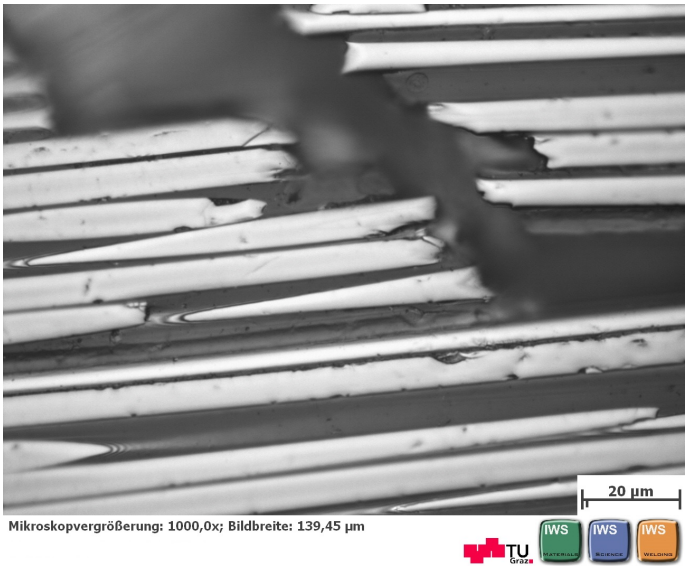

Fig. 3.1: Fiber failure

Simulation of fiber failure

Formulation of the fiber failure alters depending on the material type.

Material type 30 does not use specific condition for fiber failure in this thesis. Therefore in this thesis fiber failure is simulated with the help of damage curves also called damage curves.[21] The reason for not using the specific condition is the possibility to compare standard material types together in a better way with similar conditions.

Damage curves are prescribed curves which alter the Young's modulus and the shear modulus in all three direction depending on either volumetric or shear strain. To define the damage curve as shown in figure 3.2 it is necessary to specify either a function for the curve or three points on the curve. For three point it is valid that in the region between ϵ = 0 and ϵ_i the damage value is 0. Between points ϵ_i and ϵ_1 the damage value grows linear to the defined value. The same is valid for the next region which is ϵ_1 up to ϵ_u after this point the damage curve starts to grow asymptotically to the value of 1. [21]

Volumetric and shear strains are defined in the equation (3.3) and equation (3.4) [21].

$$\epsilon_v = \epsilon_{kk} \tag{3.3}$$

where

ϵ_v – Volumetric strain
ϵ_{kk} – Trace of the total tensor. For fiber phase: $\epsilon_{kk} = \epsilon^f$

$$\epsilon_s = [(1/2)\, e_{ij} e_{ij}]^2 \quad \text{with} \quad e_{ij} = \epsilon_{ij} - (1/3)\epsilon_{kk}\delta_{ij} \tag{3.4}$$

where

e_{ij} – component of deviatoric strain tensor

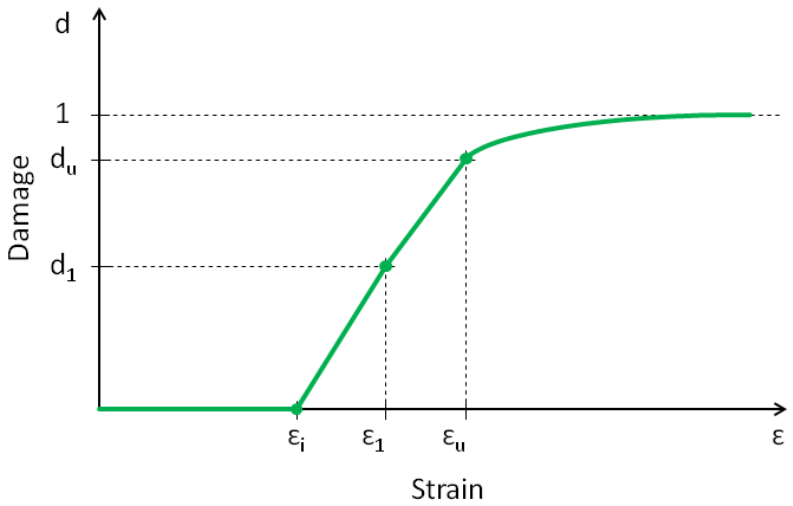

Fig. 3.2: Damage-Strain curve. d - Damage, d_u - Ultimate damage, d_1 - Intermediate damage, ϵ - Strain, ϵ_u - Ultimate strain, ϵ_1 - Intermediate strain, ϵ_i - Initial strain

When the damage curve is defined it is possible to calculate the residual Young's modulus after the damage with help of equation (3.5). The result is illustrated in figure 3.3.

$$E(\epsilon) = (1 - d(\epsilon))E_0 \tag{3.5}$$

where

E – elastic modulus
E_0 – initial elastic modulus

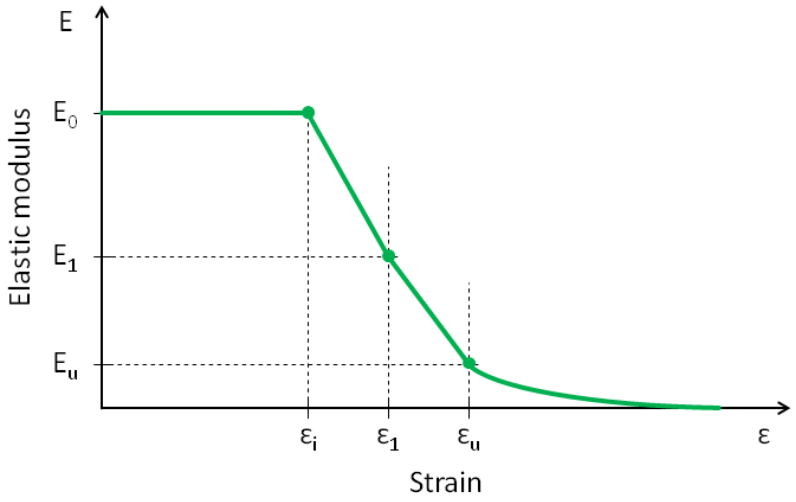

Fig. 3.3: Elastic modulus-Strain curve. E_1 - Intermediate elastic modulus, E_u - Ultimate elastic modulus

User-material type 81 is a user defined material type which works with the fiber fracture criterion as defined in equation (3.1) and (3.2) which means that if the ultimate strength in the specific direction is reached fiber failure occurs. The user material type allows to directly prescribe the ultimate strength values for each lamina. [22]

Material type 131 is a standard shell material type for multilayered structures. This material allows to define fiber failure criterion for each ply with help of Yamada Sun model which is defined by equations (3.6) and (3.7). If the variable e reaches the value 1 fiber failure occurs. In our case the values for R_{12}^+ and R_{13}^+ are set to zero because the $Puck's$ fiber failure criterion is used. As a result of R_{12}^+ and R_{13}^+ beeing zero the same equation as in (3.1) or (3.2) is obtained. [21]

$$e = \sqrt{\left(\frac{\sigma_1}{R_1^+}\right)^2 + \left(\frac{\tau_{12}}{R_{12}^+}\right)^2 + \left(\frac{\tau_{13}}{R_{13}^+}\right)^2} \qquad \text{if} \qquad \sigma_1 > 0 \tag{3.6}$$

$$e = \sqrt{\left(\frac{\sigma_1}{R_1^-}\right)^2 + \left(\frac{\tau_{12}}{R_{12}^-}\right)^2 + \left(\frac{\tau_{13}}{R_{13}^-}\right)^2} \qquad \text{if} \qquad \sigma_1 < 0 \tag{3.7}$$

where

e – Fiber failure value
τ_{12} – Shear stress in the plane 23 acting in the 2-direction
τ_{13} – Shear stress in the plane 23 acting in the positive 3-direction
R_{12}^+ – Maximum for shear stress in the plane 23 acting in the positive 2-direction
R_{12}^- – Maximum for shear stress in the plane 23 acting in the negative 2-direction
R_{13}^+ – Maximum for shear stress in the plane 23 acting in the positive 3-direction
R_{13}^- – Maximum for shear stress in the plane 23 acting in the negative 3-direction

3.4.2 Inter-fiber failure

Theory

Inter-fiber failure is a type of failure phenomena in which the failure occurs in the matrix while the fibers do not fracture.

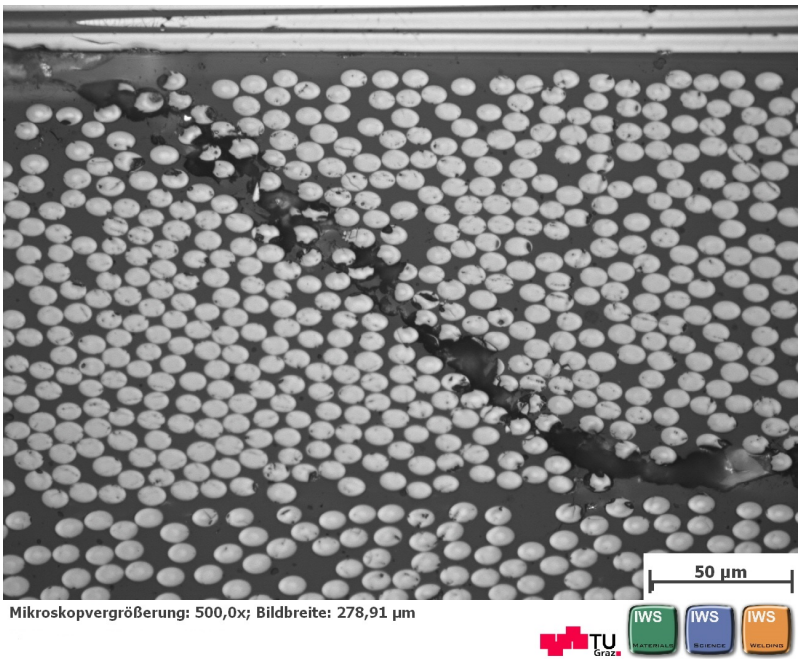

Fig. 3.4: Inter-fiber failure

According to $Puck$ three basic modes of inter-fiber failure can be distinguished as shown in figure 3.5.

Mode A is obtained if the tensile stresses perpendicular to the fiber direction are much higher than the shear stresses. If the compression stresses are small and the shear stresses are larger than mode B occurs, however after a specific limit for $R_{2\perp}^{-}$ is reached Mode C is reached. [25]

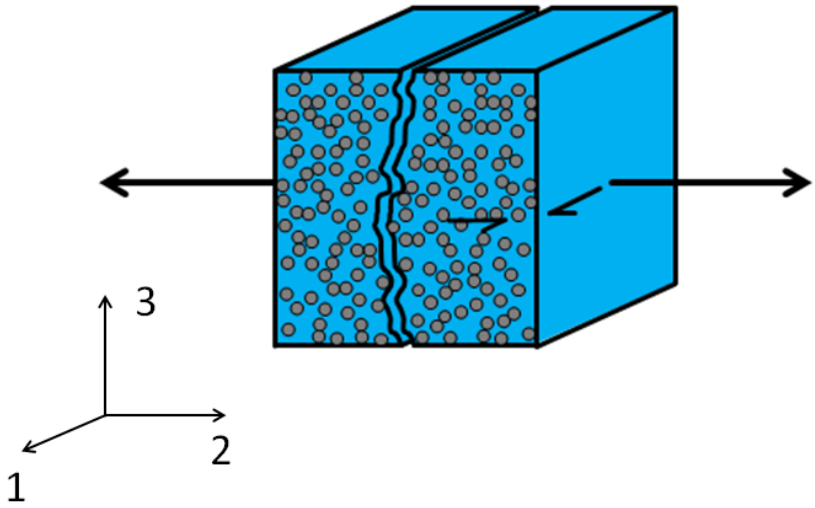

(a) Mode A

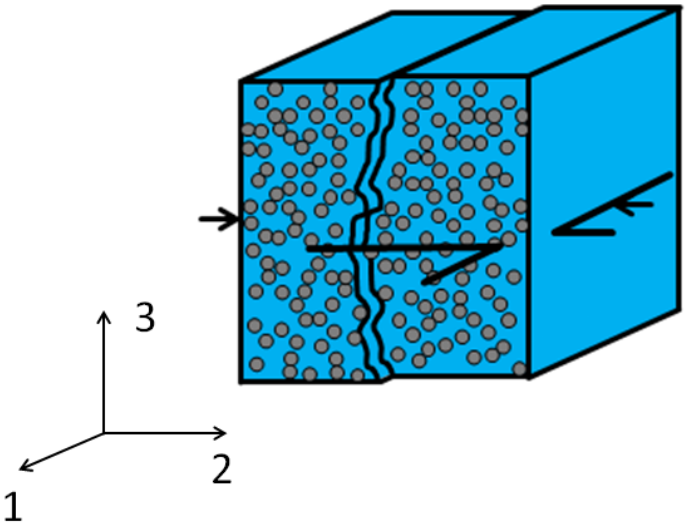

(b) Mode B

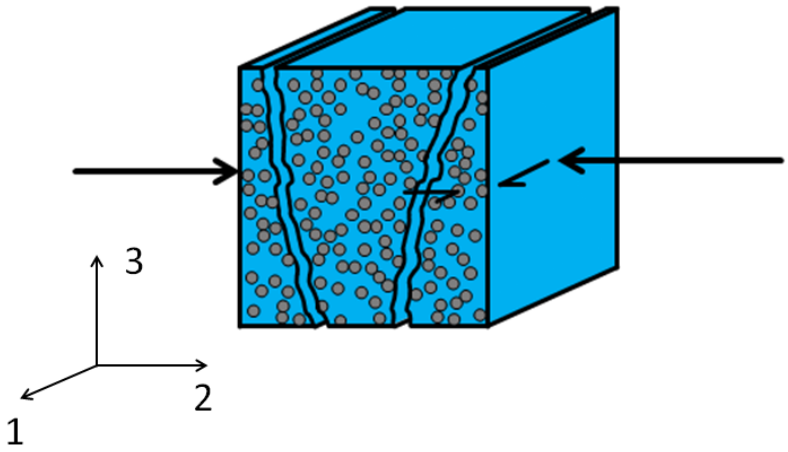

(c) Mode C

Fig. 3.5: Inter-fiber failure modes according to $Puck$ [25]

The fracture curve shown in figure 3.5 prescribes the strength limits for each of the modes in one figure and therefore makes it easier to imagine. The 2D State of stress illustrated in figure 3.6 helps to understand the terms in figure 3.5.

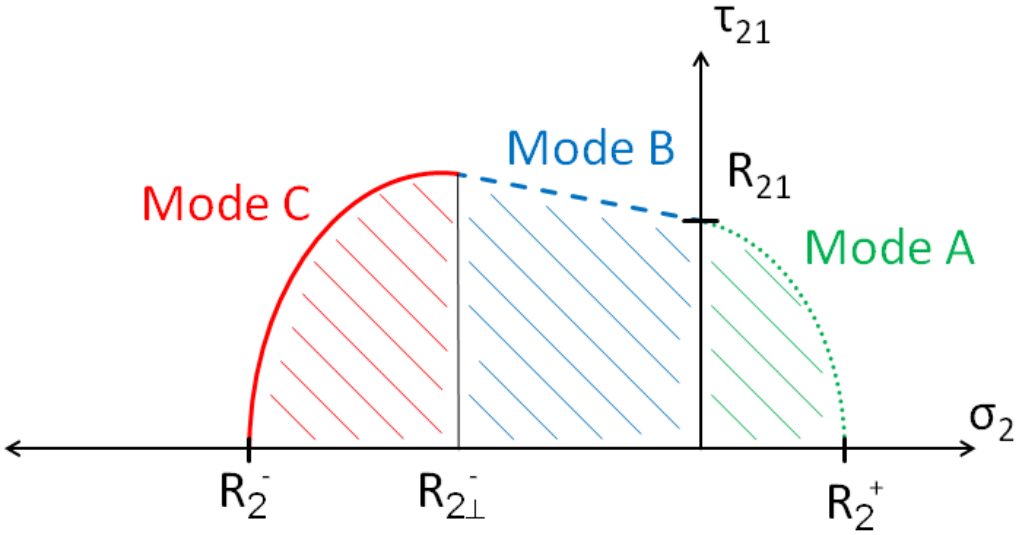

Fig. 3.5: Fracture curve for inter-fiber failure. τ_{21} - Shear stress in the x_1-x_3 plane acting in the fiber direction, σ_2 - Stress in the 2-direction, R_{21} - Shear strength of the shear stress τ_{21}, R_2^+ - Tensile strength in the /mbox2-direction, R_2^- - Compression strength in the 2-direction, $R_{2\perp}^-$ - Compression strength in the direction transverse to the fiber direction

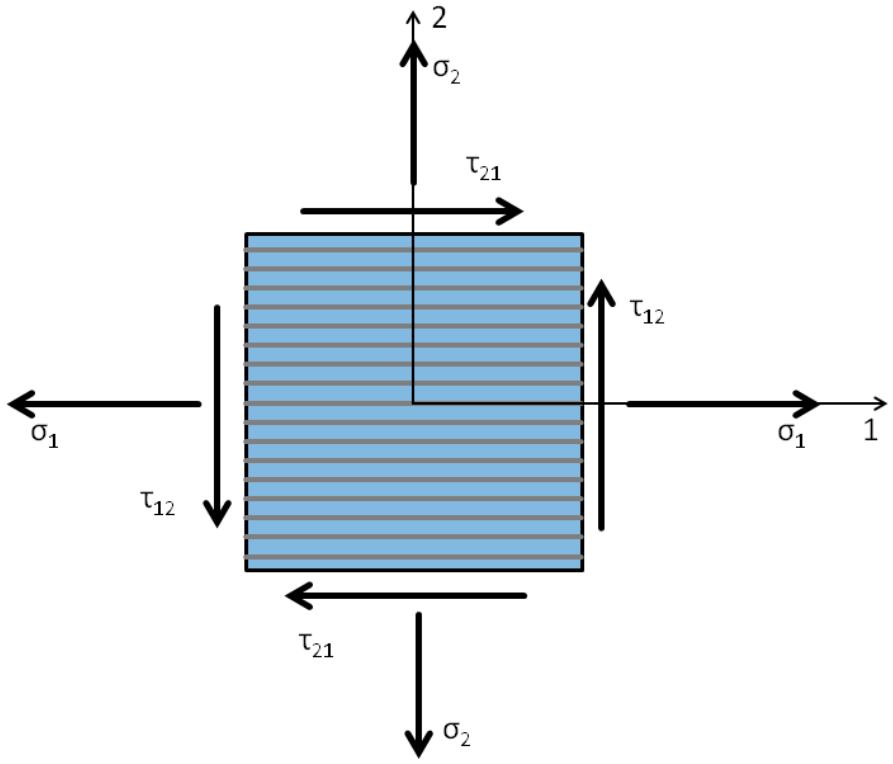

Fig. 3.6: 2D State of Stress. 1 - Fiber direction, 2 - Direction perpendicular to fiber direction

$Puck's$ hypotheses for inter-fiber failure:

1. Inter-fiber failure on a plane parallel to the fibers is caused by the stresses σ_n, τ_{nt} and τ_{n1} acting on the fracture plane.
2. If σ_n is a tensile stress it promotes fracture together with the shear stresses τ_{nt} and τ_{n1} or even alone. In contrast to that σ_n impedes fracture if it is a compressive stress by raising the fracture resistance of the fracture plane against shear fracture with increasing compressive stress σ_n. [25]

The raising fracture resistance in a 2D case is clearly visible in the left part of the figure 3.5.

According to the theory of $Puck$ the mode of failure depends on the stresses σ_n, τ_{nt} and τ_{n1} acting on the fracture plane. Fracture plane is the plane in which fracture occurs. Action plane is the plane in which the forces act. Between these two planes an angle θ_{fp} described as angle of the fracture plane exists. This angle varies strongly depending on the stresses σ_n, τ_{nt} and τ_{n1}. For a better understanding the stresses are displayed in the figure 3.7. [25]

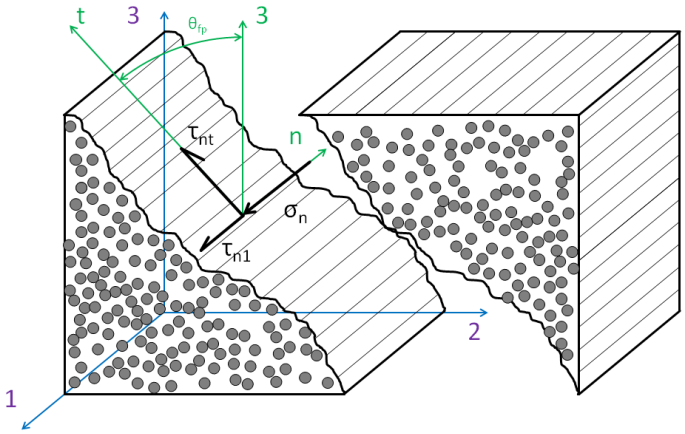

Fig. 3.7: Coordinate systems and the fracture plane. 3 - Coordinate perpendicular to coordinates 1 and 2, n - Coordinate normal to the fracture plane, t - Transversal coordinate, σ_n - Stress normal to the fracture plane, τ_{nt} - Shear stress acting on the fracture plane in the transverse direction, τ_{n1} - Shear stress acting on the fracture plane in the fiber direction, θ_{fp} - Angle between the fracture and action plane

Simulation of inter-fiber failure

Material type 30 does not allow to explicitly define criterions for inter-fiber failure and therefore it must be implemented in the damage curves based on the volumetric and shear strain as for fiber failure mention in subsection 3.4.1, page 36.

User-material type 81 allows to fully design the inter-fiber failure criterion according to the theory of $Puck$. With a number of variables which can be defined it is possible to fully adjust the failure curve as shown in figure 3.5 for 3D inter-fiber failure in agreement with the needs. This material type allows also to display the exact inter-fiber failure mode for each element for a better understanding and analysis of results. [22]

Material type 131 allows as well to fully design the inter-fiber failure criterion of $2DPuck'scriterion$ with the help of user defined parameters.

3.4.3 Delamination

Theory

Delamination is an inter-laminar failure which separates the laminas from each other. The reason for this failure is the weakness of the areas where the laminas are joined together. The weakness exists due to the lack of reinforcement in that region. Delamination is mainly caused by the stresses σ_3, τ_{13} and τ_{23}, where the stress σ_3 must be positive.

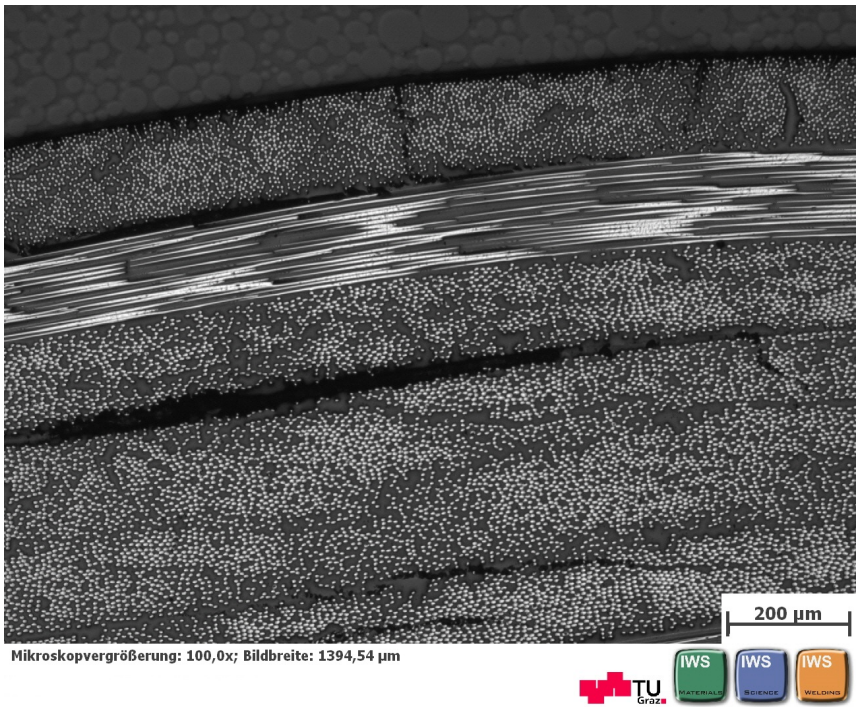

Fig. 3.8: Delamination

There are three basic configurations of delamination depending on the direction in which the laminate is loaded. It can distinguish between mode I (opening), mode II (shear) and mode III (tearing) which are illustrated in figure 3.9 [26].

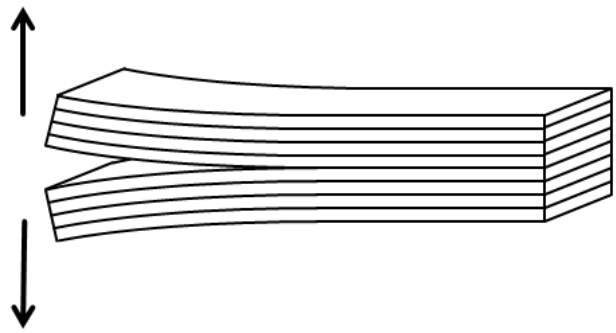

(a) Mode I

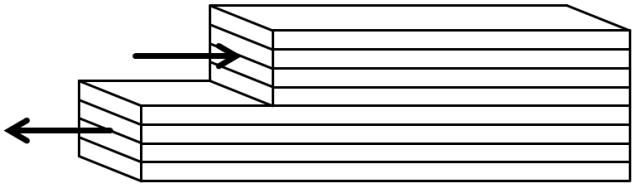

(b) Mode II

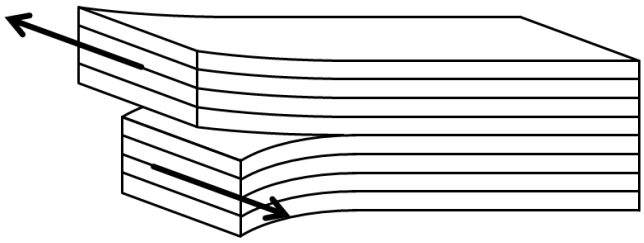

(c) Mode III

Fig. 3.9: Delamination modes

Simulation of delamination

In this thesis all the simulation were calculated without the consideration of delamination. The reason is that with the delamination the work would go beyond the its scope. An excessive study in this field was done by [26].

3.4.4 Damage

Theory

It is always necessary to investigate the damage of the laminate. The first cracks appear in the areas with the highest strain between the fibers. Due to the crack appearance, propagation and creation of more cracks the stresses have to be redistributed and the stress strain development of the whole laminate becomes non-linear degressive. [4]

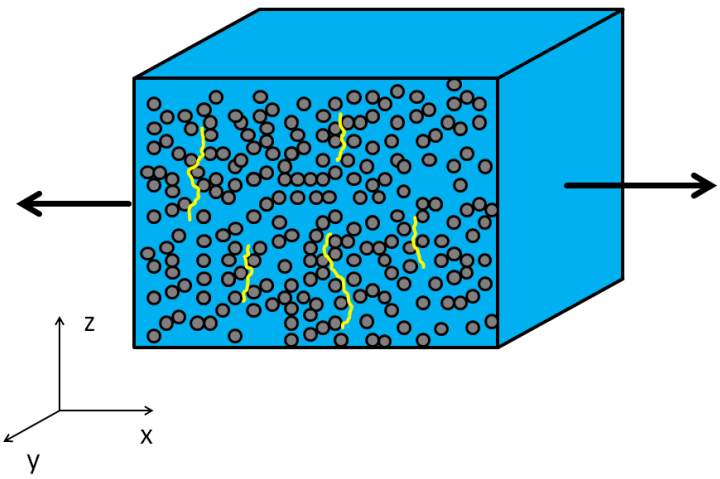

Fig. 3.9: Damage

Damage simulation

Material type 30 does have a possibility to define a damage curve as mentioned in subsection 3.4.1. In this thesis the damage curve was used to design the fiber and inter-fiber failure. Due to the interaction between these phenomena it is not possible to simulate all failure types with one curve.

User-material type 81 allow to simulate the damage according to an assumption [27] defined in in the way, that when the stress reaches a specific value, which can be defined, the stress remains constant even when the strain does not and therefore the Young's and shear modulus have to be reduced asymptotically as shown in figure 3.10 and figure 3.11 [27], [22].

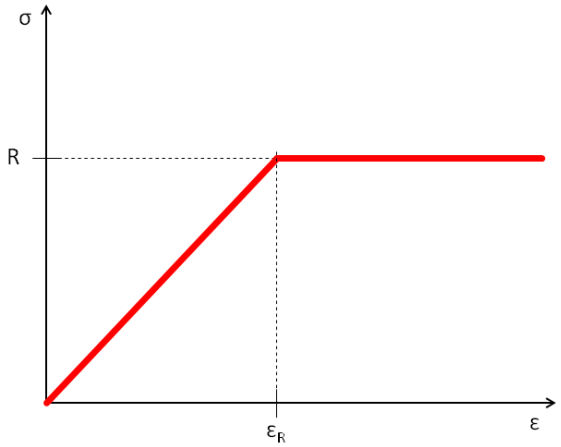

Fig. 3.10: Assumed damage curve for user-material type 81. σ - Stress, R - Strength, ϵ_R - Strain at strength level

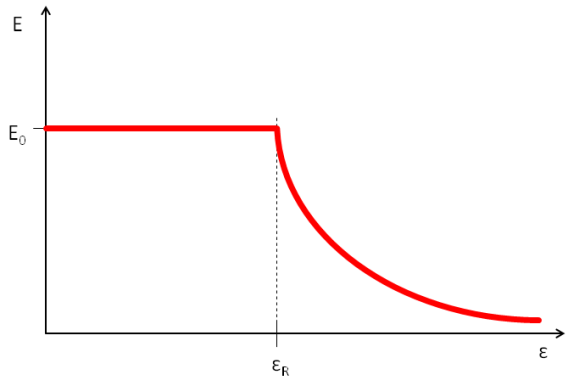

Fig. 3.11: Young's modulus reduction depending on damage for user-material type 81

Material type 131 is capable to portray damage of the material with damage curves. Preliminary simulations have shown a strong interconnection between the $Puck's\ inter-fiber$

$failure\ criterion$ and the damage. This is one of the reasons why damage is excluded from this model. The other reason is that it concentrates on the fundamental comparison of material type and therefore the base for the standard material would not be the same, because material type 30 would not simulate the damage and material type 131 would. [21]

3.4.5 Element elimination

In reality specimens are continuums. In a case of a loading the specimen start to crack in the weakest part and the crack propagates till it comes to a material separation.

In the simulation this phenomenon is displayed and simulated differently. In the simulation continuum is transformed in an object with finite amount of elements which are hold together by common nodes. A crack cannot be simulated in a way that just two nodes out from one are created and propagate such a created crack. The simulation is done by element elimination which under fulfillment of certain conditions removes an element and a crack appears. Conditions for element elimination alter with the material type.

Material type 30 includes a very simple condition for the element elimination. It is just necessary to set a value for volumetric strain and if the strain is reached an element is removed. Due to the nature of the damage which is supposed to simulate failures, the setting of the element elimination condition plays only a minor role. This is due to the fact that the damage occurs always first and after the damage the volumetric strain increases rapidly and reaches almost immediately after the damage condition for element elimination. [21]

User-material type 81 has got multiple conditions to a better determination and simulation of the failure. These conditions are explained in [28].

Material type 131 uses a simple condition as well. If the fiber failure occurs no matter in what state the element is removed [21].

4 Model setup and material type validation

To present the real advantages of the simulation it is necessary to compare the results with experimental test with the same initial conditions. As a reference point the study from *T. A. Collings* was chosen. He presents in his study [5] experiments, where he tried to determine the different conditions, which predict certain type of failure mode of double lap bolted joints. As mentioned in the subsection 2.3.2 on page 25 there are four basic failure modes.

4.1 Testing facility

The testing facility used in the study is represented in figure 4.1. The tensile test device consist of machine head, pin jointed loading head, pins, loading lugs, bolted screw for lateral constraint and a shear pin.

In the simulation some simplification are applied. They do not affect the results significantly. Considering that the whole testing facility with the CFRP specimen is symmetrical, it was possible to save computational time by just simulating the half of the facility. The other simplification involves the components of the testing facility. As a result of the fact that the deflection of steel compared to CFRP specimen is minor and not important it was decided to remove the test machine head, the pin joined loading head and the pin. With this idea it was possible to save another computational time. As a material for the steel loading lugs standard structural steel S355 was used. The model used in the simulations is shown in figure 4.2

The loading lugs have small raised pads which are equivalent to standard washer to control the clamping area around the loaded hole. The lateral constrain had a value of 22 MPa. The edge of the loading lugs is moved with a movement prescription and the edge of the CFRP specimen is fixed in x-direction. [5]

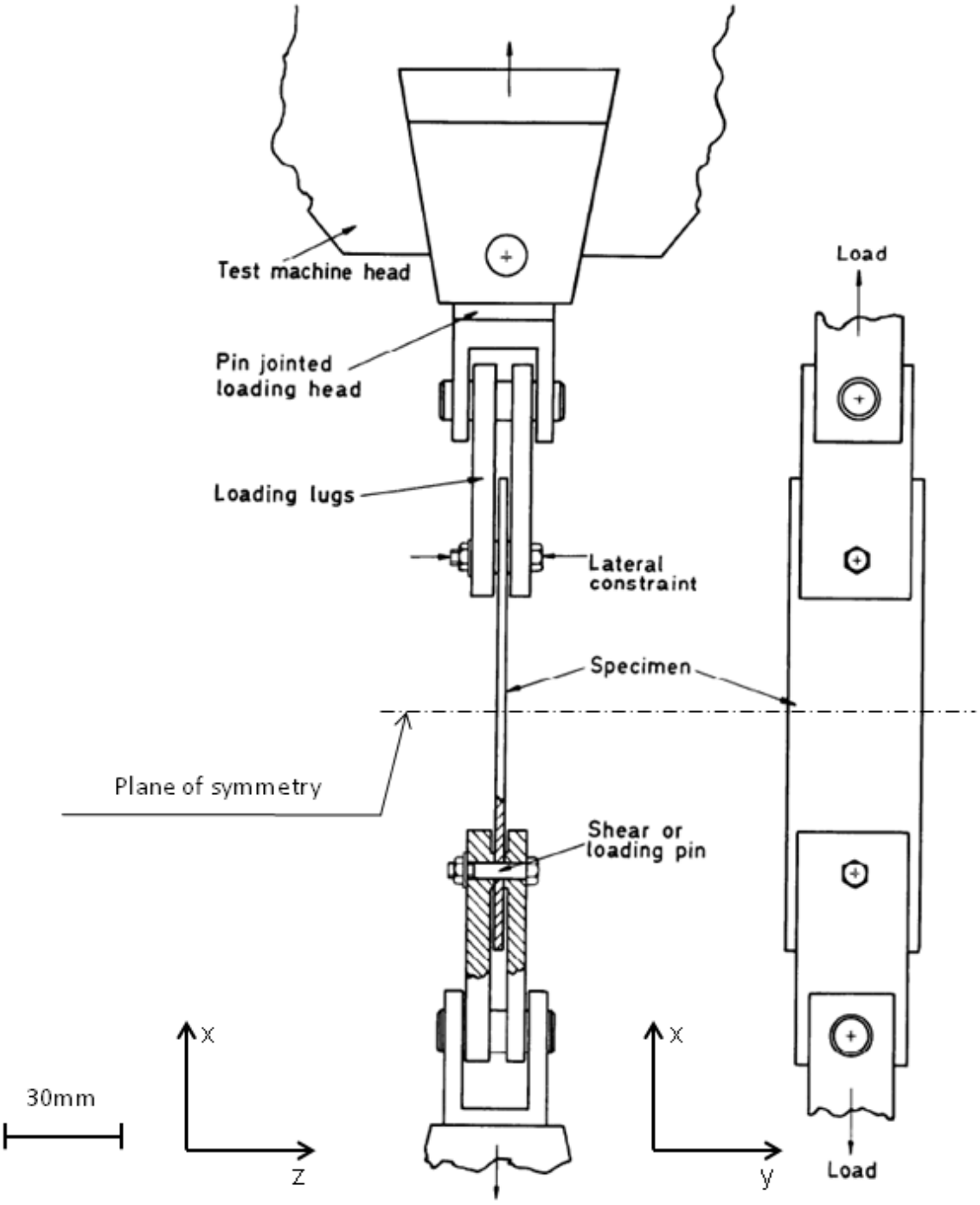

Fig. 4.1: Real testing facility [5]

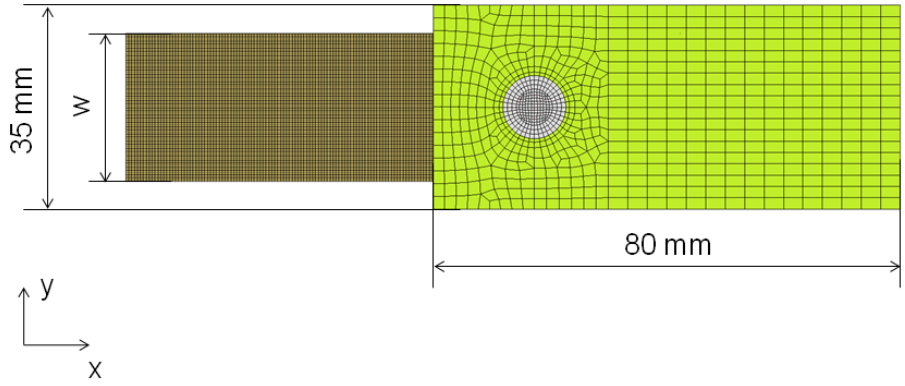

(a) Top view

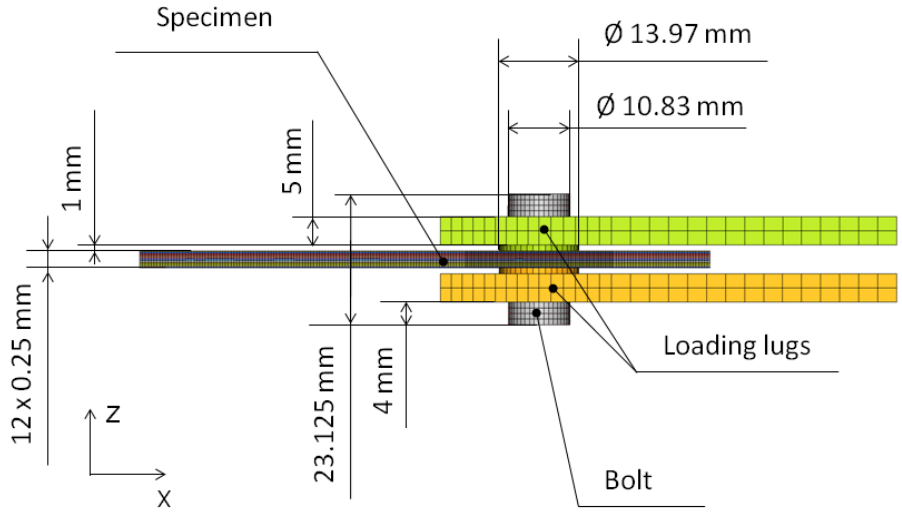

(b) Front view

Fig. 4.2: Model of the testing facility

4.2 Test CFRP specimen

In the study of *T. A. Collings* the CFRP specimen length was approximately 200 mm, the 0° fiber direction was in the length direction and the amount of plies varied.

In this work a specific laminate type was chosen. This laminate includes 12 plies with a ply thickness of 0.25 mm with stacking sequence $(0°/45°/\text{-}45°)_{2s}$. The CFRP specimen had a hole with a diameter of 6.35 mm and the edge distance e and the bolt distance w were altered.

The material in the experiment was described as fiber type 130SC/10000 and it was supposed to be preimpregnated with an epoxy resin system (Union Carbide ERLA 4617/DDM). Due to the fact that it was not possible to find any detailed information

about this material, it was decided to use a standard CFRP material called AS4/3501-6, described in [7]. Figure 4.3 illustrate the CFRP specimen dimensions. [5]

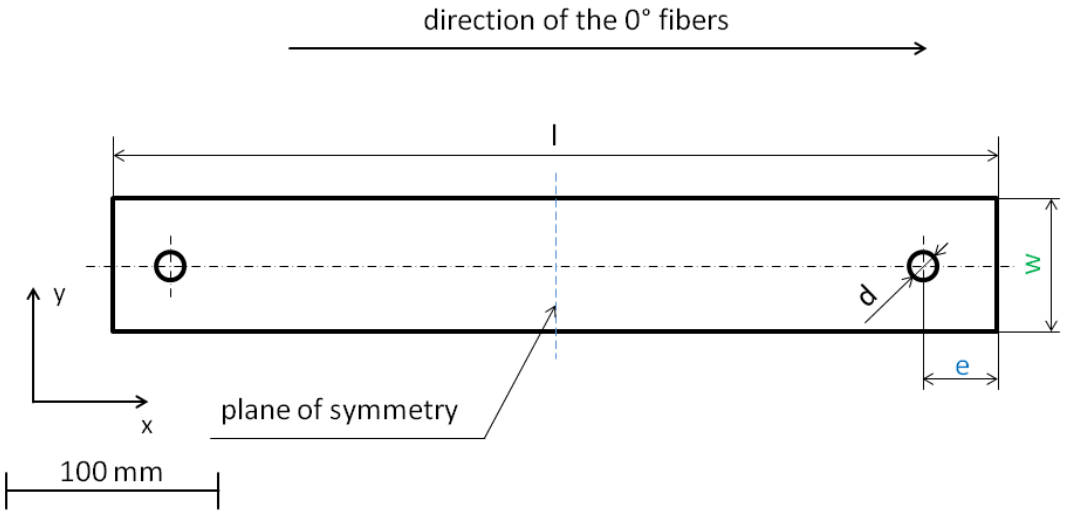

Fig. 4.3: Test CFRP specimen

4.3 Simulation of the bolt pretension

In reality firstly the bolt is pretensioned by a worker to a specific stress. In the simulation this is done by a multistage simulation.

Multistage simulation enables to combine multiple load steps, which would had to be started after each other, into one calculation which does that automatically. The load steps are called stages. The results of the first load step are taken to the second load step. In this case that means, that the pretension of the bolt is simulated first and then the bolt movement is simulated.

Bolt pretension is done by specifying the pretension stress. All the other components of the testing facility are fixed. After the specified simulation time is reached, this stage ends. The time is specified in a way that the bolt can reach the defined pretension.

The next stage is the movement of the bolt. To be able to keep the bolt pretensioned even after the first stage, it is simulated as a rigid body in the second stage. This keeps the bolt in the form as it was at the edge of first stage and therefore the pretension stress remains constant. Then the bolt is moved through the CFRP specimen to simulate the failure modes as described in next sections.

4.4 Simulations with variable edge distance *e*

In this section simulation of shear and bearing failure depending on the variation of the edge distance e and the transition point between these failures is discussed. Edge distances e from 1 to 4 times the diameter of the hole were chosen. To avoid tensile failure the bolt distance w was designed with the bolt distance of $w = 35\,\text{mm}$, which is $w = 5.52 \cdot d$ and therefore meets the conditions mentioned in the subsection 2.3.2 on the page 27. Figure 4.4 portrays the CFRP specimen for these simulations.

The achieved results of all three material types are then compared with the results provided by *T. A. Collings* in his study.

To be able to better understand and imagine the failure phenomena the CFRP specimen is divided into three regions as shown in figure 4.4.

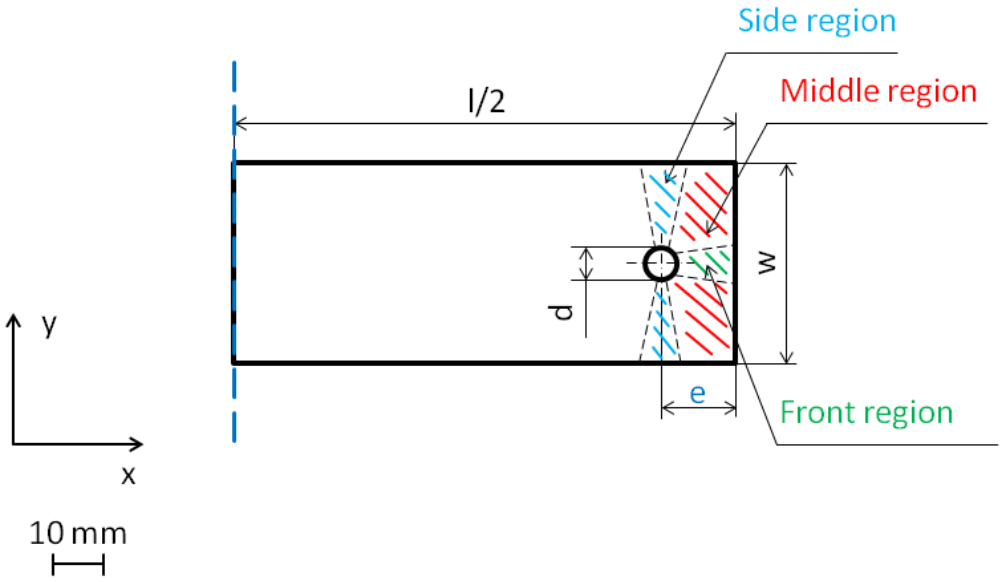

Fig. 4.4: Geometry of the test CFRP specimen

4.4.1 Material type 30

Results

The results in figure 4.5 represent simulations with material type 30 with the edge distances e 1, 2, 3 and 4 times the hole diameter.

Every curve from figure 4.5 can be divided in four sections.

The first section starts at a displacement of $0\,\text{mm}$ and is represented by a curve inclination. This section describes the overcoming of the friction force caused by the pretension and is colored yellow in figure 4.5.

When the friction force is overcome, second section begins. This section is representing the movement of the bolt towards the edge of the hole until a contact is established. This part can be identified by the flat curve. The displacement depends on the size of the gap between the bolt and the edge of the hole. In figure 4.5 this part is colored blue.

In the third section of the curve the bolt is already in contact with the edge of the hole and the bolt starts to deform and damage the elements of the CFRP specimen. This can be identified by the inclination of the curve up to a peak, where the first element failure and elimination occurs. The element failure depends on the damage curve. If an element reaches specific volumetric or shear strain, it starts to damage but it is not removed. The condition for element elimination depends only on the volumetric strain. Due to this condition it can be assumed that the element failure and elimination occur almost at the same time. This section is colored green in figure 4.5.

The last section begins with the downfall of the curve and results often in numerical instability. The downfall is cause by the element elimination, which occurs when an element reaches specific strain conditions. For the results comparison the curve peaks play a major role. This section is colored red in figure 4.5 and is valid only for the edge distance $e = 1 \cdot d$.

The fact that the curves fall down to zero is caused by the element elimination. When the whole row in front of the bolt is removed the contact force between the bolt and the CFRP specimen fall to zero. When the residual elements of the CFRP specimen stretch and a contact is established the curves reach positive values again. For the investigation only the maximal force is important. Due to this fact the curves are trimmed after they reach the zero value and therefore the whole behavior cannot be seen.

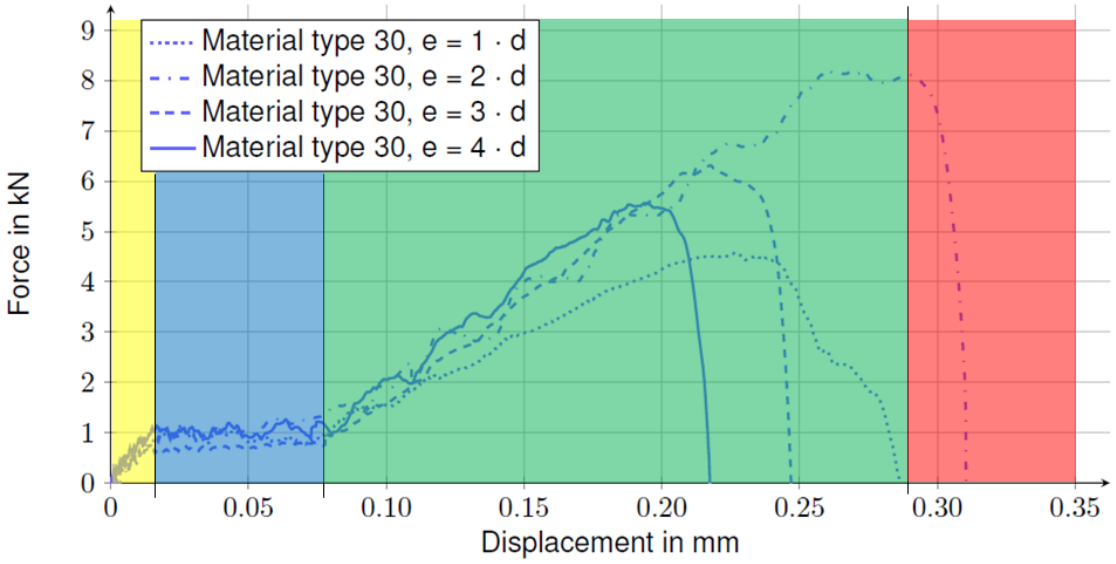

Fig. 4.5: Tensile test with material type 30 with variable edge distance e

In figure 4.6 failures of the material type 30 with various edge distances e are displayed. The CFRP specimens are colored grey and the bolts are blue.

The bearing failures in figures 4.6(b) - 4.6(d) can be identified by the elements which are eliminated in front of the bolt.

The shear failure can be identified by the removed front region as shown in figure 4.6(a).

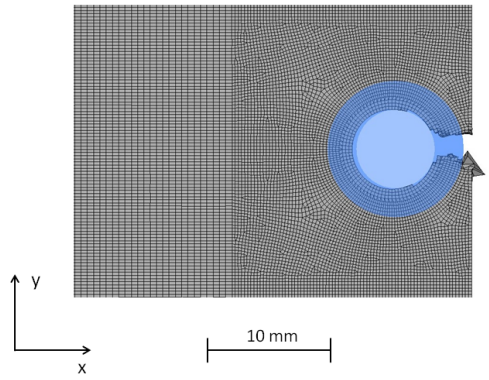

(a) Shear failure of material type 30 with the edge distance $e = 1 \cdot d$ at a displacement of 0.291 mm

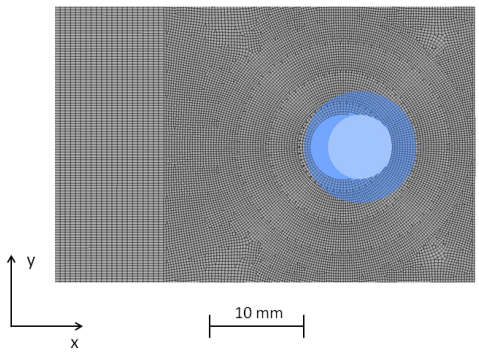

(b) Bearing failure of material type 30 with the edge distance $e = 2 \cdot d$ at a displacement of 1.703 mm

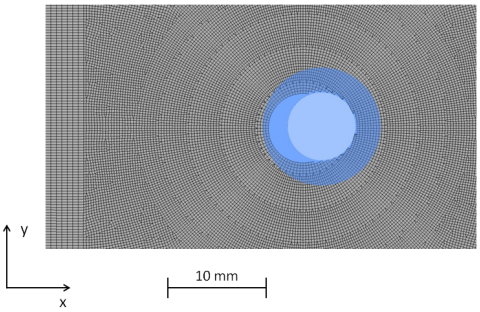

(c) Bearing failure of material type 30 with the edge distance $e = 3 \cdot d$ at a displacement of 1.703 mm

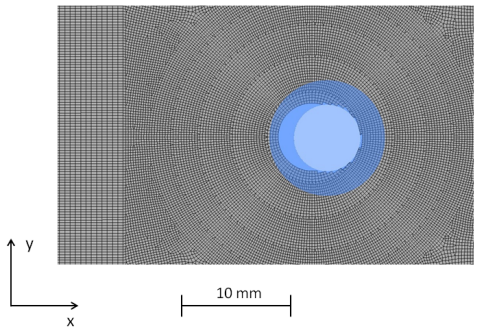

(d) Bearing failure of material type 30 with the edge distance $e = 4 \cdot d$ at a displacement of 1.703 mm

Fig. 4.6: Failures of material type 30 with variable edge distance e

Edge distance $e = 1 \cdot d$

The edge distance $e = 1 \cdot d$ is the only case where the shear failure occurs. This is a result of the small edge distance e.

In all variation of edge distance e the first element failures and eliminations occur in the front region due to compression stresses.

The edge distance *e = 1 · d* alters by the inclination and the displacement at which the element failure and elimination occurs. This is caused by the edge distance e, which affect the stiffness of the CFRP specimen in the middle and front region. The lower ultimate force is caused by the shear failure.

Edge distance *e = 2,3,4 · d*

These three variations can be interpreted together because they behave in a similar way.

Due to their edge distances e shear failure can be avoided and bearing failure occurs as illustrated in figure 4.6(b) - 4.6(d). The first element eliminations occur in the front region due to the compression stresses.

The differences between these three variations are in the inclination and the maximal force reached. This is due to the different edge distances e. With the increasing edge distance e the front and middle region become stiffer. This results in a smaller contact surface between the bolt and the CFRP specimen. If the contact surface is smaller and the ultimate compressive pressures are approximately the same, a lower force is needed to reach this limit. Therefore the maximum forces get lower with the increasing edge distance e.

4.4.2 User-material type 81

Results

The results of the simulation with user-material type 81 with variable edge distance e are shown in figure 4.7. The curves can be as well divided in four sections: friction overcome, bolt movement, damage and downfall. These sections are described in the subsection 4.4.1 on the page 52. The only difference is that in the curve section where element damage occurs. This is due to the fact that fiber and inter-fiber failure occur independently and are not combined together in element failure. This is possible due to the nature of the material type 81 which allows a more detailed simulation and analysis.

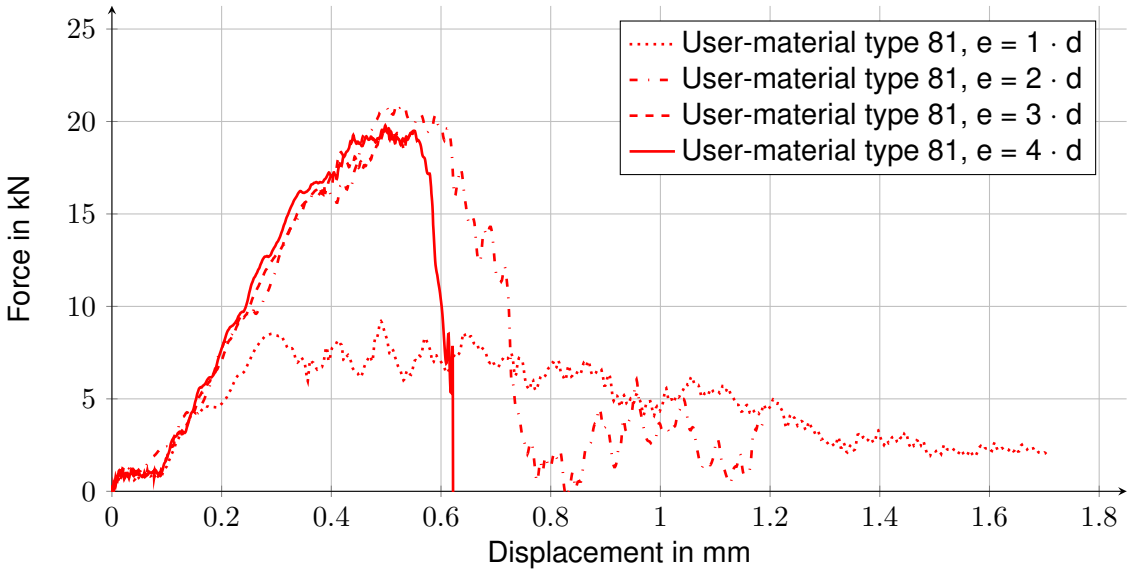

Fig. 4.7: Tensile test with user-material type 81 with variable edge distance e

Figure 4.8 illustrates failures of the CFRP specimens with various edge distances e are illustrated.

In figures 4.8(a) and 4.8(b) shear failures are displayed. This shear failures are caused by the lower edge distance e.

Figures 4.8(c) and 4.8(d) display bearing failures.

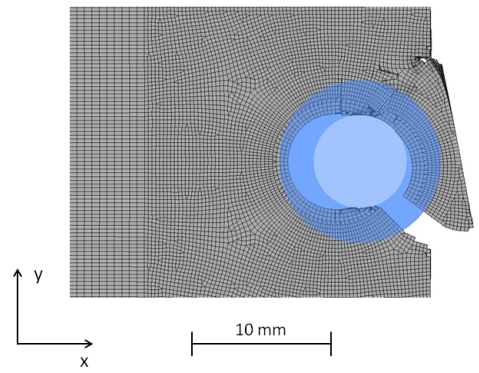

(a) Shear failure of user-material type 81 with the edge distance $e = 1 \cdot d$ at a displacement of 1.708 mm

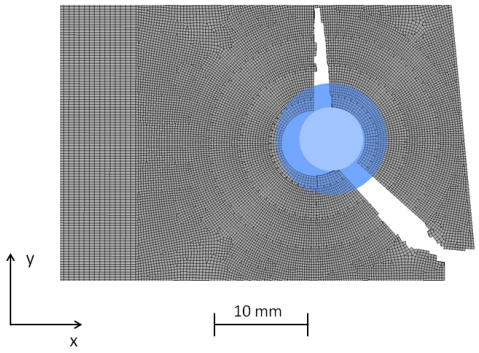

(b) Shear failure of user-material type 81 with the edge distance $e = 2 \cdot d$ at a displacement of 1.71 mm

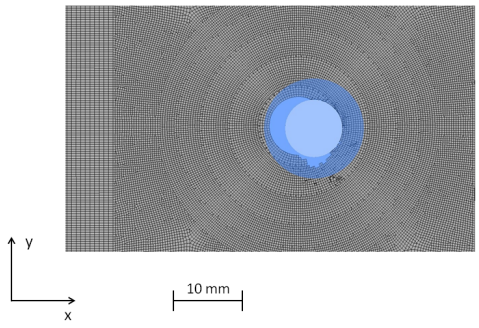

(c) Bearing failure of user-material type 81 with the edge distance $e = 3 \cdot d$ at a displacement of 1.695 mm

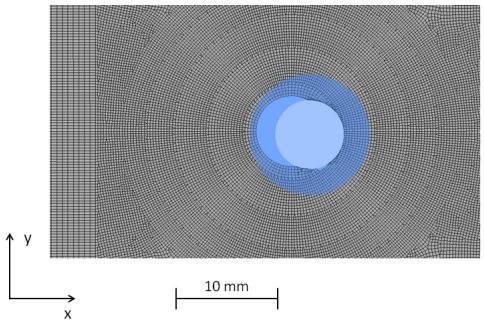

(d) Bearing failure of user-material type 81 with the edge distance $e = 4 \cdot d$ at a displacement of 1.7 mm

Fig. 4.8: Failures of user-material type 81 with variable edge distance e

Edge distance $e = 1{,}2 \cdot d$

These two variations share similar behavior. The friction overcome and the bolt movement are the same due to the same friction coefficient, pretension and the geometry. In the third section, which is the damage and deformation of the elements, inter-fiber failure occurs. This happens mostly in the front region due to compression stress. Inter-fiber failure is present as well partially in the side and middle region and is caused by tension.

Both of these variations fail in shear failure. The reason is that even, when elements in the front region reach fiber failure in compression, they must fulfill further conditions to be removed. Elements in the middle region fulfill all necessary conditions and are then removed and this results in shear failure.

The variations alter in force at which the first element eliminations appear. These forces are a result of the various edge distances e, which change the stiffness of the front and middle region. This stiffness affects the stress distribution and this results in higher compression stresses.

Edge distance $e = 3{,}4 \cdot d$

As can be seen in figures 4.8(c) and 4.8(d) CFRP specimens with the edge distances $e = 3{,}4 \cdot d$ fail in bearing failure. This bearing failure can be identified by the elements, which are removed in front of the bolt. This is caused by the higher edge distance e, which changes the stiffness of the middle and front region. This causes the elements in the front region to fulfill all conditions before the elements in the middle region and results in bearing failure.

The difference between these two variants is in the force at which the element elimination occurs. This is caused by the edge distance e, which through the change of the stiffness affects the force at which an element fulfills all conditions needed for an element elimination.

Edge distance $e = 3 \cdot d$ does not show the downfall of the curve. The reason is a numerical instability. This instability occurs after the maximal force is reached and the failure type is already reached.

4.4.3 Material type 131

Results

The figure 4.8 represents the results of the test CFRP specimens with variable edge distances e with the material type 131.

The curves in figure 4.8 can be divided in three section as mentioned in the subsection 4.4.1 on the page 52. The reason why there are only three sections is the numerical instability, which occurs in every simulation with the material type 131. Therefore a downfall of the curve cannot be seen. Due to the fact that the numerical instabilities occur after the maximal forces are reached and failure modes can be indentified it can be accepted. The nature of the material type 131 allows as in the case of material type 81 to simulate inter-fiber and fiber failure separately.

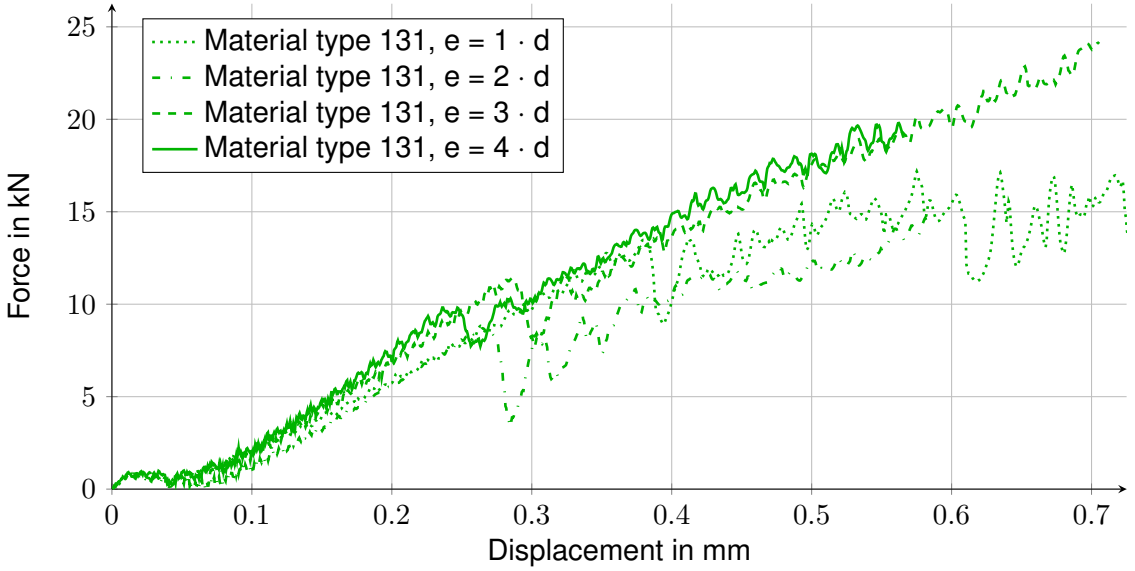

Fig. 4.8: Tensile test with material type 131 with variable edge distance e

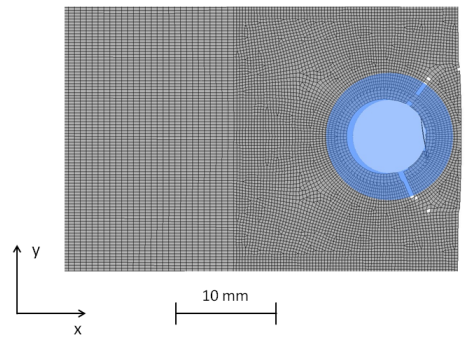

(a) Shear failure of material type 131 with the edge distance $e = 1 \cdot d$ at a displacement of 0.754 mm

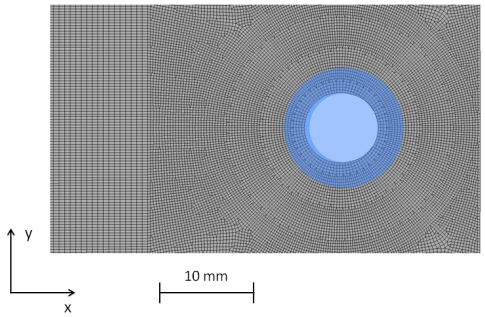

(b) Bearing failure of material type 131 with the edge distance $e = 2 \cdot d$ at a displacement of 0.585 mm

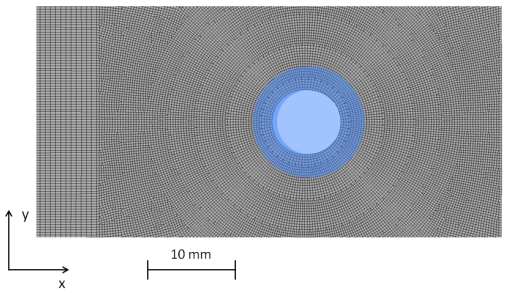

(c) Bearing failure of material type 131 with the edge distance $e = 3 \cdot d$ at a displacement of 0.706 mm

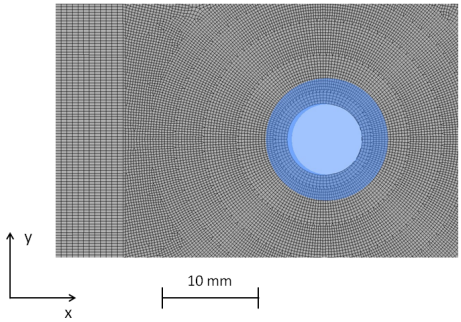

(d) Bearing failure of material type 131 with the edge distance $e = 4 \cdot d$ at a displacement of 0.566 mm

Fig. 4.9: Failures of material type 131 with variable edge distance e

Figure 4.9 illustrates simulations of CFRP specimens with various edge distances e at their failure.

Figure 4.9(a) is the only case of material type 131, where shear failure is reached.

Figures 4.9(b) - 4.9(d) show bearing failures. These bearing failures are difficult to be identified, because the numerical instabilities occur after the first rows of elements are eliminated. Due to the fact that any other failure mode occurred, bearing failure is assumed. The numerical instabilities are caused by the poor support of the elements in the z-direction.

Edge distance $e = 1 \cdot d$

Edge distance $e = 1 \cdot d$ is the only case of material type 131 where shear failure occurs. This is caused by the small edge distance e.

At the beginning of the deformation inter-fiber and fiber failure occur due to compression stress. After few elements are removed and the edge distance e decreases the stiffness decreases also and this causes the elements in the middle region to fail in tension and being removed. These eliminated elements create wedge shaped part of the CFRP specimen which is separated.

The deformed elements, which cause the numerical instability, are visible in figure 4.9(a).

Edge distance *e = 2,3,4 · d*

These three variants share similar behavior. The higher edge distance e, increases the stiffness in the middle and side region and limits the stress distribution. Therefore higher compressive stresses act on the elements on the edge of the hole in the front region and smaller tensile stresses act in the side region. Shear failures are avoided and bearing failures occur in all three variations. The higher the edge distance e the sooner the fiber failure and element elimination occur.

It possible to observe a slight downfall of the curve in figure 4.9. This is caused by elements that are eliminated. Due to the nature of this material type not all elements are removed and therefore the curve increase further. The residual elements, which are not removed, cause then numerical instability. Therefore the force at the peak before the first element elimination is understood as the maximal force.

4.4.4 Comparison of the results with experimental data and conclusion

Results

Experimental data obtained from the study performed by *T. A. Collings* and the simulation results are compared in two ways. Firstly the bearing stress at failure, which is defined by equation (4.1) by *T. A. Collings* and secondly the transition between shear and bearing failure depending on the edge distance e will be compared. The results are present in figure 4.10 [5].

$$\sigma_{b(u)} = \frac{F_u}{n \cdot d \cdot t} \tag{4.1}$$

where

$\sigma_{b(u)}$ – Ultimate bearing stress
n – Amount of holes

The table 4.2 presents the failure modes of CFRP specimens with certain material type and edge distance e.

Tab. 4.1: Failure modes of material types with various edge distances e. B - Bearing failure, S - Shear failure

	$e = 1 \cdot d$	$e = 2 \cdot d$	$e = 3 \cdot d$	$e = 4 \cdot d$
Material type 30	S	B	B	B
User-material type 81	S	S	B	B
Material type 131	S	S	B	B

Figure 4.10 displays bearing stresses over the edge distance to diameter ratio e/d. Results are portrayed as points. The color of a point represents the material type. Material type 30 is blue. User-material type 81 is illustrated red and material type 131 is filled with green color. If the point has a check mark next to it that means the simulated failure mode equals to the forecasted one by the study. If there is an x mark placed it does not equal.

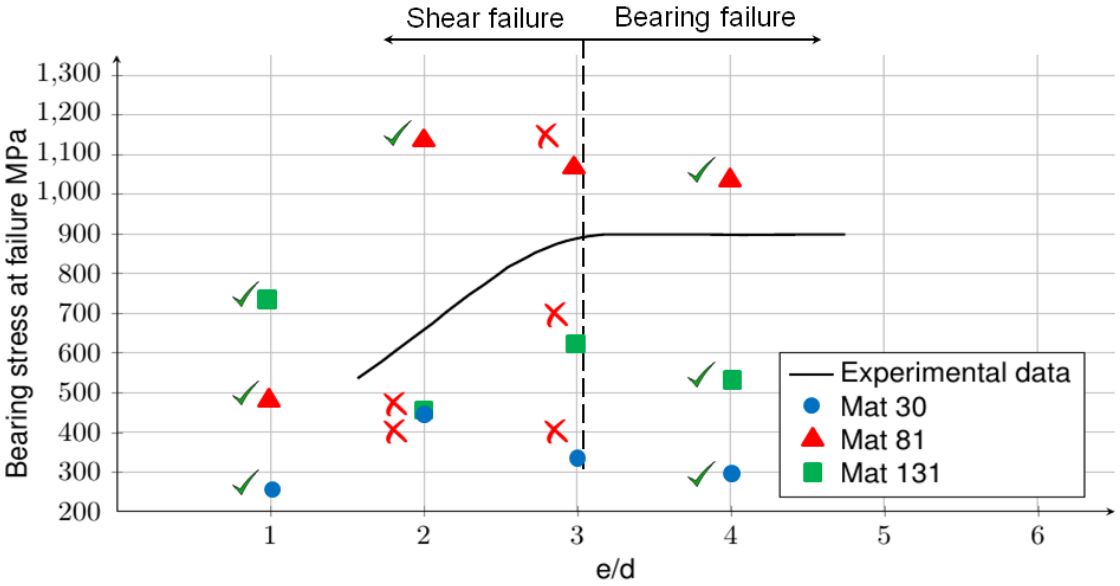

Fig. 4.10: Ultimate bearing stress with variation of the e/d ratio

Result interpretation

Due to the fact mentioned in the section 4.2 on the page 50, that the material properties were not known, similar material properties were used and they caused that the absolute

values do not match. For the investigation the major role plays the behavior.

Material type 30 has issues to simulate shear failure due to the simple condition for element failure. It was successful only when the edge distance e was very small. The simple conditions are given from simple tensile test with unidirectional plies and do not allow an explicit simulation of fiber or inter-fiber failure. It is necessary to understand that an element fails when a certain elastic strain is reached. This elastic strain can be caused by stress from any direction and therefore this model does not consider the fiber direction effect on the failure.

User-material type 81 shows the best results when it comes to absolute values as well as behavior. It is capable to take in consideration almost all phenomena which can occur in the CFRP and all parameters that influence the failure mode and the behavior. It allows to display the specific inter-fiber failure mode and exceed other material types in possibilities, result accuracy and visualization abilities. The reason for the higher results compared to the study from *T. A. Collings* are explained in the subsection 4.2 on the page 50 and are a result of different material properties due to the information confidentiality.

Material type 131 is placed between material type 30 and user-material type 81. It takes in consideration the fiber direction in the fiber failure condition. But the conditions for the element elimination lack on complexity, which is necessary to simulate the failure modes in the right way. Material type 131 is a double-edged sword. Due to the fact that it is a shell the computational costs decrease, but the numerical instability increases and therefore the user-material type 81 is much more suitable for this type of simulations.

4.5 Simulations with variable bolt distance *w*

As opposed to the simulations of CFRP specimens with variable edge distances e, in this part simulations of CFRP specimens the variable bolt distances w are covered. The edge distance e is designed in a way that it prevents shear failure in all situations and therefore it is possible to investigate the transition between tensile failure and bearing failure. The geometry of the CFRP specimen is portrayed in the figure 4.4. The conditions for the suggested edge distance e are covered in the subsection 2.3.2 on the page 28. The designed edge distance is $e = 30\,\text{mm}$, which equals $e = 4.72 \cdot d$, and meets all requirements to avoid shear failure mentioned in 2.3.2 on the page 28.

4.5.1 Material type 30

Results

The results in figure 4.11 show simulations with material type 30 with the bolt distances w 2, 3, 4 and 5 times the hole diameter. The curves can be divided in four sections as in the subsection 4.4.1 on the page 52.

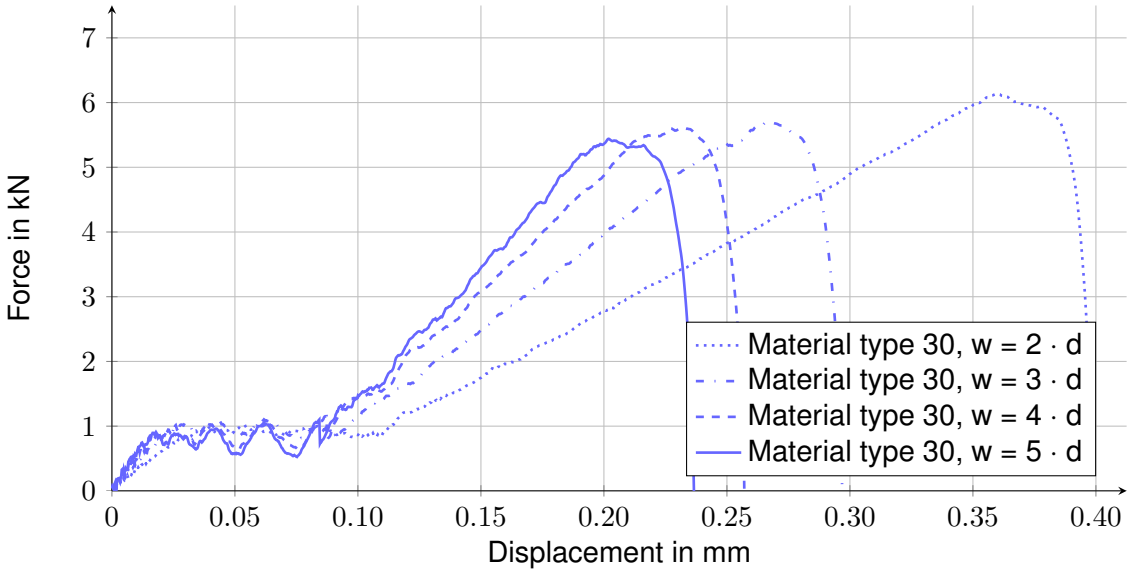

Fig. 4.11: Tensile test with material type 30 with variable bolt distance w

Figure 4.12 illustrates failure modes of CFRP specimens with various bolt distances w. All four variants show bearing failure.

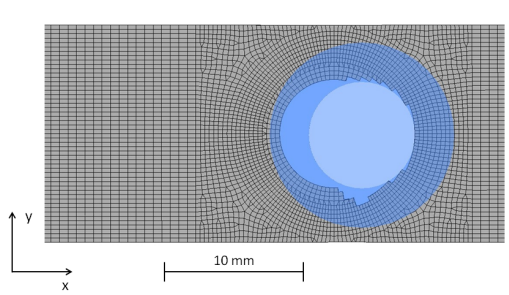

(a) Bearing faiulre of material type 30 with the bolt distance $w = 2 \cdot d$ at a displacement of 1.704 mm

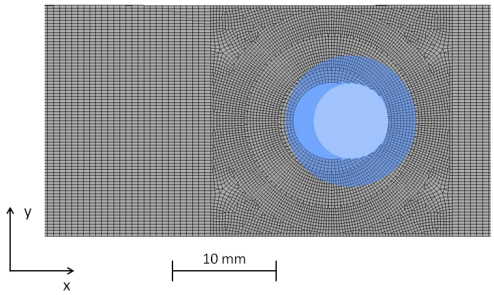

(b) Bearing failure of material type 30 with the bolt distance $w = 3 \cdot d$ at a displacement of 1.701 mm

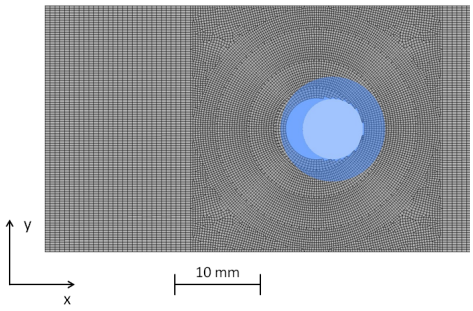

(c) Bearing failure of material type 30 with the bolt distance $w = 4 \cdot d$ at a displacement of 1.707 mm

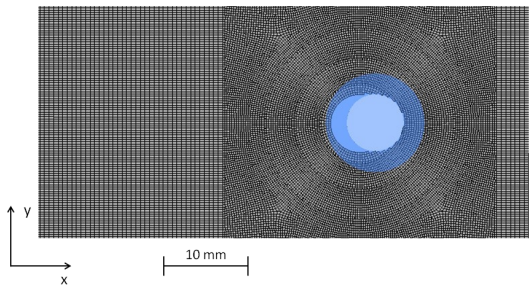

(d) Bearing failure of material type 30 with the bolt distance $w = 5 \cdot d$ at a displacement of 1.707 mm

Fig. 4.12: Failures of material type 30 with variable bolt distance w

Bolt distance $w = 2,3,4,5 \cdot d$

All four variants show similar behavior. The friction overcome and the bolt movement are almost the same. The reason is that the geometry and the pretension are designed identically. The fluctuations in these phases are caused by numerical uncertainty.

The differences between the variants are in the inclination of the curve in the damage phase and the maximum force reached. This is caused as mentioned in the subsection 4.4.1 on the page 55 by the different bolt distance w, which alters the stiffness. The maximum force reached decreases with the increasing bolt distance w. This is a result of the changing cross-section that alters the stiffness. If the stiffness is higher the contact surface between the bolt and the hole is smaller. Element failure and elimination occur when an element reaches specific volumetric or shear strain. Due to the nature of the condition for element failure and elimination the maximum force decreases. The first element elimination occurs in the front area as a result of compression stress and is then followed by more element eliminations. The bearing failures can be identified by the eliminated elements in front of the bolt and the movement of the bolt through the CFRP specimen.

4.5.2 User-material type 81

Results

The simulation results of the user-material type 81 with variable edge distance e are shown in figure 4.12. The curves can be divided in four sections as in the subsection 4.4.1 on the page 52. Figure 4.13 illustrates all variations of the CFRP specimen with variable edge distance e at their failure.

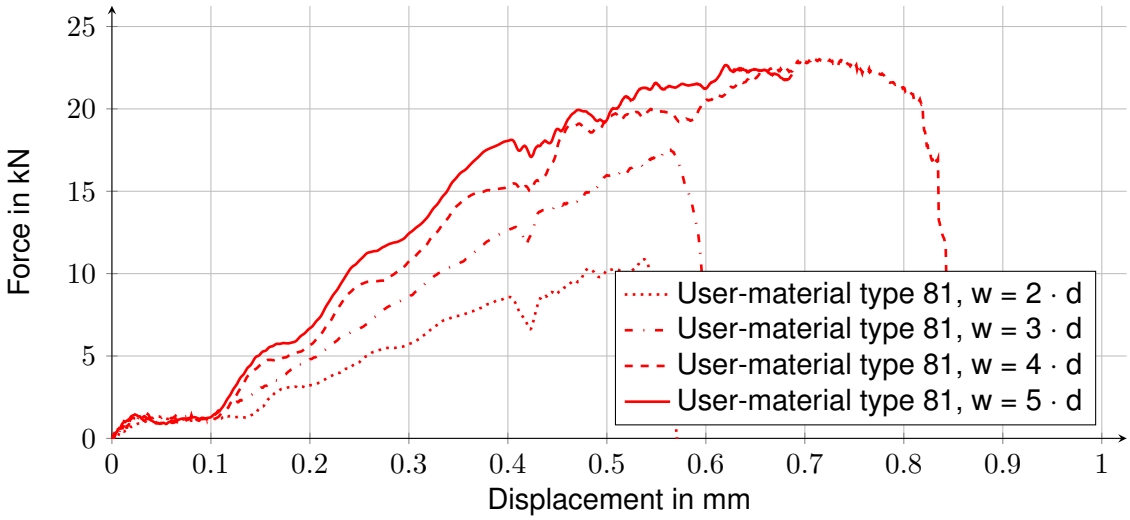

Fig. 4.12: Tensile test with user-material type 81 with variable bolt distance w

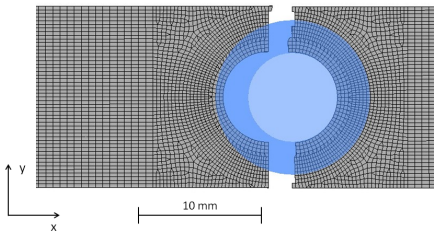

(a) Tensile failure of user-material type 81 with the bolt distance $w = 2 \cdot d$ at a displacement of 1.714 mm

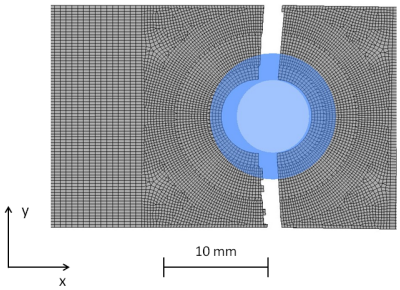

(b) Tensile failure of user-material type 81 with the bolt distance $w = 3 \cdot d$ at a displacement of 1.716 mm

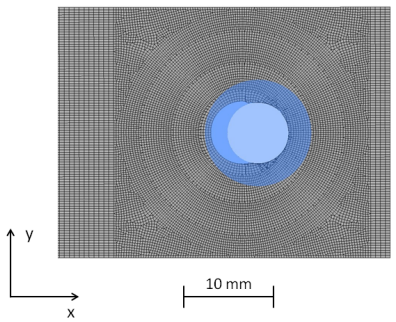

(c) Bearing failure of user-material type 81 with the bolt distance $w = 4 \cdot d$ at a displacement of 1.698 mm

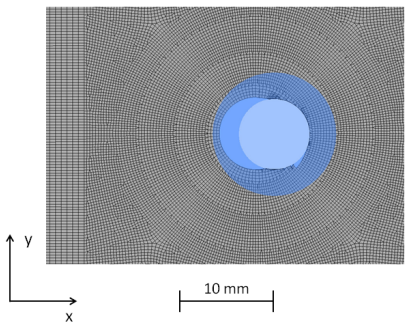

(d) Bearing failure of user-material type 81 with the bolt distance $w = 5 \cdot d$ at a displacement of 1.700 mm

Fig. 4.13: Failures of user-material type 81 with variable bolt distance w

Bolt distance *w = 2,3 · d*

CFRP specimens in figures 4.13(a) and 4.13(b) fail in tensile failure.

First inter-fiber failures occur in the front region due to compression but also in the middle and side region due to tension. As a result of the small bolt distance w first fiber failure occurs in the case of CFRP specimen with the bolt distance *w = 2 · d* in the side region due to tension and is then followed by element elimination, when all conditions are reached. Afterwards more elements are eliminated and a separation of the CFRP specimen occurs.

The first fiber failure of the CFRP specimen with the bolt distance *w = 3 · d* occurs in the front region due to compression. The elements do not fulfill all conditions and therefore are not eliminated. The elements, which experience fiber failure and are eliminated afterwards, are the elements in the side region and cause as a result tensile failure.

Bolt distance *w = 4,5 · d*

Figures 4.13(c) and 4.13(d) show that these two CFRP specimens fail in bearing failure.

First inter-fiber failure occurs in the front region due to compression and is followed by more inter-fiber failures in all three regions. First fiber failure occurs in the front region due to compression but the conditions for element elimination are not reached. The first element elimination occurs at the side region because the tensile stress exceeds the ultimate tensile strength and the conditions for element elimination are reached. Due to the higher bolt distance w a further propagation of the tensile failure is avoided and after reaching the condition for element elimination in compression a bearing failure occurs. This bearing failure can be identified by the removed elements in the front region and the bolt displacement.

4.5.3 Material type 131

Results

The figure 4.14 represents the results of the CFRP specimens with the variable edge distances e with the material type 131. Some curves can be divided in four section and some just in three because of a numerical instability.

Figure 4.15 shows CFRP specimens with variable bolt distance w at their failure.

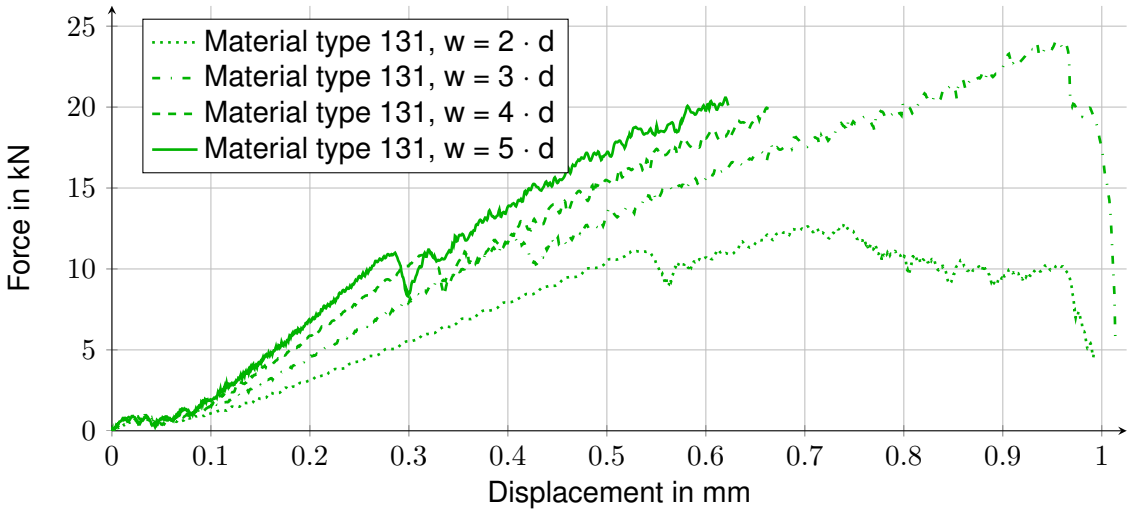

Fig. 4.14: Tensile test with material type 131 with variable bolt distance w

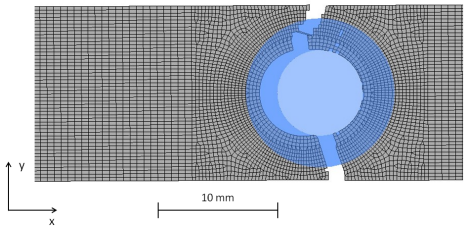

(a) Tensile failure of material type 131 with the bolt distance $w = 2 \cdot d$ at a displacement of 1.763 mm

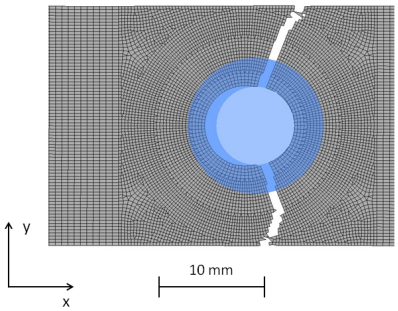

(b) Tensile failure of material type 131 with the bolt distance $w = 3 \cdot d$ at a displacement of 0.997 mm

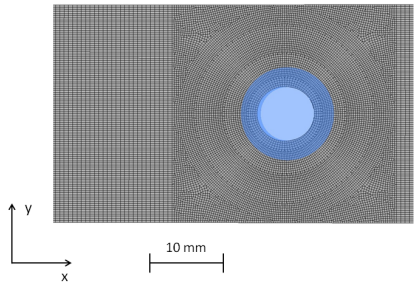

(c) Bearing failure of material type 131 with the bolt distance $w = 4 \cdot d$ at a displacement of 0.669 mm

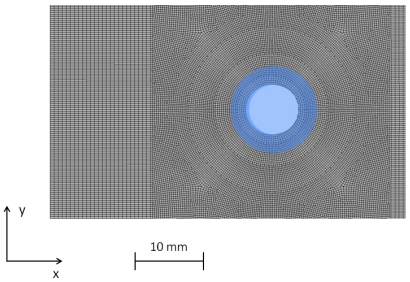

(d) Bearing failure of material type 131 with the bolt distance $w = 5 \cdot d$ at a displacement of 0.623 mm

Fig. 4.15: Failures of material type 131 with variable bolt distance w

Bolt distance *w = 2,3 · d*

In these two cases the CFRP specimens fail in tensile failure. The difference is in the curve inclination in the damage phase and the maximum force reached.

This inclination difference is cause by the cross-section which is smaller with the smaller bolt distance w. Smaller cross-section reduces the stiffness and therefore a small inclination is obtained.

The maximum force reached alters as a result of different bolt distance w. This causes for bolt distance $w = 2 \cdot d$ then the higher stiffness. That avoids immediate tensile failure and firstly elements in the front region are eliminated. These elements are eliminated due to compression stress. When the elements in the side region reach the conditions for element elimination in tension they start to eliminate and tensile failure occurs.

Bolt distance *w = 4,5 · d*

These two CFRP specimens fail in bearing failure. This bearing failure is cause by the higher bolt distance w, which avoids tensile failure. The difference in the inclination is caused by the stiffness, which is a result of higher bolt distance w. These CFRP specimen simulations end with a numerical instability. The results from these CFRP specimens can be used. The reason for this is that the force at first element elimination is taken as the maximal bearing force. Due to the conditions of this material type not all elements are removed and therefore the curve increase further. The residual elements, which are not removed, cause then numerical instability.

4.5.4 Comparison of the results with experimental data and conclusion

Results

Similar as mentioned in the subsection 4.4.4 on the page 60 the results are represented in figure 4.15 with the help of singular points.

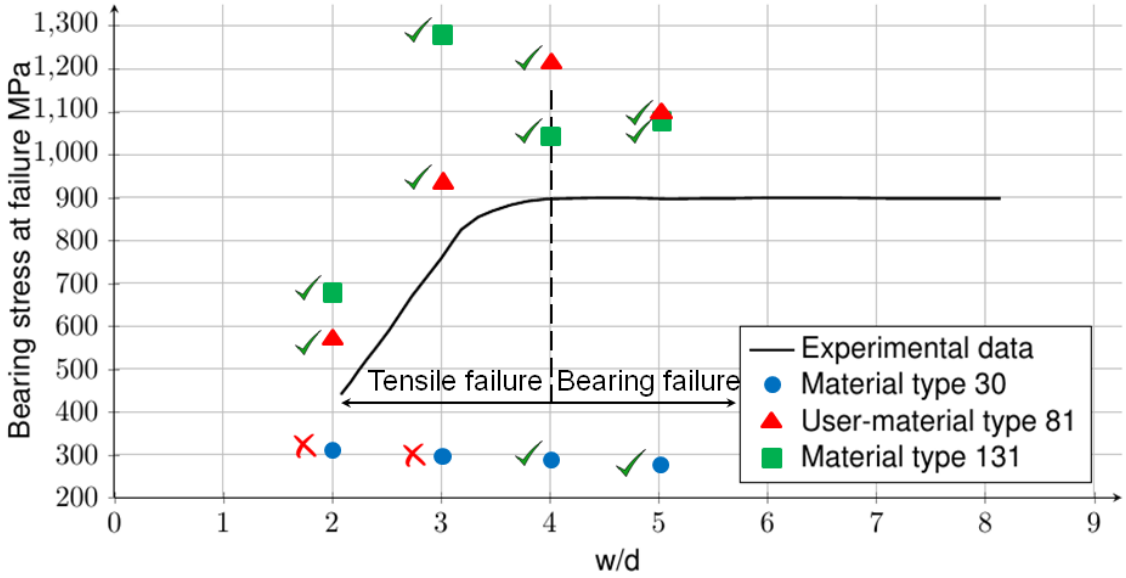

Fig. 4.15: Ultimate bearing stress with variation of the w/d ratio

The table 4.2 presents the failure modes of CFRP specimens with certain material type and bolt distance w.

Tab. 4.2: Failure modes of material types with various edge distances e. B - Bearing failure, T - Tensile failure

	$e = 1 \cdot d$	$e = 2 \cdot d$	$e = 3 \cdot d$	$e = 4 \cdot d$
Material type 30	B	B	B	B
User-material type 81	T	T	B	B
Material type 131	T	T	B	B

Results interpretation

The results in figure 4.15 show that the absolute values of the bearing stresses at failure do not match. This happened because as mentioned in the section 4.2 on the page 50, the exact material properties of the CFRP specimen used in the tests were unknown. Therefore the deviation occurs. For the investigation the behavior is much more important than the absolute values.

Material type 30 shows that due to its very simple failure conditions it cannot simulate tensile failure and the result is always bearing failure. The bearing stresses at failure

are very low, because the values for failure are defined as elastic strains and not as ultimate strengths as it should be. These values are given from simple tensile tests with unidirectional plies. It is necessary to understand that the elements fail when a certain elastic strain is reached. This elastic strain can be caused by stress from any direction and therefore this model does not consider the fiber direction effect on the failure.

User-material type 81 shows the best results when it comes to absolute values and behavior. It was capable to display all failure types properly depending on the geometric properties. This is due to its extensive definition of almost every phenomenon, which occurs in CFRP, and precise conditions for element elimination, which are based on real phenomena. It is capable to distinguish between inter-fiber and fiber failure and even display the inter-fiber failure mode, which any other material type is not capable of.

Material type 131 stands between material type 30 and user-material type 81. It shows advanced possibilities compared to material type 30. It is possible to set up conditions for fiber and inter-fiber failure and therefore overcomes the material type 30. These conditions are simpler than that used in the user-material type 81. The other property of the material type 131 is more of a double-edged sword. Due to the fact that it is a shell the computational costs decrease but the numerical instability increases and therefore the user-material type 81 is much more suitable for this type of simulations.

5 Experimental testing and verification

As a part of a research project this master thesis compared numerical and experimental data with flow drill screw joint tests. This has allowed to confirm the simulation results from chapter 4 with experimental data obtain from tests.

5.1 Experimental tests

In this section experimental tests are introduced. This section takes a closer look at the test CFRP specimen, testing facility, measuring techniques and then at the provided results.

5.1.1 Test CFRP specimen

Flow drill screws represent in automotive industry a good way to assemble fiber-reinforced plastic and metals together. This is a result of their minimal thermal input and a possibility to access the assembly from one side only. The CFRP specimen contains of CFRP with high-tenacity fibers T700 and a thermoset polymer, an aluminum U-shape profile and a flow drill screw.

The thesis concentrates on the CFRP specimen and not on the aluminum and the bolts, because it is expected that the CFRP specimen fails first.

The CFRP specimens were made of 8 unidirectional plies. Each ply had a thickness of 0.15 mm. The CFRP specimens obtained from the supplier needed to be modified. It was necessary to drill three holes in the test CFRP specimen through which the CFRP specimen was fixed to the bottom part of the testing facility. The aluminum U-shape profile was fixed to the top part of the testing facility. Figure 5.1 illustrate the drilling process which was done with a bench drilling machine. The predrill was done with a 3 mm drill and then a 6 mm drill was used. In these holes pins were inserted and through these pins the CFRP specimen was fixed to the testing facility. Three stacking sequences $(90°/0°/\text{-}45°/45°)_s$, $(0°/90°/0°/90°)_s$ and $(45°/\text{-}45°/45°/\text{-}45°)_s$ and two edge distances 10 mm and 14 mm were tested.

The test CFRP specimen is shown in figure 5.2. Due to the fact that the test CFRP specimen was designed a new modification to the testing facility had to be done as well [29].

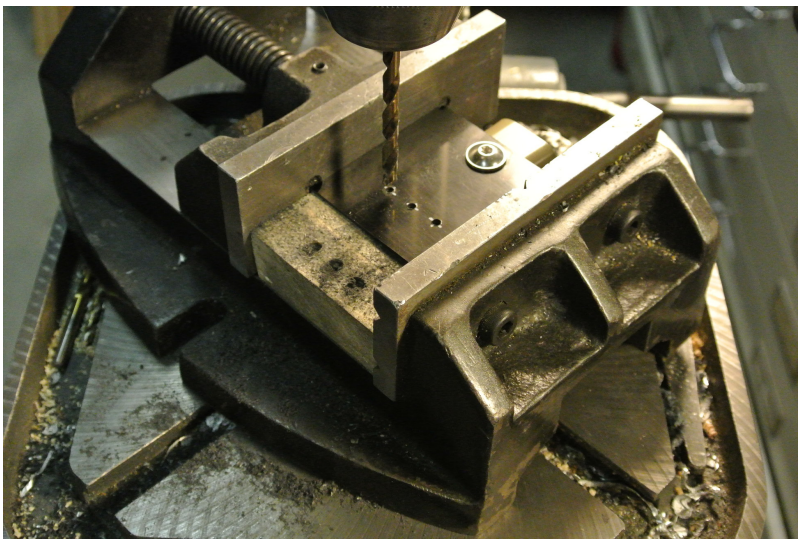

Fig. 5.1: Drilling process

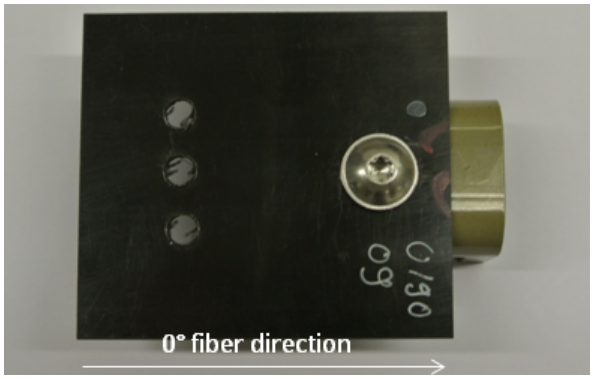

(a) Top side

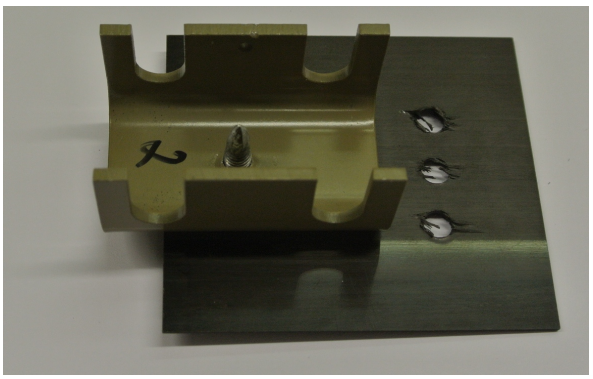

(b) Bottom side

Fig. 5.2: CFRP specimen after drilling

5.1.2 Testing facility

Figure 5.3 taken form [29] shows the testing facility. This facility was constructed to allow multiple types of testing. For the purposes of this thesis only the shear test is interesting, that means that the forces are applied in the 0° direction. The bottom part of the facility is fixing the CFRP plate and the top part of it is attached to the U-shaped aluminum profile. The testing facility capable to lock rotation and is designed in a way that the forces are transmitted directly through the joining point. To be able to reproduce and compare the results boundary conditions have to by always the same. The tests were done on a common tensile test device. The CFRP specimens were tested on the Institute of Material Science and Welding of Graz University of Technology.

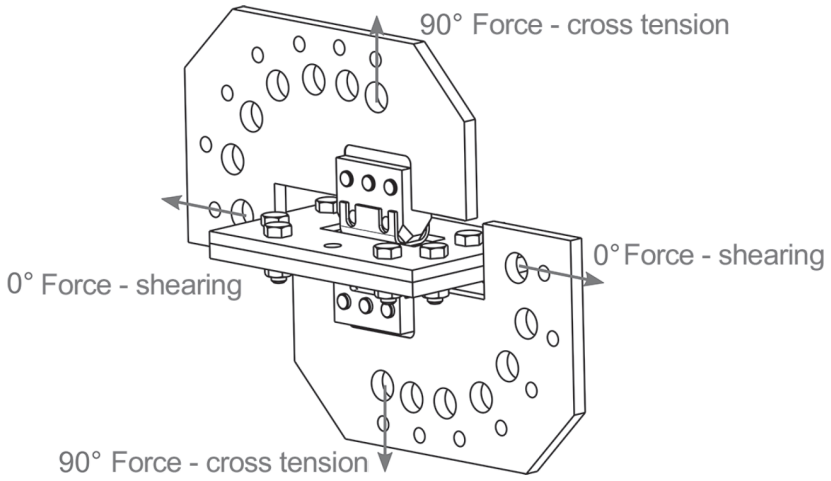

Fig. 5.3: Testing facility [28]

5.1.3 Measuring techniques

The tensile test device measures the force displacement but does implement the test device rigidity and the deformation of CFRP and aluminum. Therefore just one curve is obtained from the test device. In the testing two measurement techniques were used to be able to measure in more exact way.

To be able to distinguish between the deformation of CFPR and aluminum a optical analysis that uses photographs was used. This method even eliminated the influence of the test device rigidity. [29]

Endoscopic camera recorded visually the behavior of the CFRP specimen from a view that a normal camera would not be possible to reach.

5.1.4 Results

Results were always scaled in a way that the maximal reached force of all curves compared together in one figure represented 100 %. Therefore mostly only one curve reached 100 %. This was done for a better comparability. The displacement was scaled in the same way.

Laminate with a stacking sequence of (90°/0°/-45°/45°)$_s$ and an edge distance *e* of 10 mm

Figure 5.4 presents the results from the tensile test with the laminate (90°/0°/-45°/45°)$_s$. It is possible to distinguish four regions.

The first region is between the displacement approximately 0 % and 2 %. In this region the flow drill screw, which is pretensioned, has to overcome the friction caused by the pretension. The deviations between the tests might be caused by different pretensions or surface roughnesses, which define the friction coefficient. In figure 5.4 this region has yellow color.

The second region is the region where the flow drill screw travels to the edge of the hole and ranges from displacement approximately 2 % up to 7 %. In this region the reason for the curve deviation is the distance between the flow drill screw and the edge of the hole. This section is colored blue in 5.4.

The third region is from the displacement approximately 7 % up to 23 %, where the flow drill screw starts to damage the CFRP specimen. This continues until the ultimate force is reached. Deviation may be caused by the difference in mechanical properties caused by production scatter. In figure 5.4 this part is colored green.

The last region starts after the ultimate force is reached. Video recordings made by the endoscopic camera showed that the CFPR fails in a combination between shear and tensile failure. That should be illustrated in the figure with a steep downfall of the curve due to the separation of the CFRP. The difference is that this cannot happen because we do not have a unidirectional CFRP, but a laminate with a stacking sequence (90°/0°/-45°/45°)$_s$. That means that even when the failure initiates as tensile failure separation does not happen immediately as shown in figure 5.7. And that is why the curve does not fall down to 0 N but has a slow decrease of the force. This section is in figure 5.4 colored red and valid only for the Test 5.

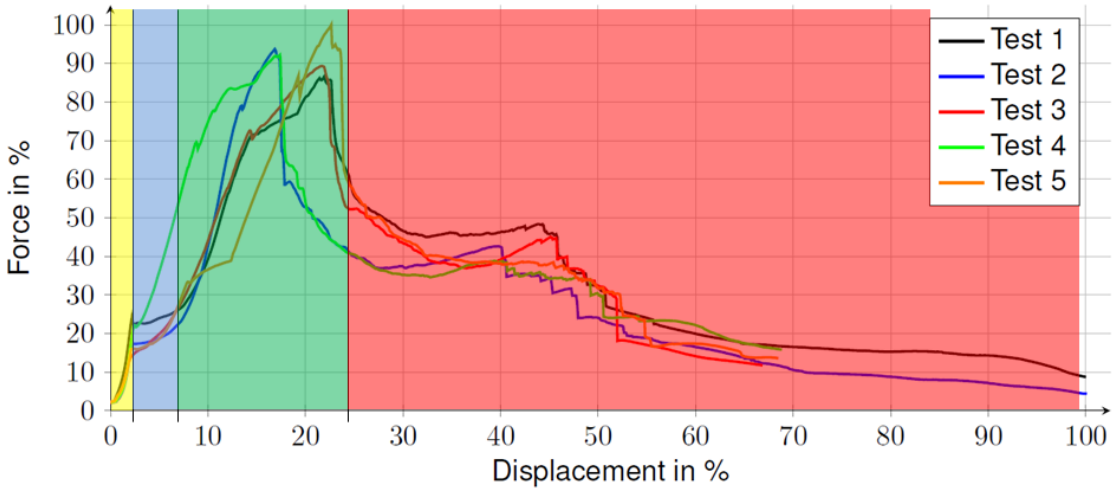

Fig. 5.4: Results of tensile test with a $(90°/0°/\text{-}45°/45°)_s$ laminate and an edge distance e of 10 mm

Laminate with a stacking sequence of $(90°/0°/\text{-}45°/45°)_s$ and an edge distance *e* of 14 mm

The regions in figure 5.5 can be interpretated analogicaly to figure 5.4. The only difference is in the region which starts after reaching the ultimate force. The edge distance is big enough that bearing failure can occur. Bearing failure can be easily identified by the stable level of force. This state remains approximately constant until the edge distance e does not decrease to a certain limit. If this limit is reached tensile failure without immediate separation appears as mentioned in the subsection 5.1.4.

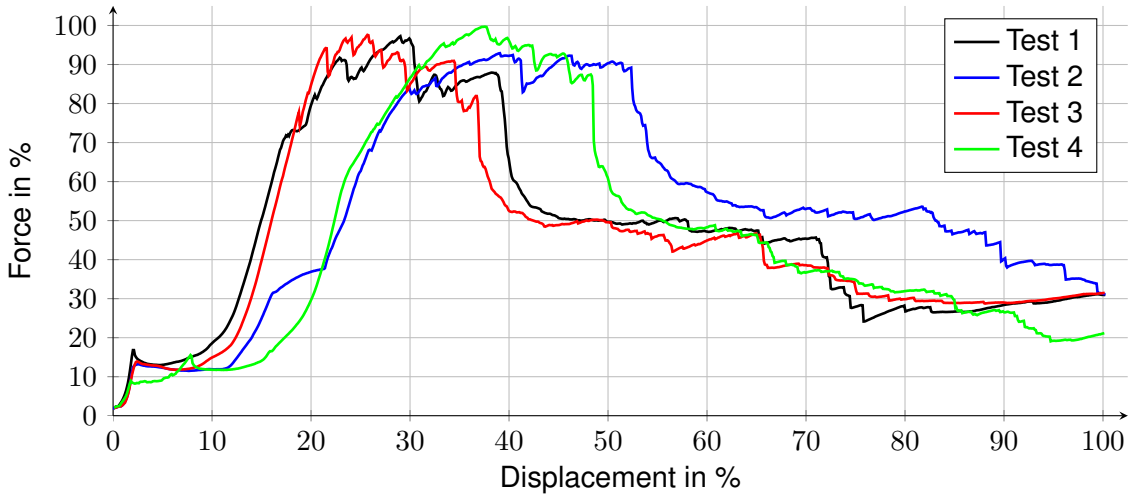

Fig. 5.5: Results of tensile test with a $(90°/0°/\text{-}45°/45°)_s$ laminate and an edge distance e of 14 mm

Laminate with a stacking sequence of $(0°/90°/0°/90°)_s$ and an edge distance *e* of 10 mm

From figure 5.6 it is possible to distinguish four known regions. At the beginning the overcome of friction force is necessary. This region is followed by the travel of the flow drill screw to the edge of the hole and after that the damage region with ultimate force begins. When the ultimate force is reached failure occurs. As can be seen in figure 5.7 the failure is a combination of shear failure in the 0° plies and tensile failure in the 90° plies. The separation of the CFRP is visible by the downfall of the curve at the end.

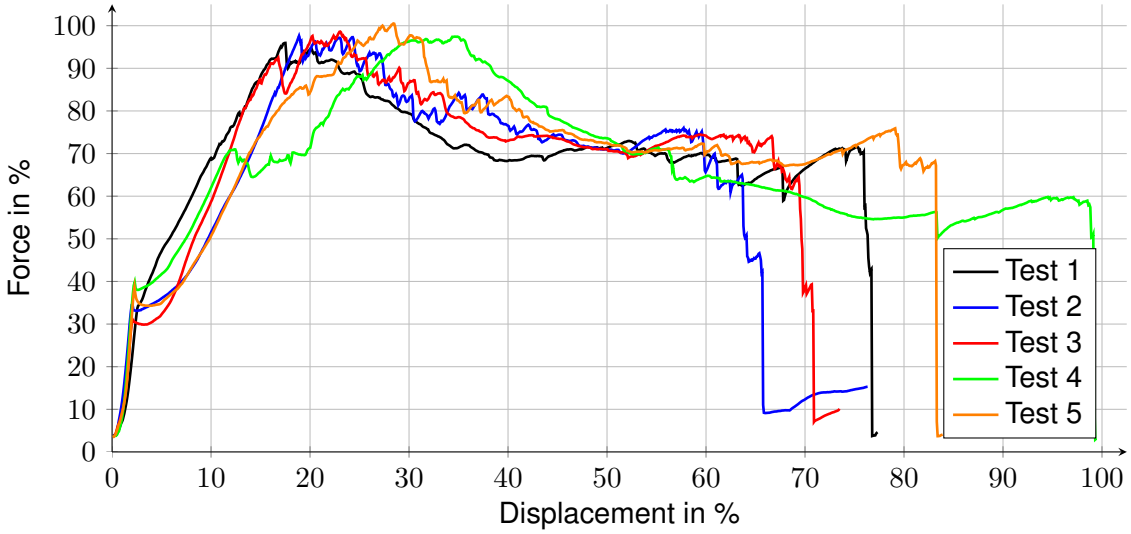

Fig. 5.6: Results of tensile test with a $(0°/90°/0°/90°)_s$ laminate and an edge distance e of 10 mm

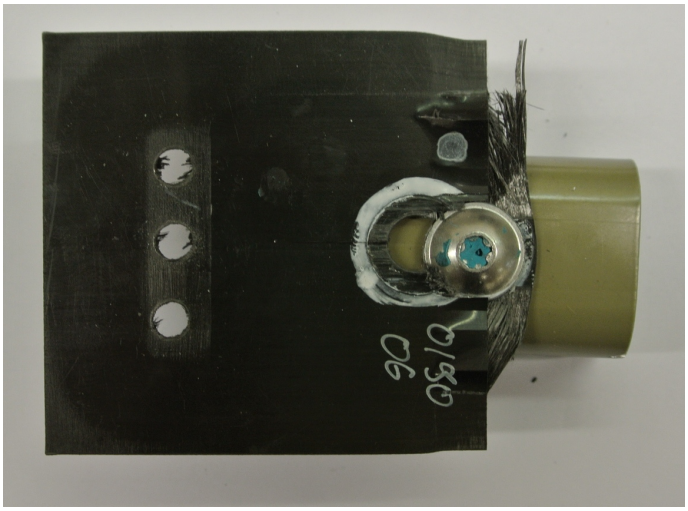

Fig. 5.7: Shear failure of $(0°/90°/0°/90°)_s$ laminate with 10 mm edge distance without immediate separation

Laminate with a stacking sequence of $(0°/90°/0°/90°)_s$ and an edge distance *e* of 14 mm

Due to the larger edge distance e it is possible to observe bearing stress until the edge distance reaches the critical value and as mentioned above a combination of shear and tensile failure occurs. Due to the fact that the failure is a combination of shear and tensile failure a downfall of the curve in the figure 5.8 is not observed. That means that even when the tensile failure occurs, separation does not happen immediately.

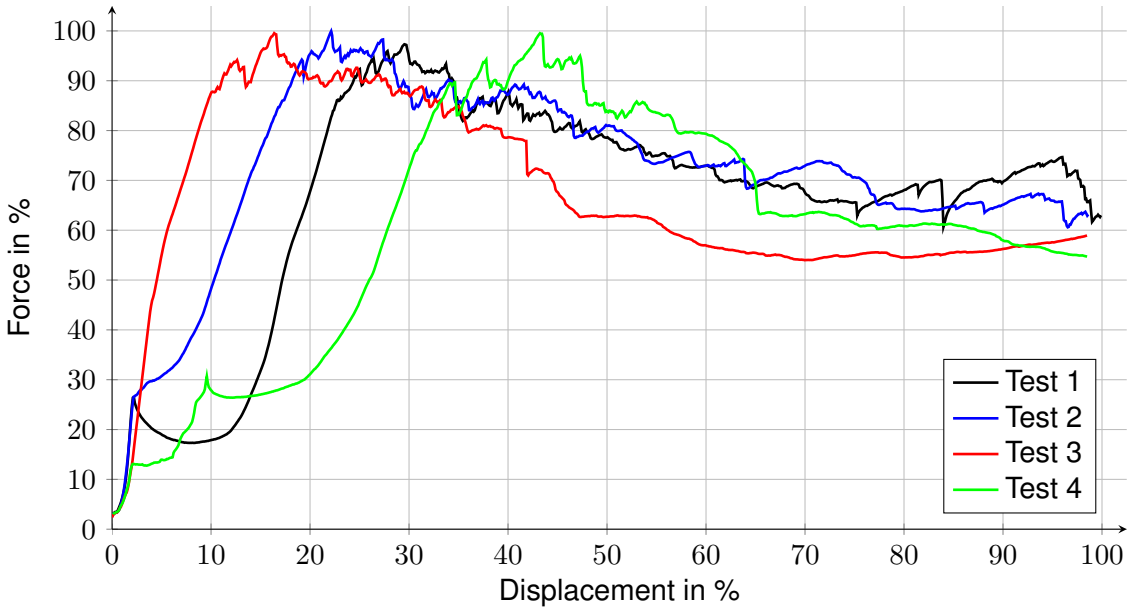

Fig. 5.8: Results of tensile test with a $(0°/90°/0°/90°)_s$ laminate and an edge distance e of 14 mm

Laminate with a stacking sequence of $(45°/-45°/45°/-45°)_s$ and an edge distance *e* of 10 mm

As a reason for the smaller edge distance e in this case shear failure occurs directly after reaching the ultimate force. The difference between the inclination of the curve after the ultimate force in case of laminate $(45°/-45°/45°/-45°)_s$ and $(0°/90°/0°/90°)_s$ is the diverse stacking sequence of the laminates. These results confirm the theory mentioned in the subsection 2.3.2 on the page 28.

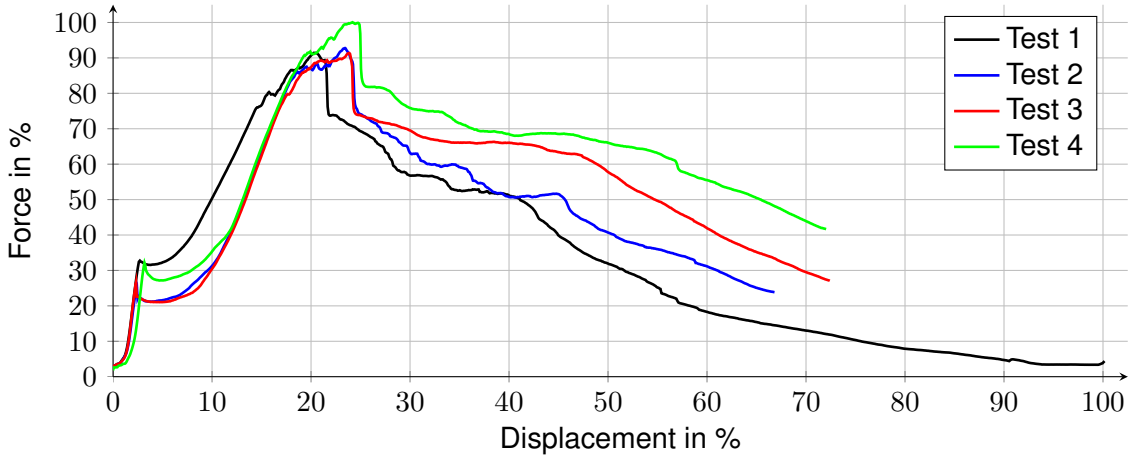

Fig. 5.9: Results of tensile test with a $(45°/-45°/45°/-45°)_s$ laminate and an edge distance e of 10 mm

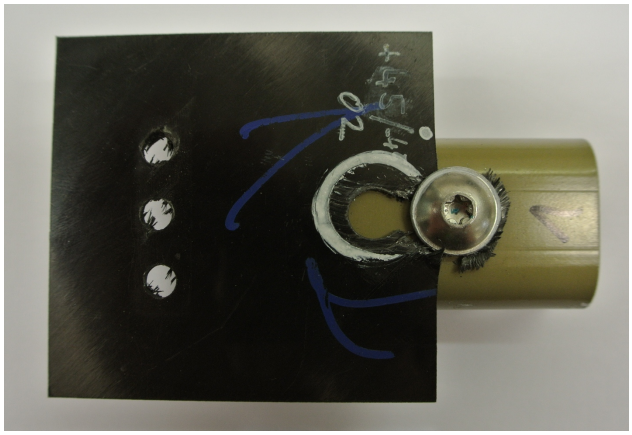

Fig. 5.10: Shear failure with a $(45°/-45°/45°/-45°)_s$ laminate

5.2 Numerical simulations - Simple tensile test

In this section simulations of simple tensile tests are discussed. These were done to be able to validate the settings of the chosen material types.

5.2.1 Tensile test with 0° plies

Determination of material properties from experimental data

The first step in the practical part of this thesis was to determine the material properties of the CFRP from experimental data provided.

The experimental data were gained from simple tensile test with CFRP of unknown properties. The data were acquired with a tensile test device with a strain gauge mounted on the test CFRP specimen and presented in a stress strain diagram in figure 5.11.

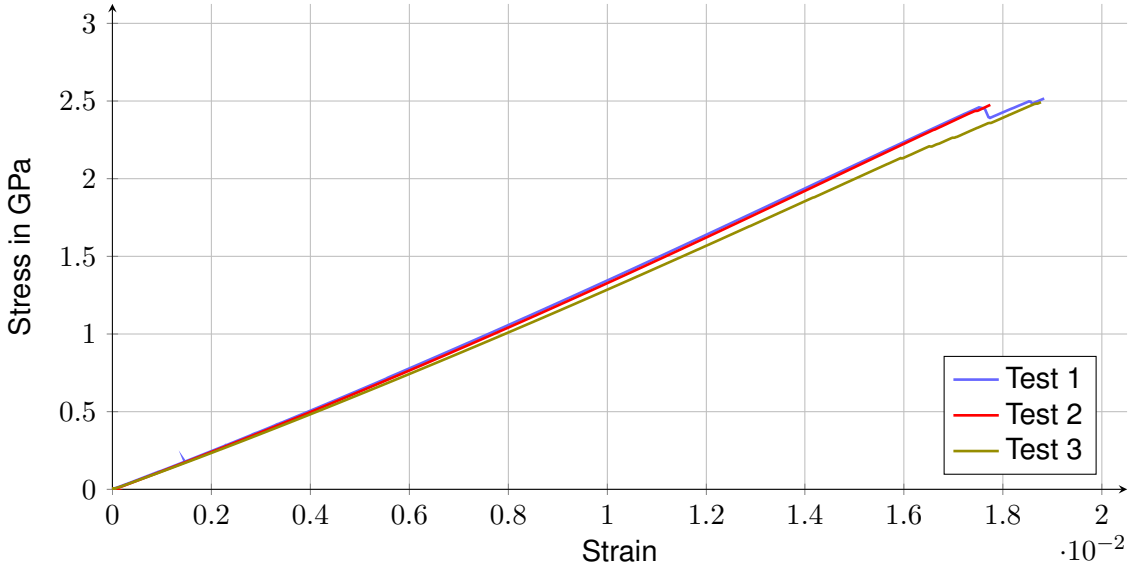

Fig. 5.11: Tensile test with CFRP specimens with 0° fiber direction

From these results and with the understanding of Hook's law it is possible to determine the Young's modulus of the ply in the fiber direction E_1. The strength of the lamina in the fiber direction R_1 can be obtained as well. Depending on the initial conditions of each material type the input variables alter. User-material type 81 requires as input data the elastic moduli and strengths for plies as whole. On the other hand material types 30 and 131 demand separated elastic moduli and strengths for matrix and fiber. In this case there is a need for more information about the plies, such as fiber volume ratio and elastic moduli at least of one phase of the ply (matrix or fiber). If this information is provided, the other parameters can be calculated from formula written bellow. In this case the fiber volume ratio and the Young's modulus of the fiber were known. [4]

$$E_1 = E_1^f \cdot \alpha_f + E^m \cdot (1 - \alpha_f) \tag{5.1}$$

where

E_1 – Young's modulus of the ply in fiber direction
E_1^f – Young's modulus of the fiber in the fiber direction
α_f – Fiber volume ratio
E^m – Young's modulus for the matrix

In the equation (5.1) new variable is mentioned - fiber volume ratio. The fiber volume ratio is defined as:

$$\alpha_f = \frac{V_f}{V} \tag{5.2}$$

where

α_f – Fiber volume ratio
V_f – Fiber volume in the ply
V – Ply volume

Control of the simulation results with experimental data

After defining the correct input values for the various material type results displayed in figure 5.12 are obtained.

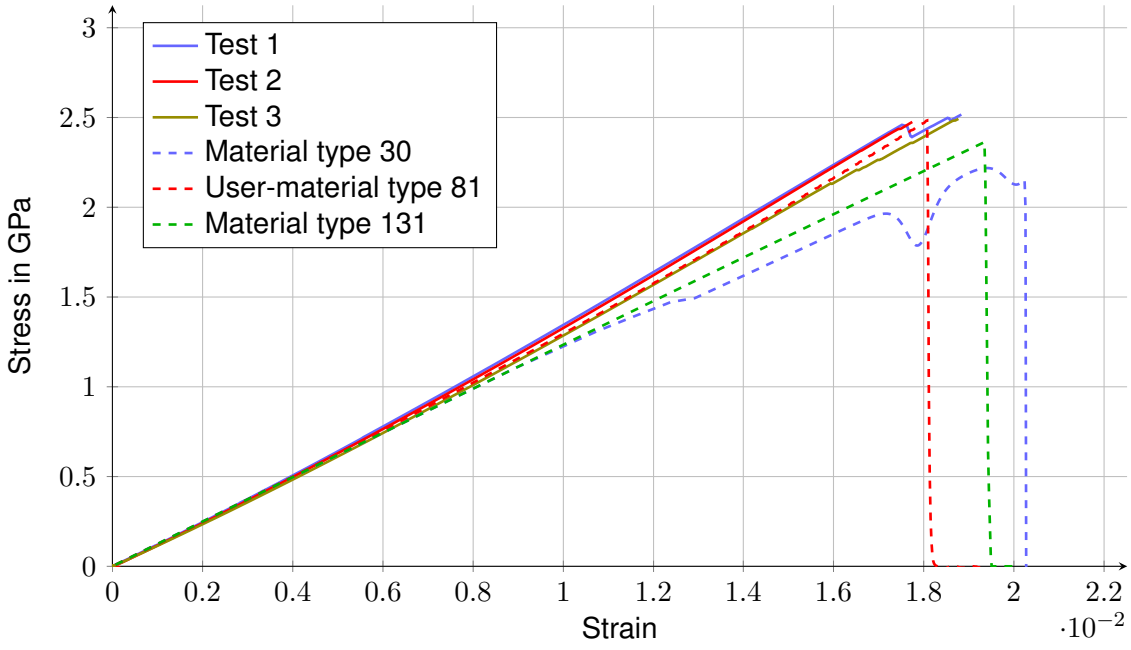

Fig. 5.12: Simulation and experimental data in a simple tensile tests with 0° ply

Material type 30 shows the right strength and the Young's modulus until the displacement reaches approximately 40 % equal to the real CFRP specimen. The difference is cause by two reasons. Firstly in the real CFRP specimen non-linear elastic behavior occurs which is a result of a non-linear behavior of the fiber material. This is not possible to simulate with material type 30 and therefore a deviation appears [28].

Second reason is that in case of material type 30 all the failures are simulated only through damages which are dependent on the volumetric or shear strain as explained in the section 3.4. Because there are only 6 input values that are supposed to simulate all possibilities an interaction cannot be avoided. The slight downfall of the curve is caused by a condition that is necessary to be able to simulate and achieve reasonable results in tensile test with CFRP with 90° plies.

User-material type 81 illustrates with its conditions a perfect behavior. It shows that it can simulate the non-linear behavior and the downfall with defined values.

Material type 131 behaves a little bit different. Based on the initial input conditions it is possible to avoid situation that happened with material type 30. In the figure it is possible to observe a linear behavior up to a failure point where the force reaches the ultimate force.

5.2.2 Tensile test with 90° plies

Determination of material properties from experimental data

Tensile test with 90° plies showed results illustrated in figure 5.13.

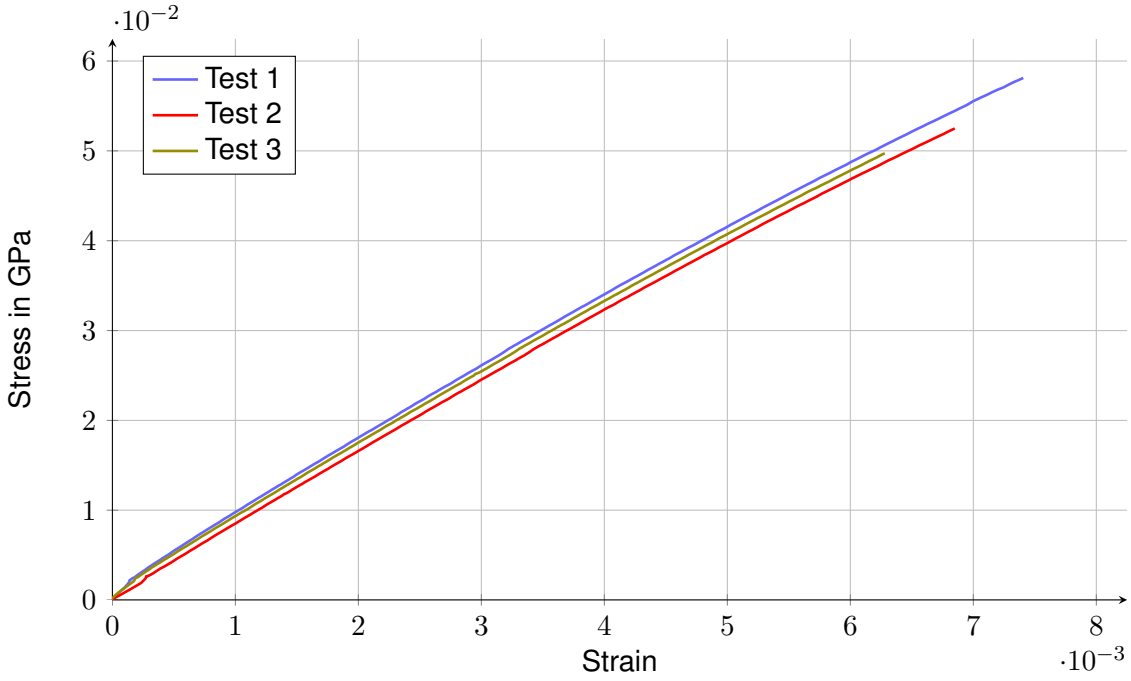

Fig. 5.13: Experimental data in a simple tensile tests with 90° ply

From figure 5.13 it is possible to obtain the strength R_2 and with the usage of the equation (5.3) to calculate the Young's modulus in the direction perpendicular to the fiber direction for the matrix. This value is a necessary input value. [21]

$$E_2^m = \frac{E_2^{UD}}{(1 + (\nu_{12}^{UD})^2 \cdot (\frac{E_2^{UD}}{E_1^{UD}}) \cdot (\frac{E_1^f}{E_1^{UD} - E_1^f}))} \tag{5.3}$$

where

E_2^m – Young's modulus of the matrix in the 2-direction
E_2^{UD} – Young's modulus of the laminate in the 2-direction
ν_{12}^{UD} – Poisson's ratio of the laminate
E_1^{UD} – Young's modulus of the laminate in the fiber direction
E_1^f – Young's modulus of the fiber phase in the laminate in the fiber direction

ν_{12}^{UD} is obtain by a measurement with a strain gauge and E_{11}^f is calculated with help of equation (5.4) [21].

$$E_{1(p)}^f = \alpha_f \cdot E_1^f \tag{5.4}$$

where

$E_{1(p)}^f$ – Young's modulus of the fiber phase in laminate in the fiber direction
α_f – Fiber volume ratio

Validation of the simulation results with experminetal data

After calculation of the input variables for the different material types simulation results shown in figure 5.14 were received.

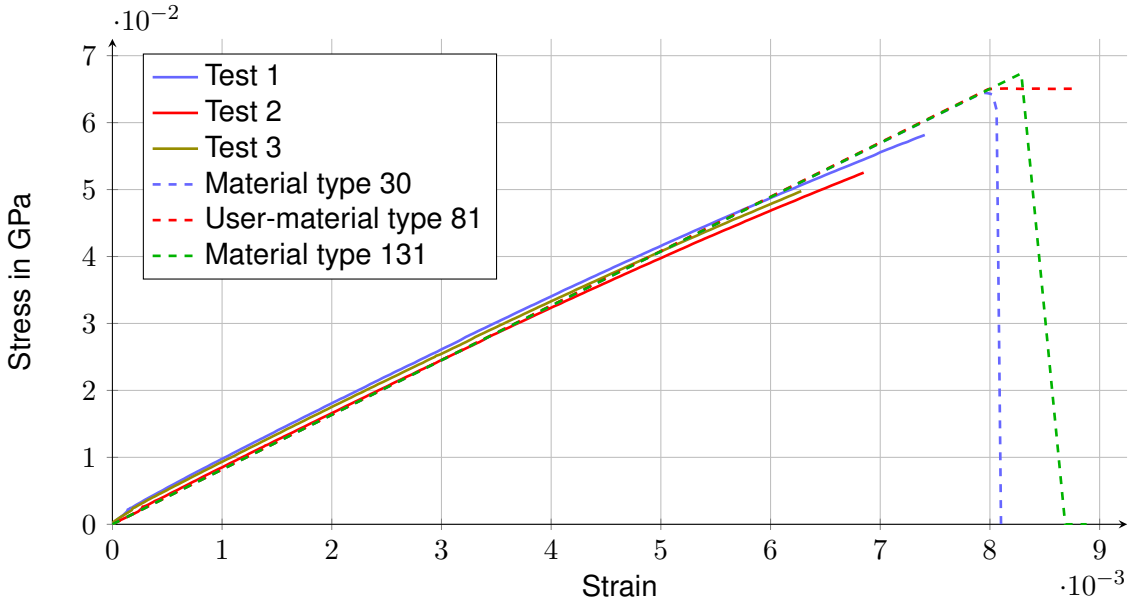

Fig. 5.14: Simulation and experimental data in a simple tensile tests with 90° ply

Material type 30 shows in this case as all the other materials a linear elastic behavior. The difference to the real tests is, that the real CFRP specimen experience from the beginning damage as described in the subsection 3.4.4 on the page 45. This is very difficult to simulate with material type 30 because the damage curve is already used for failure simulation. The curve at the ultimate stress has a smooth transition to a downfall of the curve and this is due to the damage curve which was defined in this way to prevent numerical problem in the simulation and to smoothen the interaction in other simulations.

User-material type 81 is capable to achieve the defined strength and then remains constant as already discussed in the subsection 3.4.4 on the page 45.

Material type 131 shows roughly the same result compared to the user-material type 81. Behavior of the curve could be designed so that it would copy the curves of the tests in a better way. The initial condition was not to use the damage curve but only the fiber and inter-fiber failure criterion. After the curve reaches the ultimate stress inter-fiber failure occurs and an immediate fall of the curve follows.

5.2.3 Tensile test with (45°/-45°/45°/-45°)$_s$ laminate

Determination of material properties from experimental data

Results of the simple tensile test with (45°/-45°/45°/-45°)$_s$ laminate are illustrated in figure 5.15.

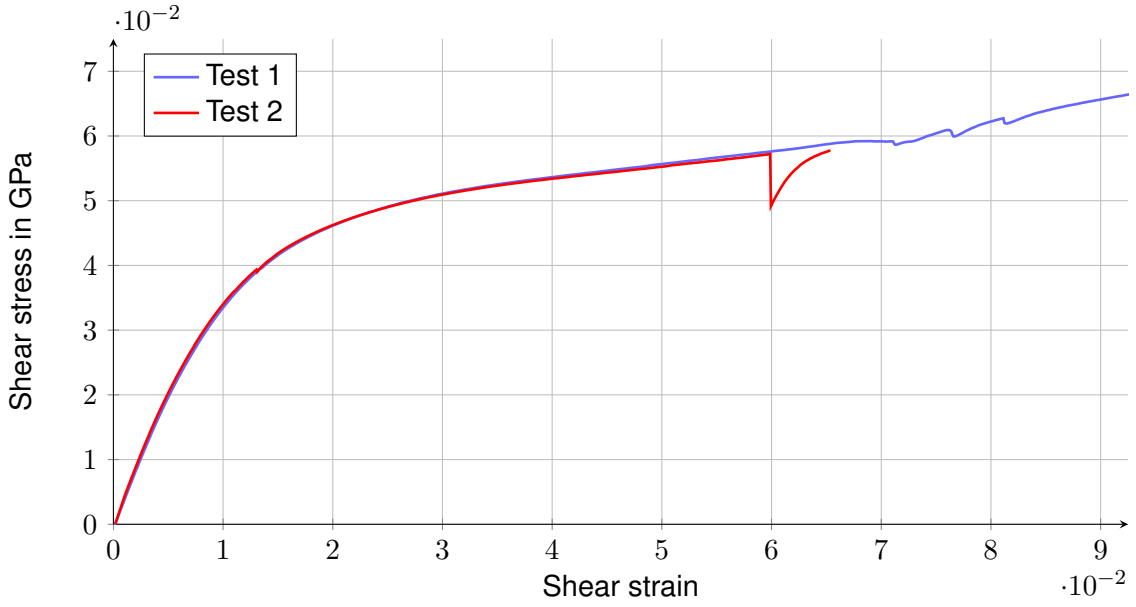

Fig. 5.15: Expermiental data in a simple tensile test with a $(45°/-45°/45°/-45°)_s$ laminate

The shear strain and shear stress were calculated with the help of values obtained using a strain gauge. The calculations were done according to equation (5.5). From this experimental data it is possible to obtain ultimate shear stress and shear modulus, which are necessary inputs for the simulations.

$$G_{xy} = \frac{\sigma_x}{2 \cdot (\epsilon_x - \epsilon_y)} \tag{5.5}$$

where

G_{xy} – Shear modulus in plane
σ_x – Normal stress in the direction of the length
ϵ_x – Strain in the direction of the length measured with strain gauge
ϵ_y – Strain in the perpendicular direction measured with strain gauge

The behavior of the curve is a result of a special phenomenon called *Nurnburger Schere* or *lazy tongs* [4]. Due to the strain caused by the loading the fibers stretch and start to change the direction from 45° up to 0°. This change of fiber direction alters the stress - strain relationship and changes the shear modulus, which is calculated with the initial inclination. The reason for the stress downfall is the missing support effect of the matrix. This phenomenon cannot be simulated with the material types considered here.

Validation of the simulation results with experimental data

With these approaches it was possible to simulate the behavior in a way displayed in figure 5.16

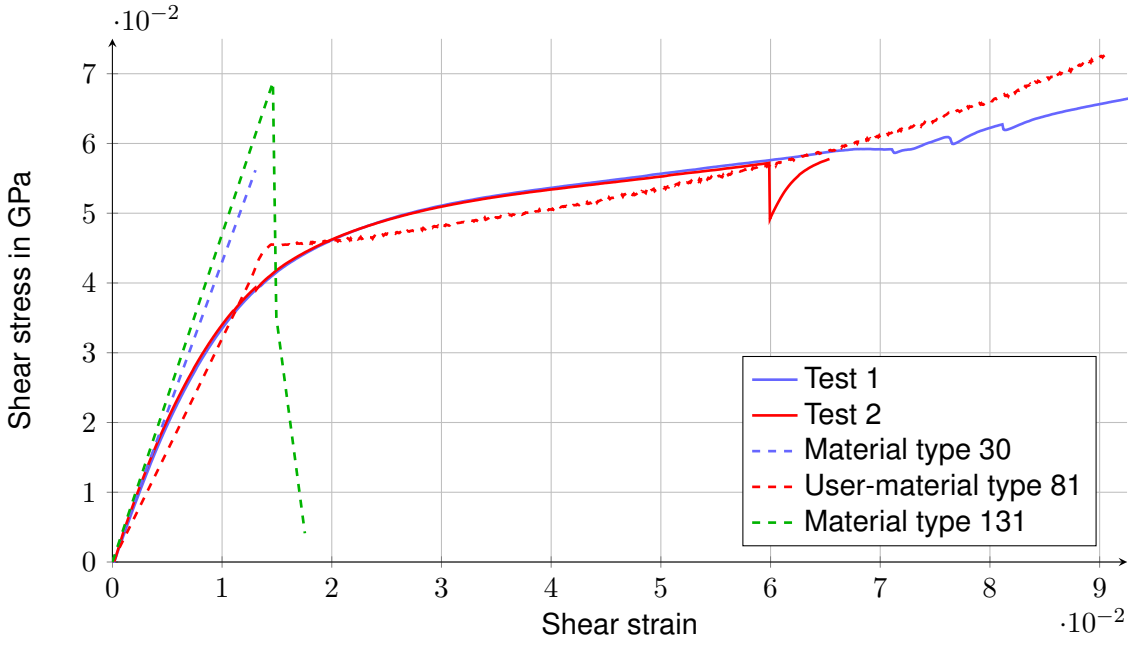

Fig. 5.16: Experimental data and simulations in a simple tensile tests with a $(45°/\text{-}45°/45°/\text{-}45°)_s$ laminate

From the results shown above it is visible, that the simulations and tests differ. This is due to the fact specified above. The simulated shear modulus in plane copies the tests at the beginning but shortly after the *lazy tongs* effect appears the curves take two separate paths. Therefore only the shear modulus at the beginning and the shear stress at the failure are approximately equal in all cases. The reason for the fact that the material type 30 does not continue up to 0 N is that a numerical instability that occurred during the simulations.

5.2.4 Tensile test with $(90°/0°/45°/\text{-}45°)_s$ laminate

The last of the simple tensile test is a test with $(90°/0°/45°/\text{-}45°)_s$ laminate. This test can be seen as a control of the input values, because it involves all types of ply. The results of the simulation and the tests are illustrated below. It is possible to see in the figure 5.17 that the material type 30 shows only poor results and the user-material type 81 and the material type 131 simulate the strength level in a good way.

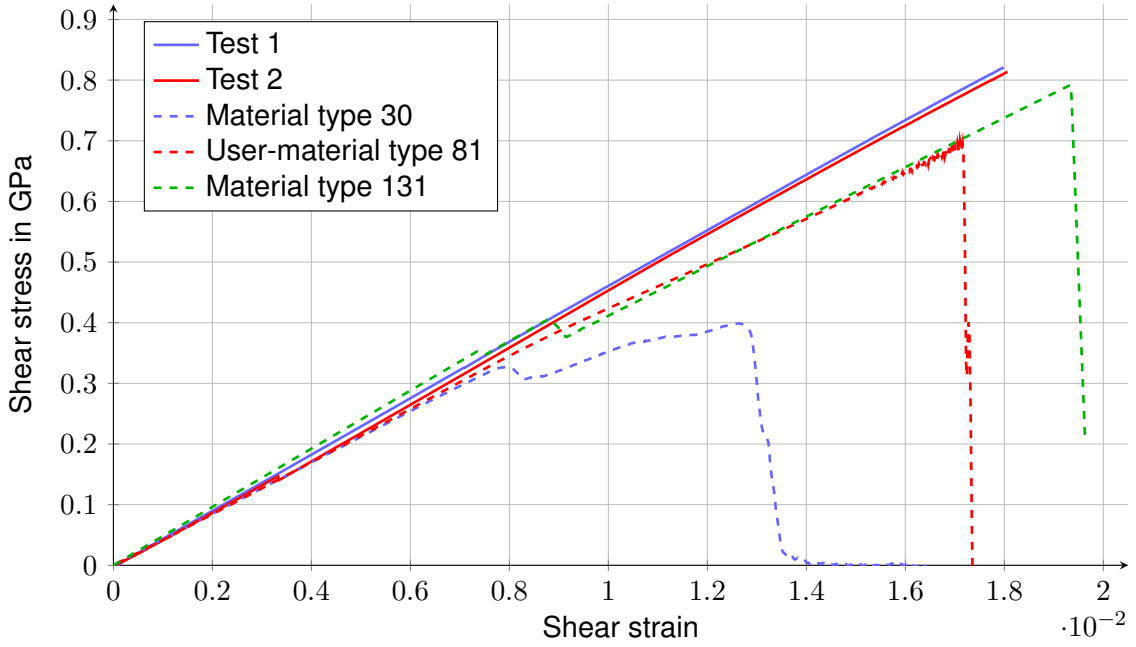

Fig. 5.17: Experimental data and simulations in a simple tensile tests with a $(90°/0°/45°/\text{-}45°)_s$ laminate

5.3 Numerical simulations - KSII testing facility

The following results were obtained from simulations with a model which represents the testing facility in figure 5.3. The CFRP specimens used in these tests were constructed according to subsection 5.1.1 on the page 71 with a stacking sequence of $(90°/0°/\text{-}45°/45°)_s$, $(0°/90°/0°/90°)_s$ and $(45°/\text{-}45°/45°/\text{-}45°)_s$. Two edge distances (10 mm and 14 mm) were tested.

The flow drill screw is pretensioned by defined force with the help of multistage approach, which is described in the section 4.3 on the page 51.

As a consequence of the flow drill process the aluminum U-shaped profile flows. This flowing aluminum wraps around the screw and enlarges its diameter. This is simulated in a way that a component, that is supposed to represent the flowed part, is constructed in a shape and dimensions that represent the reality.

For a better understanding and imagination the CFRP specimen is imaginary divided in regions as in figure 4.4.

5.3.1 Laminate with a stacking sequence of (90°/0°/-45°/45°)$_s$ and an edge distance *e* of 10 mm

Results

The results in figure 5.18 display the simulations with all three material types and the results from the experimental tests. The experimental tests are colored gray.

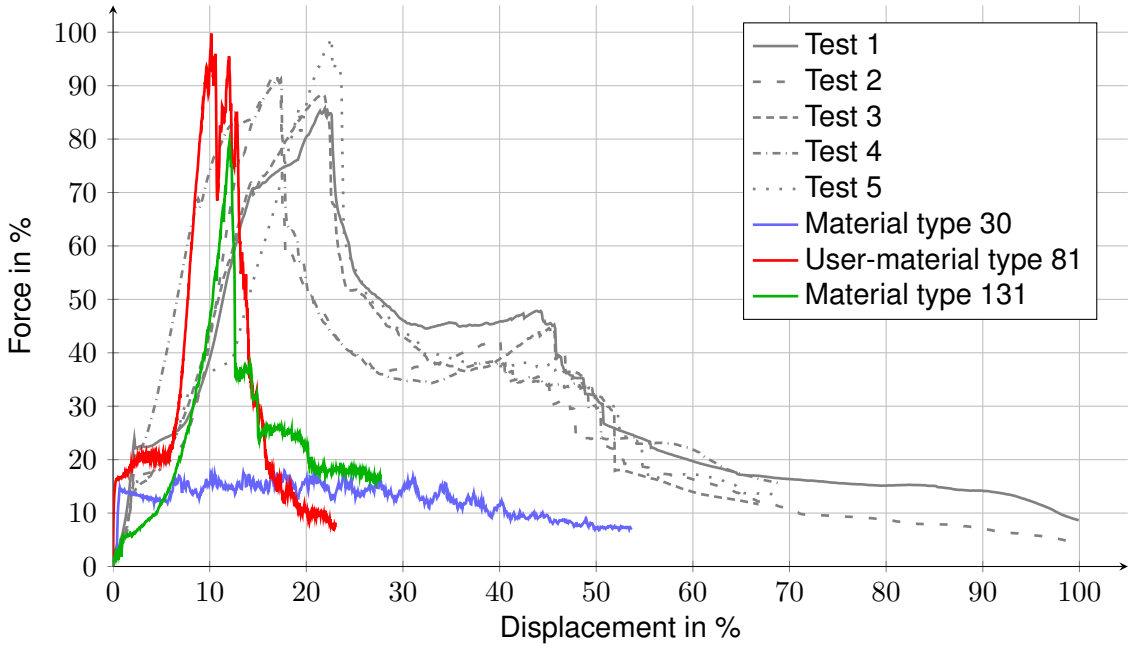

Fig. 5.18: Experimental data and simulations with a (90°/0°/-45°/45°)$_s$ laminate with an edge distance e of 10 mm

Experimental tests

The results from the experimental test are interpreted in detail in the subsection 5.1.4 on the page 74 according to which a combination of shear and tensile failure is observed.

Simulations

The simulation results of all three material types at failure are illustrated in figure 5.19.

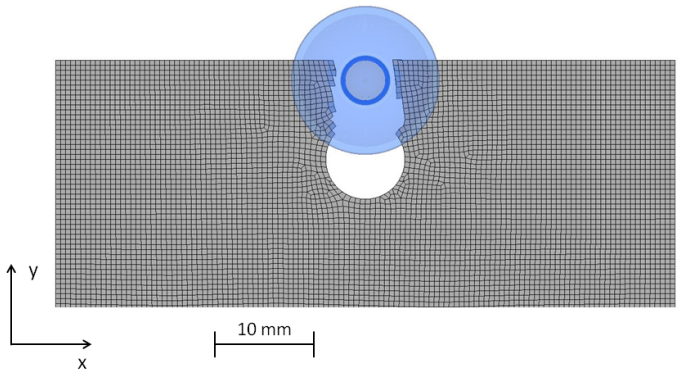

(a) Failure of material type 30 with a $(90°/0°/-45°/45°)_s$ laminate with the edge distance e of 10 mm at a displacement of 54 %

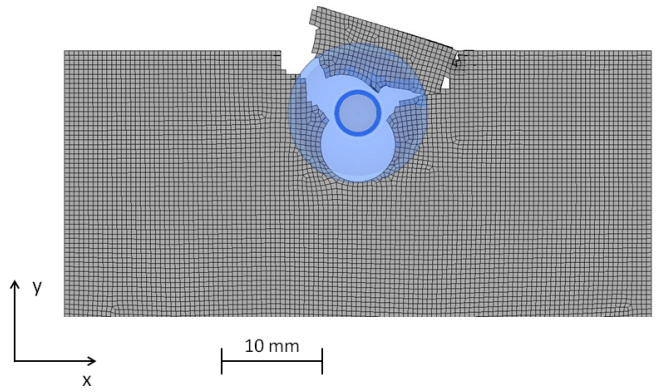

(b) Failure of user-material type 81 with a $(90°/0°/-45°/45°)_s$ laminate with the edge distance e of 10 mm at a displacement of 23 %

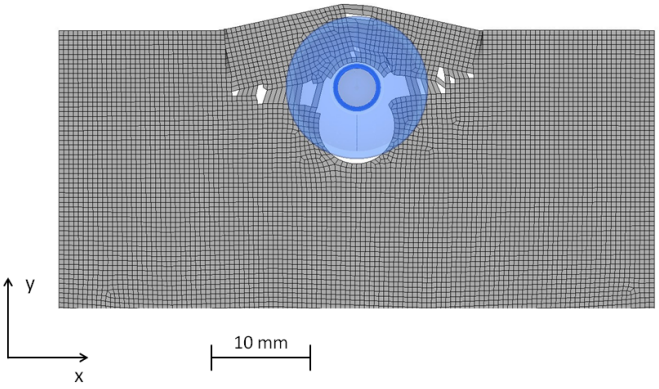

(c) Failure of material type 131 with a $(90°/0°/-45°/45°)_s$ laminate with the edge distance e of 10 mm at a displacement of 27 %

Fig. 5.19: Failure of various material types with a $(90°/0°/-45°/45°)_s$ laminate with the edge distance e of 10 mm

The friction overcome and bolt displacement phases are in all three material type simulations similar. Material type 131 shows a difference, which is caused by the shell element. To simulate the pretension with shell elements was not possible in a proper way.

Bolt displacement is in the solid element material types very similar. The difference in the shell material type is caused by the fact that the flowed aluminum component could not be simulated and that the pretension differs.

The most important difference in the simulations appears in the damage section. These differences are a result of different simulation approaches.

Material type 30 has very simple conditions for element elimination and does not allow an explicit definition of fiber and inter-fiber failure conditions. The conditions for element failure are fulfilled when defined volumetric or shear strain is reached. The conditions for element elimination are fulfilled when elements reach a defined volumetric strain. The elements are eliminated in the front region and bearing failure can be observed there. Due to the simplicity of the element elimination conditions the force level is low.

User-defined material type 81 allows an explicit definition for fiber and inter-fiber failure and includes multiple conditions for element elimination. Therefore even when the first fiber failure in the front region due to compression occurs element elimination does not happen. First elements are removed due to tension in the middle region when all conditions are fulfilled. As a result of these conditions a tensile failure occurs.

Material type 131 behaves similar to the user-defined material type 81. It allows explicit definition for fiber and inter-fiber failure, but includes simpler conditions for element elimination. First element eliminations occur in the middle region and results finally in a combination of shear and tensile failure.

5.3.2 Laminate with a stacking sequence of $(0°/90°/0°/90°)_s$ and an edge distance *e* of 10 mm

Results

The simulation results of all three material types and the experimental tests are compared in figure 5.20. The experimental tests are colored gray.

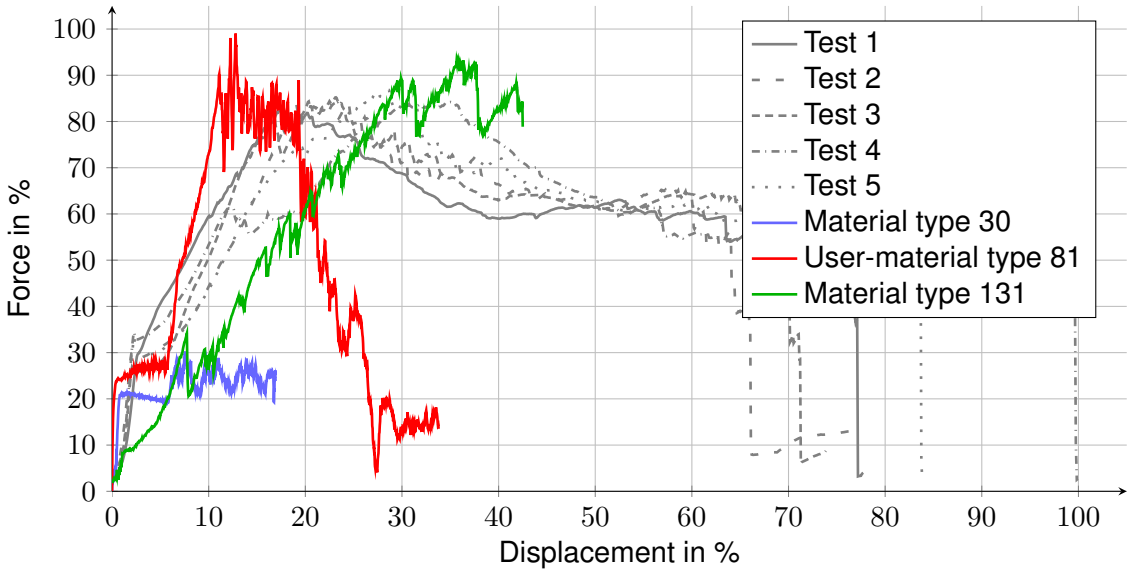

Fig. 5.20: Experimental data and simulations with a $(0°/90°/0°/90°)_s$ laminate with an edge distance e of 10 mm

Experimental tests

Interpretation of the results of the experimental tests is already given in the subsection 5.1.4 on the page 74. This interpretation and figures show that the failure mode should be a combination of shear and tensile failure.

Simulations

The simulations of all three material types at failure are illustrated in 5.21

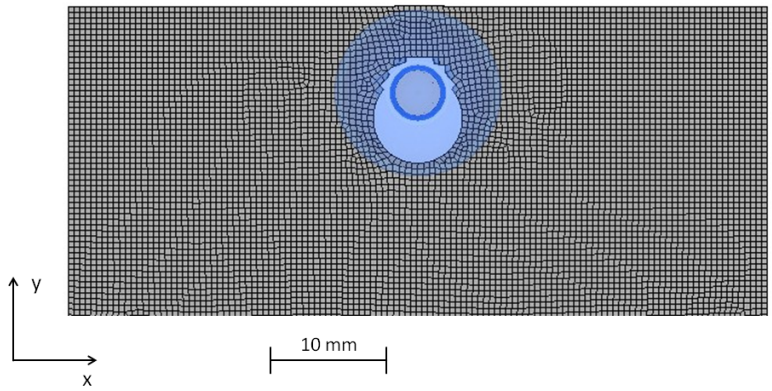

(a) Failure of material type 30 with a $(0°/90°/0°/90°)_s$ laminate with the edge distance e of 10 mm at a displacement of 17 %

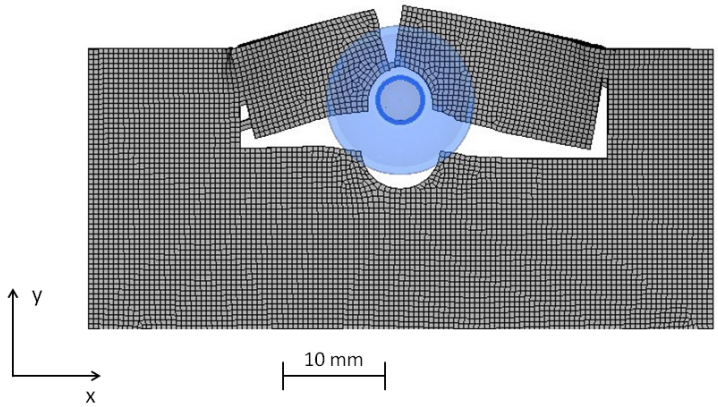

(b) Failure of user-material type 81 with a $(0°/90°/0°/90°)_s$ laminate with the edge distance e of 10 mm at a displacement of 34 %

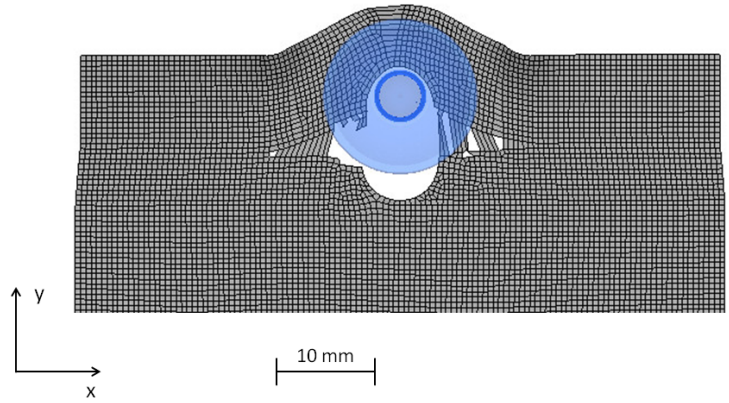

(c) Failure of material type 131 with a $(0°/90°/0°/90°)_s$ laminate with the edge distance e of 10 mm at a displacement of 43 %

Fig. 5.21: Failure of various material types with $(0°/90°/0°/90°)_s$ laminate with the edge distance e of 10 mm

The results of all three material types can be divided in the four sections mentioned before.

Material type 30 displays the friction overcome and bolt displacement in the proper way. The difference is in the damage phase where the force reaches only low levels. This is a result of simple conditions for element failure and elimination. These are based on volumetric and shear strain and are therefore not capable to simulate the phenomena in the right way. As a result it simulates bearing failure.

Material type 81 is capable to simulate the friction overcome and bolt displacement also

in the proper way. Due to its explicit definition for inter-fiber and fiber failure it is able to simulate all phenomena and predict the right failure mode. Even when the first fiber failure occurs in the front region due to compression stresses there is not element elimination. This is a result of the conditions for element elimination. The first element elimination appears in the side region due to tensile stresses.

Material type 131 alters from the other two material types in the friction overcome part. This is caused by the shell element. The result of this fact and the fact that the component for the flow of aluminum could not be used is that the bolt displacement behavior alters also. The damage phase is influenced by the conditions for fiber and inter-fiber failure which are simpler than in the case of user-material type 81. Therefore a slightly different failure occurs.

5.3.3 Laminate with a stacking sequence of (45°/-45°/45°/-45°)$_s$ and an edge distance *e* of 10 mm

The comparison of the simulations with the tests is illustrated in figure 5.21.

Results

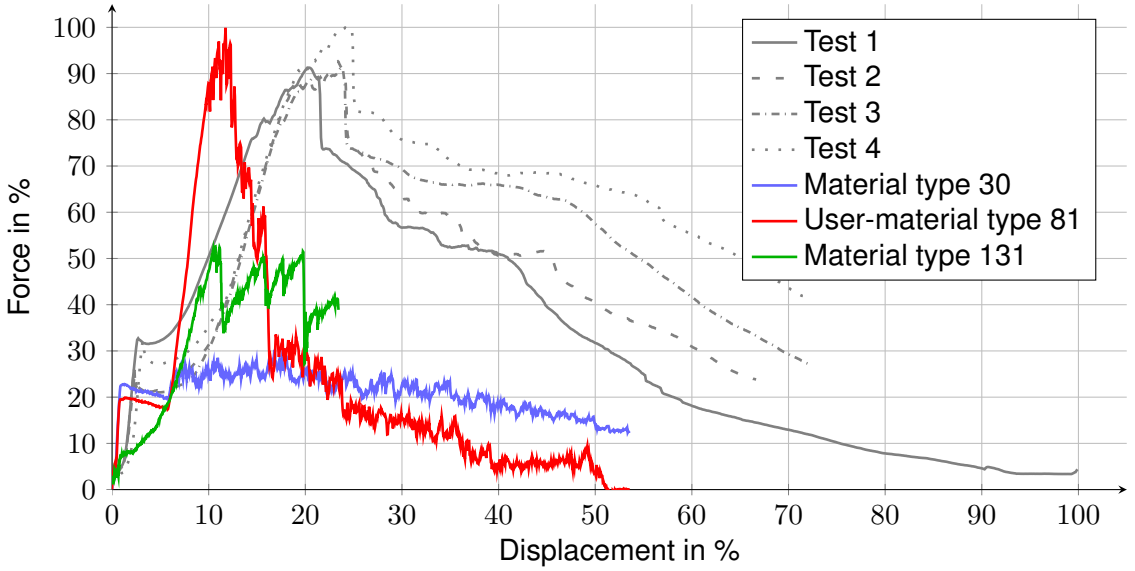

Fig. 5.21: Experimental data and simulations with a (45°/-45°/45°/-45°)$_s$ laminate with an edge distance e of 10 mm

Experimental tests

Interpretation of the results from experimental tests can be founded in the subsection 5.1.4 on the page 74. The results of the experimental tests are colored gray in figure 5.21.

Simulations

The simulation results at failure of all three material types are illustrated in figure 5.22

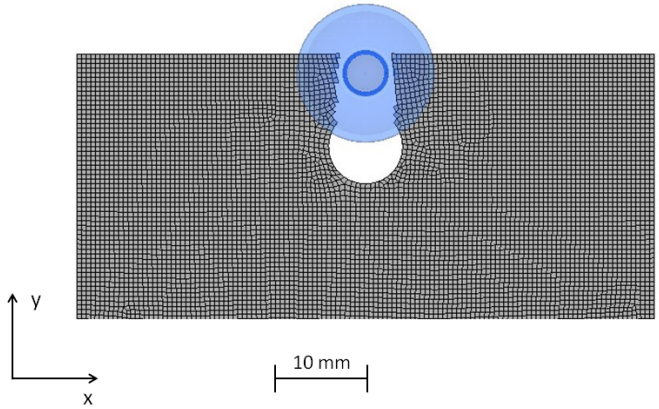

(a) Failure of material type 30 with a $(45°/-45°/45°/-45°)_s$ laminate with the edge distance e of 10 mm at a displacement of 54 %

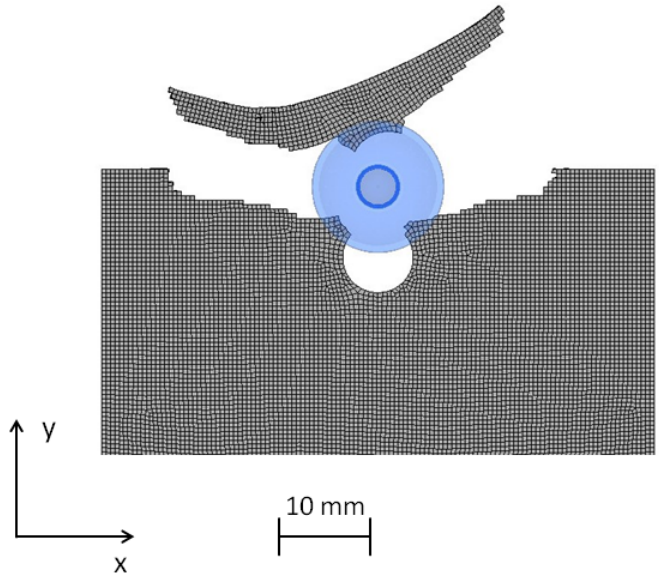

(b) Failure of user-material type 81 with a $(45°/-45°/45°/-45°)_s$ laminate with the edge distance e of 10 mm at a displacement of 54 %

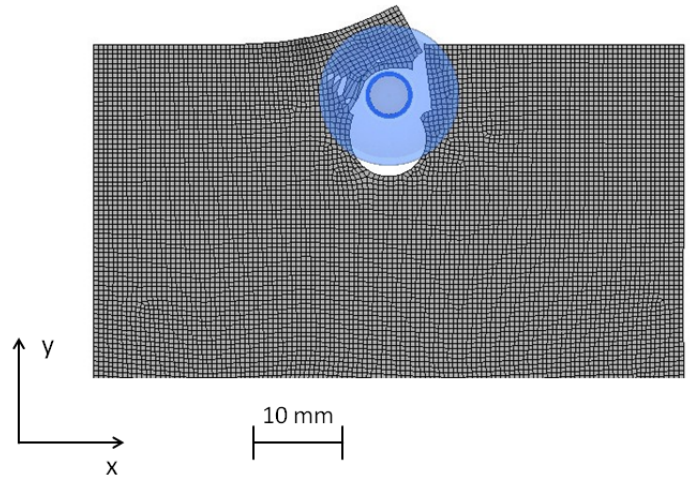

(c) Failure of material type 131 with a (45°/-45°/45°/-45°)$_s$ laminate with the edge distance e of 10 mm at a displacement of 23 %

Fig. 5.22: Failure of various material types with a (45°/-45°/45°/-45°)$_s$ laminate with the edge distance e of 10 mm

As can be seen the results of the various material types vary from each other.

Material type 30 is able to simulate the friction overcome and the bolt displacement toward the edge of the hole in the proper way. The difference between this material type and the other two is in the damage phase. Due to the simplicity of the conditions for element failure and elimination the material type 30 reaches low force level and results in bearing failure. This is due to the fact that the elements in the front region reach the defined volumetric and shear strain and are removed.

User-material type 81 shows the best behavior and the best force level compared with the experimental tests. This is a result of the possibility to define conditions for fiber and inter-fiber failure and the conditions for element elimination. As a result of the conditions for element elimination is that even when the fiber failure occurs in the front region due to compression the first element elimination occurs in the side region due to tension.

Material type 131 shows differences in the friction overcome and bolt displacement phases. This is as mentioned before caused by the shell element. Due to the conditions for element elimination, which are simpler that those of user-material type 81, is the material type 131 not able to reach the correct force level.

5.3.4 Laminate with a stacking sequence of (90°/0°/45°/-45°)$_s$ and an edge distance *e* of 14 mm

Results

The results of the experimental tests and the simulations are displayed in figure 5.22. The experimental tests are colored gray.

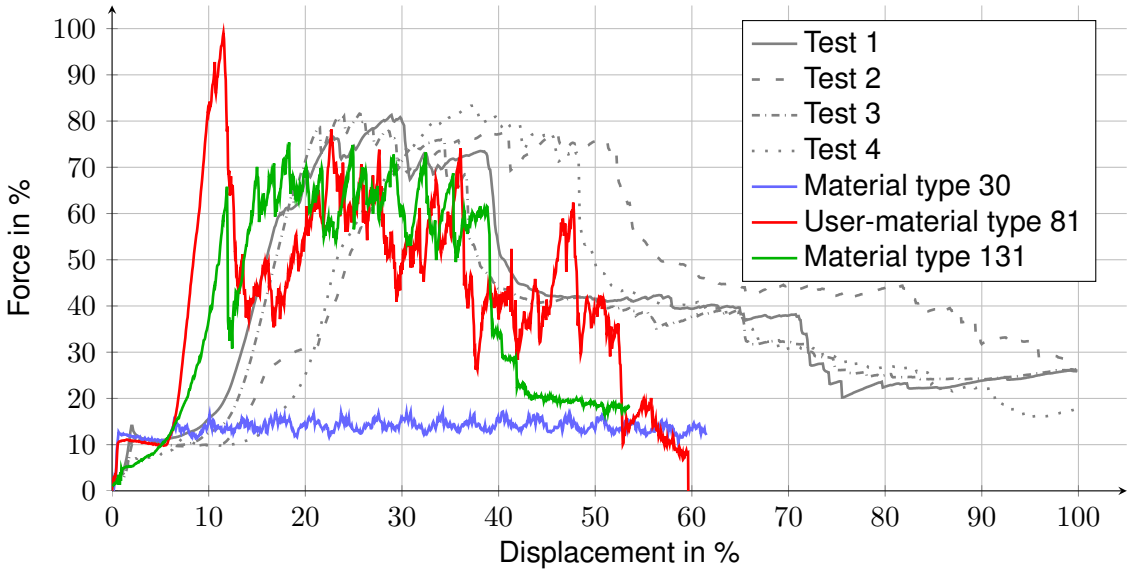

Fig. 5.22: Experimental data and simulations with a (90°/0°/45°/-45°)$_s$ laminate with an edge distance e of 14 mm

Experimental tests

The results of the experimental tests are fully interpreted in the subsection 5.1.4 on the page 74. The experimental tests of the (90°/0°/45°/-45°)$_s$ laminate with an edge distance e of 14 mm fail in a combination of bearing and tensile failure.

Simulations

The simulation results of all three material types at different failures are displayed in figure 5.23.

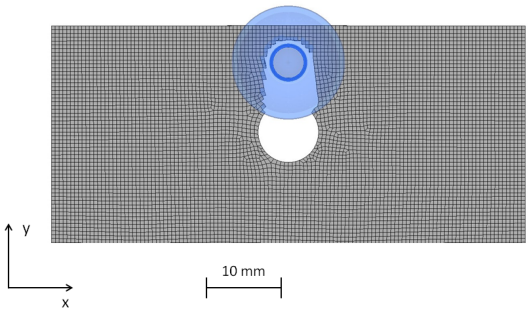

(a) Failure of material type 30 with a $(90°/0°/-45°/45°)_s$ laminate with the edge distance e of 14 mm at a displacement of 62 %

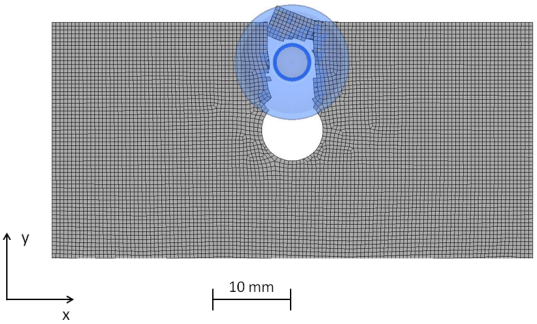

(b) Failure of user-material type 81 with a $(90°/0°/-45°/45°)_s$ laminate with the edge distance e of 14 mm at a displacement of 59 %

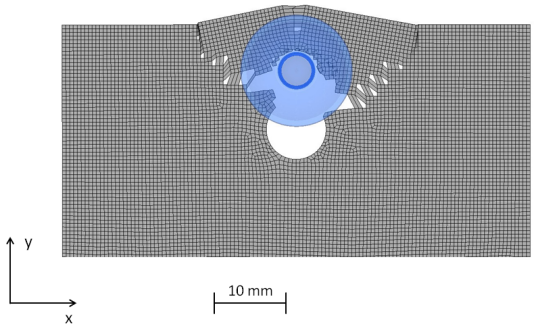

(c) Failure of material type 131 with a $(90°/0°/-45°/45°)_s$ laminate with the edge distance e of 14 mm at a displacement of 54 %

Fig. 5.23: Failure of various material types with a $(90°/0°/-45°/45°)_s$ laminate with the edge distance e of 14 mm

From figures above it is possible to see the differences in the failure modes reached.

Material type 30 can simulate the friction overcome and the bolt displacement well. It reaches again only bearing failure. This is a result of its simple conditions for element failure and elimination. Due to this conditions the force level reached is low as can be seen in figure 5.22. In the simulation the elements in the front region fail first and are then removed.

User-material type 81 simulates the first two phases in the proper way. It reaches a high force level. Due to its capabilities to define conditions for inter-fiber and fiber failure it predicts the failure mode correctly. The first fiber failure occurs in the front region due to compression and elements are removed when the conditions for element elimination are fulfilled.

Material type 131 shows good results which is a result of the possibility to define conditions for inter-fiber and fiber failure and due to the conditions for element elimination. These conditions are able to simulate bearing failure in a precise way and therefore the force level of the results is correct.

5.3.5 Laminate with a stacking sequence of $(0°/90°/0°/90°)_s$ and an edge distance *e* of 14 mm

Results

The comparison of the tests and the simulations are illustrated in figure 5.23. The experimental tests are colored gray.

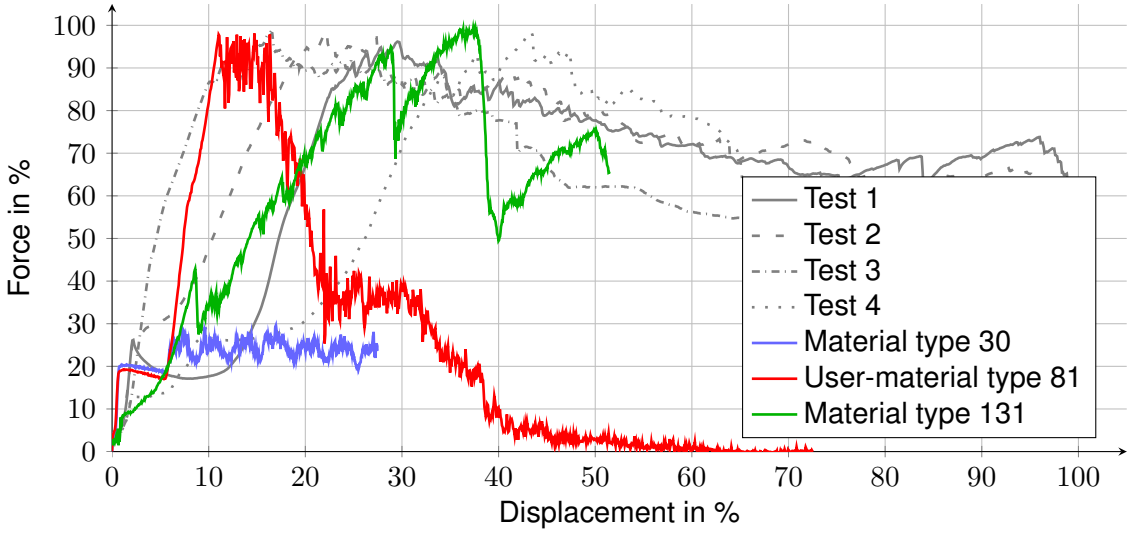

Fig. 5.23: Experimental data and simulations with a $(0°/90°/0°/90°)_s$ laminate with an edge distance e of 14 mm

Experimental tests

In the subsection 5.1.4 on the page 74 the results of the experimental tests are interpreted.

Simulations

The simulation results are illustrated in figure 5.24.

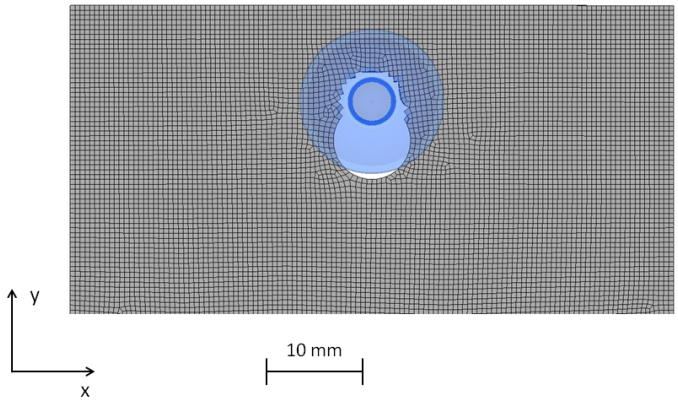

(a) Failure of material type 30 with a $(0°/90°/0°/90°)_s$ laminate with the edge distance e of 14 mm at a displacement of 27 %

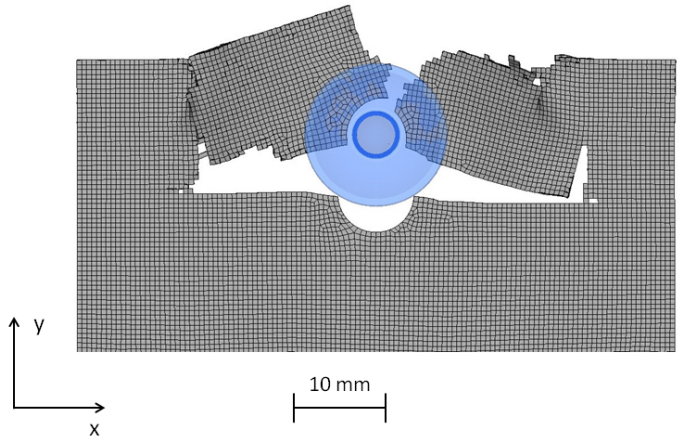

(b) Failure of user-material type 81 with a $(0°/90°/0°/90°)_s$ laminate with the edge distance e of 14 mm at a displacement of 73 %

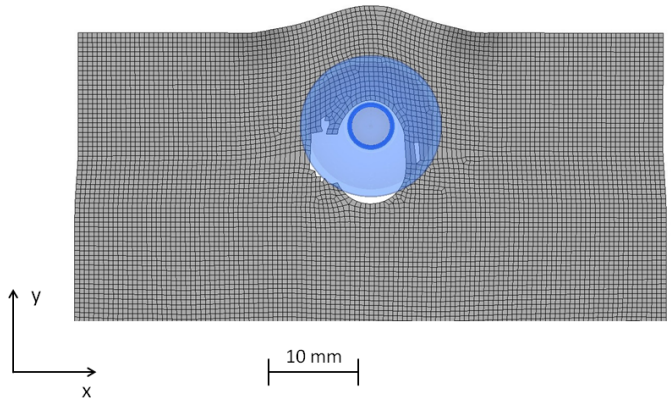

(c) Failure of material type 131 with a $(0°/90°/0°/90°)_s$ laminate with the edge distance e of 14 mm at a displacement of 52 %

Fig. 5.24: Failure of various material types with a $(0°/90°/0°/90°)_s$ laminate with the edge distance e of 14 mm

As can be seen in 5.24 a different failure modes occur.

Material type 30 reaches only bearing failure. This is again a result of its simple conditions for element failure and elimination, which is based on volumetric and shear strain. When this defined strain is reached element failure and elimination occurs. Therefore even when the friction overcome and bolt displacement phase are simulated in the proper way the force level is low.

User-material type 81 reaches the correct force level and is able to simulate the first two phases in the correct way. This is due to the nature of the material type, which allows definition of conditions for inter-fiber and fiber failure and due to the amount of conditions for element elimination. Even when the fiber failure occurs in the front region due to compression the conditions for element elimination do not allow element elimination. This happens when all conditions are fulfilled as it is in the middle region.

Material type 131 differs from the other material types in the first two phases. This is a result of the shell elements which cannot simulate the bolt pretension in the same way as the solid elements and the fact that the aluminum component for aluminum flow could not be used. The force level in the damage phase is correct and the failure is not perfectly right. This is a result of the conditions for element elimination. The simulation end with a numerical instability as in almost all simulations with the material type 131. This is caused by the nature of shell elements.

5.3.6 Conclusion from the simulations with the KSII testing facility

Material type 30

Due to the simplicity of the conditions for damage and element elimination it is obvious that the simulation possibilities of the standard material for solid elements are restricted. Almost in every simulation the failure mode was bearing failure. This is due to the fact, that the element elimination was achieved after reaching a specified value for compression, which would not happen in the reality. This material type does not allow a detailed simulation of inter-fiber and fiber failure and all this phenomena have to be included in the damage, which takes as a parameter only the elastic and shear strain of the element, which is just not sufficient.

User-material type 81

The user-defined material type allows explicit simulation of the inter-fiber and fiber failure and provides the most accurate results. This is a result of the conditions for element elimination and the simulation of almost all phenomena, which can happen in the CFRP, which were defined in an extensive research work done. This material type allows as well to display the inter-fiber failure mode and makes this material type not only the most accurate on but also unique.

Material type 131

Even, when the curves in the graphs seem to be comparable with the material type 81, there are still major differences between them. The biggest one is the amount of conditions for element elimination, which is in case of the material type 131 not sufficient.

The other important thing is the stability of the model. The shell model has stability issues, which are caused by its minimal thickness. The thickness causes as well problems with the pretension, where the flowing aluminum, which is created by the flow drill screw process, could not be displayed.

The other issue with the pretension was the fact that the pretension force is strongly depending on the duration of the pretension. This is caused by the fact, that the shell model cannot be deformed in the thickness direction.

The definition of the material type 131 as well describes that an element is removed, when the condition is reached in all plies, which can cause other uncertainties.

This shows that even when the material type 131 is able to provide better understanding and results of the simulation with CFPR as the material type 30 it does not reach the accuracy and the possibilities of the material type 81.

6 Summary

The advantages of the bolted joints between the aluminum and CFRP were explained in this thesis. These advantages are significantly influenced by the failure mode reached. As already mentioned there are safe and non-safe failure modes. To be able to fully utilize the energy absorption potential of CFRP a safe failure mode must be achieved. The bearing failure is the only safe mode from all. The energy absorption ability of the bearing failure depends on many variables, like matrix and fiber material properties, stacking sequence, bolt diameter and thickness of the laminate. If the bearing failure is not achieved, the energy potential cannot be utilized and the joint separates. Therefore a transition between the bearing failure and other failures caused by the geometry is important.

Simulation of the flange bolt joint between CFRP and aluminum make it possible to save manufacturing costs and time and forecast the failure mode in a precise way.

Experimentals revealed that the failure modes strongly depend on the geometry of the CFRP specimen. Multiple tests with various stacking sequence and edge distance were done to prove this fact. With the help of endoscopic camera and photo analysis it was not only possible to precisely isolate the results in the form of a force-displacement curve but to visually validate the failure mode. It was shown that the failure modes with stacking sequences cannot provide ideal results in the case of shear and tensile failure. This is a result of the residual lamina, which do not fail. Therefore the ideal tensile or shear failure with immediate CFRP specimen separation can only occur in the case of unidirectional CFRP.

The finite element simulations in this thesis were done with an explicit solver called $PAMCrash$. These simulations were done with three material types. One user-defined material type for solid, one standard material type provided by the software company for solids and one standard material provided by the software company for shells. Each of these material types had different parameters that could be set to simulate the CFPR. This parameters can be separated into two group. In the physical based parameters information like Young's modulus, shear modulus, poisson's ratio, strengths and stacking sequence were defined. In the numerical based parameters various parameter for numerical stability were defined.

7 Conclusion

The results of the simulation has shown that the user-defined material type has much better ability to simulate the failure modes and predict the right one and provides enhanced visualization possibilities helpful for engineers. The ability to predict and simulate the failure modes in a right way is caused by its specific conditions which are very detailed and based on the real phenomena. The standard material type for shells provided just average results, where sometimes it was capable to predict the failure mode and the energy absorption and sometimes it failed. As a shell model it had as well more numerical instability issues. The standard material type for solids has shown only less than average result, where due to lack of variables it was mostly not capable to predict the right failure mode and not even the energy absorption. This was as well caused by the fact, that the thesis wanted to compare these three material types with similar setting and therefore the full potential of the standard material type for solids was not utilized. Even with all setting, the accuracy and prediction ability would not be much better.

Due to the comparison of the different material types, the gap between the abilities was obvious. The user-defined material type for solids is the future in the finite element simulation. The standard material types lack of ability and their conditions are limited and can therefore simulate the real behavior.

8 Outlook

The furter steps in the simulation should go in the direction of the change of the conditions on which the material types work and try to fully utilize the potential of these material types to improve the simulation between of the failure modes of CFRP. The work should focus on a goal to achieve a material type that is numericaly stable, result accurate, can predict the right failure mode and its computational costs are low.

Bibliography

[1] G. S. Cole and A. M. Sherman. Light weight materials for automotive applications. *Materials Characterization*, 35(1):3 – 9, 1995. Microstructural Characterization of Lightweight Structural Materials Transportation.

[2] P. K. Mallick. *Fiber-Reinforced Composites: Materials, Manufacturing, and Design, Second Edition*. Dekker Mechanical Engineering. Taylor and Francis, 1993.

[3] D. D. L. Chung. *Carbon Fiber Composites*. Butterworth-Heinemann, Boston, 1994.

[4] H. Schürmann. *Konstruieren Mit Faser-Kunststoff-Verbunden*. VDI-Buch. Springer-Verlag Berlin Heidelberg, 2007.

[5] T. A. Collings. The strength of bolted joints in multi-directional cfrp laminates. *Composites*, 8(1):43 – 55, 1977.

[6] Handout, porsche.

[7] I. M. Daniel and O. Ishai. *Engineering Mechanics of Composite Materials*. Number Bd. 13 in Engineering mechanics of composite materials. Oxford University Press, 2006.

[8] L. F. Mondolfo. *Aluminum alloys: structure and properties*. Butterworths, 1976.

[9] F. C. Campbell. *Structural Composite Materials*. ASM International, 2010.

[10] M. Flemming and S. Roth. Analogien zwischen faserverbunden der natur und technik. In *Faserverbundbauweisen Eigenschaften*, pages 11–29. Springer Berlin Heidelberg, 2003.

[11] I. V. K. AVK. *Handbuch Faserverbundkunststoffe: Grundlagen Verarbeitung Anwendungen*. Vieweg + Teubner, 2010.

[12] M. Flemming, G. Ziegmann, and S. Roth. *Faserverbundbauweisen: Fasern und Matrices*. Faserverbundbauweisen. Springer Berlin Heidelberg, 1995.

[13] P. Morgan. *Carbon Fibers and Their Composites*. Materials Engineering. Taylor & Francis, 2005.

[14] Thorne. *in Strong Fibers*. North-Holland, Amsterdam, 1985.

[15] S. D. Thoppul, J. Finegan, and R. F. Gibson. Mechanics of mechanically fastened joints in polymer-matrix composite structures - a review. *Composites Science and Technology*, 69(3-4):301 – 329, 2009.

[16] F. L. Camanho, P. P.; Matthews. Stress analysis and strength prediction of mechanically fastened joints in frp: a review. *Composites Part A: Applied Science and Manufacturing*, 28(6):529 – 547, 1997.

[17] L. J. Hart-Smith. Design and analysis of bolted and riveted joints in fibrous composite structures. In L. Tong and C. Soutis, editors, *Recent Advances in Structural Joints and Repairs for Composite Materials*, pages 211–254. Springer Netherlands, 2003.

[18] F. L. Matthews, P. F. Kilty, and E. W. Godwin. Load-carrying joints in fibre reinforced plastics. *Plastic and Rubber Process and Applications*, 2:19–25, 1982.

[19] S. S. Quek and G. R. Liu. *Finite Element Method: A Practical Course*. Elsevier Science, 2003.

[20] U. F. Meißner and A. Maurial. *Die Methode der finiten Elemente: Eine Einführung in die Grundlagen*. Springer-Lehrbuch. Springer Berlin Heidelberg, 2000.

[21] esi - group. *Virtual Performance Solution 2013,Solver Reference Manual - Online Help*, 2013.

[22] R. Szlosarek, T. Karall, C. Hahne, A. Berger, N. Meyer, and N. Enzinger. Entwicklung eines dreidimensionalen materialmodells für faser-kunststoff-verbunde mit hilfe simulationsbegleitender festigkeitsuntersuchungen an fließformschraubverbindungen cfk - aluminium. In *Simulation und Erprobung in der Fahrzeugentwicklung: Berechnung, Prüfstands- und Straßenversuch*, volume 2224, pages 149 – 168. VDI Verlag - Düsseldorf, 2014.

[23] J. Ruge and H. Wohlfahrt. *Technologie der Werkstoffe: für Studenten des Maschinenbaus und Bauingenieurwesens, der Verfahrenstechnik und der Werkstoffkunde ; mit 66 Tabellen*. Studium Technik. Vieweg, 2002.

[24] Cambridge University Engineering Department. *Structures Data Book*. Cambridge University, 1999.

[25] M. Knops. *Analysis of Failure in Fiber Polymer Laminates: The Theory of Alfred Puck*. Engineering Materials and Processes. Springer, 2008.

[26] Ch. Gradwohl. Experimentelle charakterisierung und finite elemente simulation des delaminiervorgangs von faserverbundkunststoffen. Master's thesis, Technische Universität Graz, April 2013.

[27] T. Weber. *Nichtlineare Analyse von Faser-Kunststoff-Verbunden: Grundlagen, Methoden und Auswirkungen auf den Konstruktionsprozess*. Schriftenreihe Konstruktiver Leichtbau mit Faser-Kunststoff-Verbunden. Shaker, 2009.

[28] R. Szlosarek. *Experimentelle und numerische Untersuchungen zur mechanischen Festigkeit von Fliessformschraubverbindungen zwischen Faser-Kunststoff-Verbunden und Aluminium*. Dissertation, Technische Universität Graz, 2015.

[29] R. Szlosarek, T. Karall, N. Enzinger, C. Hahne, and N. Meyer. Mechanische prüfung von fließlochformenden schraubverbindungen zwischen faserverstärkten kunststoffen und metallen. *Materials Testing*, 55(10):737–742, 2013.

List of figures

List of tables